



Facultad de Ciencias Geológicas



Universidad Complutense de Madrid

MÁSTER EN INGENIERÍA GEOLÓGICA

Título: Comparison of Numerical and Classical Analytical Method for Sheet Pile Wall Analyses

Darlington MENSAH
MADRID, CURSO 2013-2014

Tutor 1: Dr. Svetlana MELENTIJEVIC
UCM

Tutor 2: Vinicius GOUVEIA DE MIRANDA
MAXAM Civil Explosives



Facultad de Ciencias Geológicas



Universidad Complutense de Madrid

MÁSTER EN INGENIERÍA GEOLÓGICA

Título: Comparison of Numerical and Classical Analytical Method for Sheet Pile Wall Analyses

Darlington MENSAH
MADRID, CURSO 2013-2014

Autorizo la presentación del Trabajo de Fin de Máster.

A handwritten signature in blue ink, which appears to read 'Svetlana Melementijevic'.

Tutor UCM: Dr. Svetlana MELENTIJEVIC

ACKNOWLEDGEMENT

My sincere gratitude goes to Prof. Svetlana Melentijevic and Prof. Ángel Mateos Moreno for their guidance, advice, unlimited patience and positive attitude towards the preparation and writing of this interesting research study; without whom this research would not have been possible. I would also like to thank Vinicius Gouveia De Miranda, who continues to be a constant inspiration to me; guiding me patiently and with constructive criticism in the preparation of the software.

Gratitude also goes to the lecturers of the Faculty of Geological Engineering for contributing to my good background in geotechnics, with special mention to Prof. Meaza Tsiga.

To my parents (Ethel and Victor) and siblings (Victor Jnr, Sylvester, Clinton, Ekene, Chioma and Aka), there is no amount of words that can express my gratitude to you for believing in me and supporting me day-in-day-out. You guys are really awesome!

Special appreciation also goes to Pedro and the family for the love and support they continue to show me, especially during my academic year.

My studies and this project would not have been possible without Rishat Khabibullin, Emmanuel K.A. Effah, Francisco S. Leite and Melquides Elba. You guys made it happen and the least I can say is "THANK YOU".

Finally, I would like to thank very special people who helped me directly and/or indirectly in being able to successfully go through my studies: Emmanuel Asare-Addo, Eric Terkpertey, Paulo Fernandez, Abigail Del Carmen, Robert Fernandez Ampuero, Inma Pastrana, Danny Burbano, Gonzalo Del Leon, HoChang Lee, Ingrid Monroy and Ane Urbano.

ABSTRACT

The purpose of this study is to analyse the behaviour of steel sheet pile wall by numerical and analytical methods.

Analytical method based on the limit equilibrium approach has been used over the years in undertaking sheet pile wall analyses due to its simplicity. However it overestimates some of the results regarding maximum bending moment and maximum shear force to the sheet pile wall owing to the complexity of the soil material and the fact that the analytical method fails in considering important soil properties, such as the elastic modulus, in its analyses. This shortcoming has given way to an increase in the use of numerical methods over the last decades. That is, the difference obtained from the output values in both methods can be attributed to the fact that the numerical methods employ a wider range of input parameters in its analyses as compared to the analytical methods.

In order to achieve a proper comparison on both numerical and analytical methods in this research, the limit equilibrium method based on the USA method and the Blum's theory are used in developing a computer aided design program (*GEOWALL*), written in Visual C#.Net, for the analyses. Two commercial software's namely, *PLAXIS* (numerical software programmed using finite element method) and *PROSHEET* (analytical software based on limit equilibrium method) are used as well. Additionally, an excel macro application is developed based on formulas presented in Das (2011) which employs the limit equilibrium method as well and this excel application is also used in the analyses of the sheet pile wall.

Various output data obtained from all these methods are evaluated in detail, showing differences between numerical and analytical approaches. The difference was greatly influenced by the parameters used in the numerical analyses that are not considered in analytical modelling. Also with respect only to the analytical software, there was a little variation in the results obtained between *GEOWALL* and *PROSHEET* but a rather large variation in the results obtained between *GEOWALL* and the *Excel Macros Application* and also between *PROSHEET* and the *Excel Macros Application*. This statement is a result of the difference in lateral earth pressure theories employed by various methods.

This study involves the analyses of both cantilever and anchored sheet pile wall with and without the presence of groundwater and surcharge. In this study, a sensitivity analyses due to different geotechnical parameters used in numerical modelling is carried out in order to know the extent to which some of these soil-wall parameters considered by the numerical method affect the pile wall analyses and, how substantial is the variation in these parameters affecting the output result of the analyses.

RESUMEN

El propósito de este estudio es analizar el comportamiento de los muros de contención de tierras tipo tablestacas de acero mediante los métodos numéricos y analíticos.

En los últimos años, se ha utilizado el método analítico basado en el método de equilibrio límite en el análisis del muro de tablestacas. Sin embargo, este método sobreestima los resultados respecto al máximo momento flector y del máximo esfuerzo cortante que se produce en una tablestaca debido a la complejidad del comportamiento de suelo y el hecho de que el método analítico falla al considerar importantes propiedades del suelo, como por ejemplo su módulo de elasticidad, en sus análisis. Esta deficiencia ha dado paso al aumento en el uso de los métodos numéricos en las últimas décadas. Es decir, la diferencia obtenida a partir de los valores de salida en ambos métodos se puede atribuir al hecho de que los métodos numéricos emplean una gama más amplia de parámetros de entrada durante sus análisis en comparación con los métodos analíticos.

Con el fin de lograr una comparación adecuada entre los métodos numéricos y analíticos, en este estudio se ha empleado el método de equilibrio límite basado en el método de EE.UU. y de la teoría de Blum para el desarrollo del software (*GEOWALL*), escrito en Visual C#.Net para los análisis. También, se han utilizado utilizan dos software comerciales *PLAXIS* (software numérico basando en el método de elementos finitos) y *PROSHEET* (software analítico basado en el método de equilibrio límite). Además, se desarrolla una aplicación con Excel macro en base a las ecuaciones que se presentan en Das (2011) y que emplea el método de equilibrio límite para llevar a cabo el análisis de las tablestacas.

Varios datos de salida obtenidos a partir de todos estos métodos son evaluados en detalle, y muestran diferencias entre los métodos numéricos y analíticos. Estas diferencias en los resultados están influenciado por los parámetros utilizados en el método numérico que no se consideran en el método analítico. También con respecto a sólo al softwares que emplea los métodos analíticos, hay una variación despreciable en los resultados obtenidos entre *GEOWALL* y *PROSHEET* pero más bien una gran variación en los resultados obtenidos entre *GEOWALL* y la aplicación del Excel macros y *PROSHEET* y la aplicación del Excel macros. Estas variaciones son debidas a la diferencia en las teorías de presión lateral del terreno empleado en los distintos softwares.

Este estudio consiste en el análisis de tanto el muro en voladizo como el muro anclado con y sin la presencia de aguas subterráneas y de sobrecarga. En el estudio, se ha llevado a cabo un análisis de sensibilidad de distintos parámetros geotécnicos utilizados en la modelización numérica para conocer la medida en que estos parámetros considerados por el método numérico afectan el comportamiento de la tablestaca y si afectan, hasta qué punto la variación de estos parámetros afecta al resultado final de los análisis.

TABLE OF CONTENTS

ACKNOWLEDGEMENT	i
ABSTRACT	ii
RESUMEN.....	iii
LIST OF FIGURES.....	vi
LIST OF TABLES	ix
CHAPTER 1 INTRODUCTION.....	1
1.1 Background	1
1.2 Research Goals and Objectives.....	2
1.3 Limitations.....	2
1.4 Research Organization.....	2
CHAPTER 2 LITERATURE REVIEW	3
2.1 Introduction.....	3
2.2 Sheet Pile Walls.....	4
2.2.1 Sheet Pile Wall Type.....	5
2.2.2 Applications	6
2.2.3 Sections, Interlocks and Properties of Steel Sheet Piles	7
2.3 Lateral Earth Pressures.....	8
2.3.1 Preamble.....	8
2.3.2 Earth Pressure Theories	10
2.4 Limit Equilibrium Analysis	14
2.4.1 Cantilever Walls.....	14
2.4.2 Anchored or Propped Walls	16
CHAPTER 3 RESEARCH METHODOLOGY	19
3.1 Introduction.....	19
3.2 Cantilever Sheet Pile Wall in Granular Soils	19
3.3 Cantilever Sheet Pile Wall in a Cohesive Soil.....	23
3.4 Cantilever sheet pile wall with backfill being a cohesive soil	25
3.5 Analyses of Anchored Sheet Pile Walls.....	27
3.5.1 Free Earth Support Method	27
3.5.2 Free Earth Support Method for Cohesive Soil	29
3.5.3 Fixed Earth Support Method for Penetrating Granular Soil	30
CHAPTER 4 ANALYTICAL AND NUMERICAL MODELLING	33
4.1 Introduction.....	33
4.2 GEOWALL Software	33
4.2.1 Splash Screen and User Login.....	33

4.2.2	Project Creation	34
4.2.3	Project Modelling	35
4.2.4	Output.....	37
4.3	PROSHEET Software.....	37
4.4	Excel Macros Application	41
4.5	PLAXIS Software.....	41
4.5.1	Preamble.....	41
4.5.2	Modelling Sheet Pile Wall	42
CHAPTER 5 DATA ANALYSIS.....		48
5.1	Introduction.....	48
5.2	Lateral Earth Pressure Theories	48
5.3	Sensitivity Analysis of PLAXIS 2D	51
5.4	Data Analyses and Results.....	58
5.4.1	Cantilever Wall.....	58
5.4.2	Anchored Wall.....	63
CHAPTER 6 CONCLUSIONS AND RECOMMENDATIONS.....		67
6.1	Conclusions	67
6.2	Recommendations for Future Study.....	68
REFERENCES		69
ANNEX A BENDING MOMENT AND SHEAR FORCE DISTRIBUTION CURVES.....		71
	Cantilever Sheet Pile Wall	71
	Anchored Sheet Pile Wall	75
ANNEX B GEOWALL ALGORITHM		79

LIST OF FIGURES

Figure 2.1: Classification of earth-retaining structure (Overview of Earth Retention System: 1970-1990, 1990).....	3
Figure 2.2: Retaining wall types (Adapted after - (EN 1997-1, 2004)).....	4
Figure 2.3: Cantilever and Anchored Sheet Pile Wall (Design and Use of Sheet Pile Walls in Stream Restoration and Stabilization Projects, 2007).....	5
Figure 2.4: Pressure distribution on a cantilever wall (Murthy, 2002).....	6
Figure 2.5: Anchored sheet pile wall.	6
Figure 2.6: Section profiles of steel sheet piles (ArcelorMittal, 2008).....	7
Figure 2.7: Conditions in the case of active earth pressure (Venkatramaiah, 2006).....	8
Figure 2.8: Conditions in the case of passive earth resistance (Venkatramaiah, 2006).....	8
Figure 2.9: Relation between lateral earth pressure and movement of wall (Lambe, et al., 1969).....	9
Figure 2.10: Mohr's circle. In this case, the failure criterion of Mohr Coulomb has been reached.	9
Figure 2.11: Mohr-Coulomb failure criterion. The black circle represents an initial stress state where $\sigma_v > \sigma_h$. A cohesion c has been considered.....	10
Figure 2.12: Coulomb wedge analysis.....	12
Figure 2.13: Logarithmic spiral surface (Das, 2010).....	13
Figure 2.14: Active and passive pressure coefficients for vertical wall and horizontal backfill-based on log spiral failure surfaces [Caquot and Kerisel, 1948].....	13
Figure 2.15: Schematic version of the net earth pressure in a cantilever wall.	14
Figure 2.16: Full method of cantilever sheet pile Wall (Craig, 2004).	15
Figure 2.17: Simplified method of the cantilever sheet pile wall (Craig, 2004).....	15
Figure 2.18: Illustration for analysing cantilever sheet pile walls based on the simplified method.	16
Figure 2.19: Influences and resistance according to the USA Method (Škrabl, 2006)..	16
Figure 2.20: Schematic version of the net earth pressure in an anchored wall.....	17
Figure 2.21: Free earth support method for anchored sheet pile wall (Smith, et al., 1998)	17
Figure 2.22: Fixed earth support method for anchored sheet pile walls (Smith, et al., 1998)	18
Figure 3.1: Cantilever sheet pile wall in sand (Das, 2011)	19
Figure 3.2: Cantilever sheet pile wall in sand: (a) variation of net pressure diagram without surcharge; (b) variation of moment with depth (c) variation of net pressure diagram with depth (surcharge included) (Das, 2011).....	20
Figure 3.3: Cantilever sheet pile penetrating cohesive soil (Das, 2011)	23
Figure 3.4: Depth of embedment of a cantilever wall in a cohesive soil with a cohesive backfill soil (Murthy, 2002).	25
Figure 3.5: Nature of variation of deflection and moment for anchored sheet piles: (a) free earth support method and (b) fixed earth support method (Das, 2011)	27
Figure 3.6: Anchored sheet pile wall penetrating drained soil (Das, 2011).....	28
Figure 3.7: Free earth anchored sheet pile wall penetrating undrained cohesive soil (Das, 2011).....	29
Figure 3.8: Fixed earth support method penetrating drained soil (Das, 2011)	30
Figure 3.9: Analysing Fixed earth support method	31
Figure 4.1: Splash screen.....	33
Figure 4.2: Flowchart showing user login functionality.....	34
Figure 4.3: Flowchart showing project creation.....	34
Figure 4.4: Project creation window	35

Figure 4.5: Main window showing a completed generated project.....	36
Figure 4.6: Flowchart of software simulation	36
Figure 4.7: Maximum Bending Moment of the analyses	37
Figure 4.8: Units, configuration and Project information	38
Figure 4.9: Design data	38
Figure 4.10: Soil layers.....	39
Figure 4.11: Sheet pile section.....	39
Figure 4.12: Results: Pile check values.....	40
Figure 4.13: Results: All values.....	40
Figure 4.14: Result: Diagrams.....	41
Figure 4.15: Flowchart for general analysis procedure in PLAXIS 2D.....	42
Figure 4.16: General setting window.....	43
Figure 4.17: Typical mesh dimensions for a sheet pile wall retaining an isotropic homogenous soil (Azizi, 1999).....	43
Figure 4.18: Geometry of the model.....	45
Figure 4.19: Finite element mesh for the model.....	45
Figure 4.20: Initial pore pressure diagram.....	45
Figure 4.21: Window for entering K_0	46
Figure 4.22: Initial effective stresses	46
Figure 4.23: Calculation module	46
Figure 4.24: Stress diagram of an analysis.....	47
Figure 4.25: Bending Moment.....	47
Figure 4.26: Displacement.....	47
Figure 5.1: Variation of K_p value with δ and ϕ using the Coulomb theory.....	49
Figure 5.2: Variation of K_p value with δ and ϕ using the log spiral theory.....	50
Figure 5.3: Geometrical and geotechnical parameters for sensitivity analyses	52
Figure 5.4: Correlation between the maximum shear force, the maximum bending moment and the wall deflection with different interface values.....	54
Figure 5.5: Relationship between the maximum shear force, the maximum bending moment and the wall deflection with the different Poisson's ratio values.....	54
Figure 5.6: Correlation between the maximum shear force, the maximum bending moment and the wall deflection with varying wall normal stiffness values.....	55
Figure 5.7: Relationship between the maximum shear force, the maximum bending moment and the wall deflection with varying soil elastic modulus values.....	55
Figure 5.8: Correlation between the maximum shear force, the maximum bending moment and the wall deflection with varying wall bending stiffness values.....	56
Figure 5.9: Tornado plot for maximum shear force parameter.....	57
Figure 5.10: Tornado plot for maximum bending moment parameter.....	57
Figure 5.11: Tornado plot for displacement parameter	58
Figure 5.12: Geometrical and geotechnical parameters for cantilever analyses	59
Figure 5.13: Histogram of maximum bending moment obtained from different software analyses for the cantilever sheet pile wall	61
Figure 5.14: Histogram of maximum shear force obtained from different software analyses for the cantilever sheet pile wall	62
Figure 5.15: Histogram of maximum wall deflection obtained from different software analyses for the cantilevered sheet pile wall.....	63
Figure 5.16: Geometrical and geotechnical parameters for anchored analyses.....	63

Figure 5.17: Histogram of maximum bending force obtained from different software analyses for the anchored sheet pile wall.....	65
Figure 5.18: Histogram of maximum shear force obtained from different software analyses for the anchored sheet pile wall.....	66
Figure 5.19: Histogram of maximum wall deflection obtained from different software analyses for the anchored sheet pile wall.....	66

LIST OF TABLES

Table 2.1: Steel sheet pile sections and properties (ArcelorMittal, 2008)	7
Table 2.2: Contraflexure – Wall height relationship based on soil frictional angle.....	17
Table 4.1: Ratio of δ/ϕ (Design of Sheet Pile Walls, 1994)	44
Table 4.2: Values of δ for various interface (Design of Sheet Pile Walls, 1994).....	44
Table 5.1: Coulombs K_p values with varying ϕ and δ	48
Table 5.2: Log spiral K_p values with varying ϕ and δ	50
Table 5.3: Difference in K_p Values between Coulomb and log spiral theories.....	51
Table 5.4: Input Parameters for Sensitivity Analysis	52
Table 5.5: Output values (maximum displacement, maximum shear force and maximum bending moment) for different Poisson Ratio and E_{ref} values	52
Table 5.6: Output values (maximum displacement, maximum shear force and maximum bending moment) for different Interface, EI and EA values.....	53
Table 5.7: Percentage difference in extreme values	56
Table 5.8: Material property of the sheet pile wall.....	58
Table 5.9: Constant properties used in PLAXIS 2D throughout the analyses	58
Table 5.10: Material properties of the soil type studied for the cantilever wall analyses.	59
Table 5.11: Output result obtained from cantilever wall analyses using various software's.....	60
Table 5.12: Percentage difference in cantilever sheet pile wall height for the various software.....	60
Table 5.13: Material properties of the soil studied for the anchored wall analyses	64
Table 5.14: Output result obtained from anchored wall analyses using the various software's.....	64
Table 5.15: Percentage difference in anchored sheet pile wall height for the various software.....	64

CHAPTER 1 INTRODUCTION

This chapter presents a background to the study, which is the analyses of earth retaining structures, by comparing the numerical and analytical methods used in designing steel sheet pile walls. The research goals and objectives are enumerated in this chapter. Moreover, the limitations and the organization of the research are presented.

1.1 Background

In geotechnical applications, earth-retaining structures are used for maintaining elevation differences of ground surface. In highly populated areas, excavating self-supporting slopes is mostly not possible because of lack of empty space around the construction site. In such circumstances, earth-retaining structures, which are vertical or near vertical facilities that maintain elevation difference of ground surface, becomes a priority (Coduto, 2001). The retaining wall can be classified according to system rigidity into either rigid or flexible walls. A wall is considered to be rigid if it moves as a unit in rigid body and does not experience significant bending deformations. Most of gravity walls, such as masonry wall, simple concrete wall, or reinforced concrete wall can be considered as rigid walls. However, flexible walls, such as sheet pile walls, are the retaining walls that undergo bending deformations in addition to rigid body motion. Steel sheet pile wall is the most common example of the flexible walls because it can tolerate relatively large deformations. Due to the growing need to use scarce land efficiently, along with the improvement and development of specialized machinery with a greater efficiency, the use of flexible walls as a soil retaining structure has significantly increased over the last decade.

Sheet piling materials may be of timber, reinforced concrete, or steel. Steel sheet piling is the most common type used for walls because of several advantages over other materials such as; it is resistant to high driving stress developed in hard or rocky material, it is relatively lightweight, it may be reused several times, it has a long service life either above or below water, it is easy to increase the pile length by either welding or bolting; etc. (Bowles, 1997).

Sheet pile walls are one of the oldest earth retention systems used in civil engineering projects. They consist of continuously interlocked pile segments embedded in soils to resist horizontal pressures. They can be defined as flexible structures that depends upon the passive resistance of the soil within the confinement of the wall with the aim of achieving stability (Smith, et al., 1998). Sheet pile walls are used for various purposes; such as large and waterfront structures, cofferdams, cut-off walls under dams, erosion protection, stabilizing ground slopes, excavation support system, and floodwalls. The construction of sheet pile walls consist of either driving the sheet pile into the ground and then backfilling, or they could first be driven into the ground and the soil behind the pile dredged. In either case, the soil used for backfill behind the sheet pile wall is usually granular and the soil below the dredge line may range between sandy and clayey (Das, 2011). The sheet pile walls can be either cantilever or anchored. The selection of the wall type is based on the function of the wall, the characteristics of the foundation soils, and the proximity of the wall to existing structures. While the cantilever walls are usually used for wall heights less than 6m, anchored walls are required for higher walls or when the lateral wall deformations are needed to be restricted. Typically the anchors are installed when the wall height exceeds 6m or the wall supports heavy loads from a structure.

Design methods for sheet pile analyses have been consistently reviewed and improved, especially over the last 50 years. Despite the development of numerical methods in the last decades applied to geotechnical engineering, the classical analytical methods are still fundamental tools for soil stress analysis and are therefore broadly used with the

limit equilibrium method being one of the most powerful tools used in analysing sheet pile walls. As a result of the complexity and time-consuming nature in carrying out these analyses, computer becomes a useful instrument in undertaking the study.

1.2 Research Goals and Objectives

This research studies the behaviour of both cantilever and anchored sheet pile walls as an earth retaining structure by implementing the limit equilibrium method. A computer program (*GEOWALL*) written in Visual C#.Net is prepared for the limit equilibrium analysis method.

The following objectives are set forth in order to reach the aim of the study:

- To understand the process involved in the stability of sheet pile walls.
- To model the process using limit equilibrium method and apply this model in creating a Computer Aided Design (CAD) software, hereafter, *GEOWALL*.
- To build the application of the software for both cantilever and anchored sheet pile walls considering granular to cohesive soils.
- To analyse and compare the results of *GEOWALL* with commercial programs such as *PLAXIS* and *PROSHEET* and an *Excel Macros Application* developed based on the theory presented by Das (2011).

1.3 Limitations

The project is limited to the following:

- The distribution of both the backfill soil and the dredge soil is homogenous and without stratification.
- The groundwater is located above the dredge level.
- The anchorage is installed above the groundwater level.
- The considered surcharge distribution is continuous and uniform in nature.
- Braced wall is omitted.
- Only steel sheet pile structure is considered.

1.4 Research Organization

The research is organized into six chapters. Chapter 1 gives an introduction into the research work. It encompasses the research background, its goals and objectives and the limitation to the research work. Chapter 2 reviews previous literatures published by experts and authors in the field of geotechnics with the main focus on the sheet piling. Chapter 3 describes the methodology applied in undertaking the study. Chapter 4 describes the software developed (*GEOWALL*); how it was developed and how it is used in simulating practical sheet pile wall analysis. *PLAXIS* and *PROSHEET* software is also reviewed in the chapter, as a tool for solving sheet pile wall problems. Also, an *Excel Macros Application* designed based on the sheet pile theory presented in Das (2010) and employing the Rankine theory for lateral earth pressure is presented in Chapter 4. In Chapter 5, field data is analysed using *GEOWALL*, *PROSHEET*, *Excel Macros Application* and *PLAXIS* and the results are discussed while Chapter 6 concludes the research by giving recommendations for future studies. A bibliography containing references from all articles and books is presented at the end, and this is followed by an Annex containing relevant information for the project that does not appear in the previous chapters.

CHAPTER 2 LITERATURE REVIEW

In this chapter, the description of sheet pile walls, its properties and applications are presented. The various types of steel sheet pile walls are also explained together with the methods used in analysing these walls. Also, definitions of common geotechnical terms such as brief explanation of earth pressures are also presented.

2.1 Introduction

In geotechnical applications, earth-retaining structures are used for maintaining elevation differences of ground surface. In highly populated areas, excavating self-supporting slopes is not possible, mostly because of lack of empty space around the construction site. It is inevitable to use retaining walls in such cases, for vertical excavations.

Retaining structures are commonly divided into two groups:

- Rigid retaining structures, where the stability is provided by the use of a large volume of mass. Only rigid body movements occur.
- Flexible retaining structure, where other properties of the materials, such as stiffness, strength and wall thickness are exploited in order to provide the stability. Bending and rigid body movements are found.

O'Rourke & Jones (1990) classified earth-retaining structures into two broad categories: externally stabilized systems and internally stabilized systems as shown in Figure 2.1. Some hybrid methods combine features from both systems.

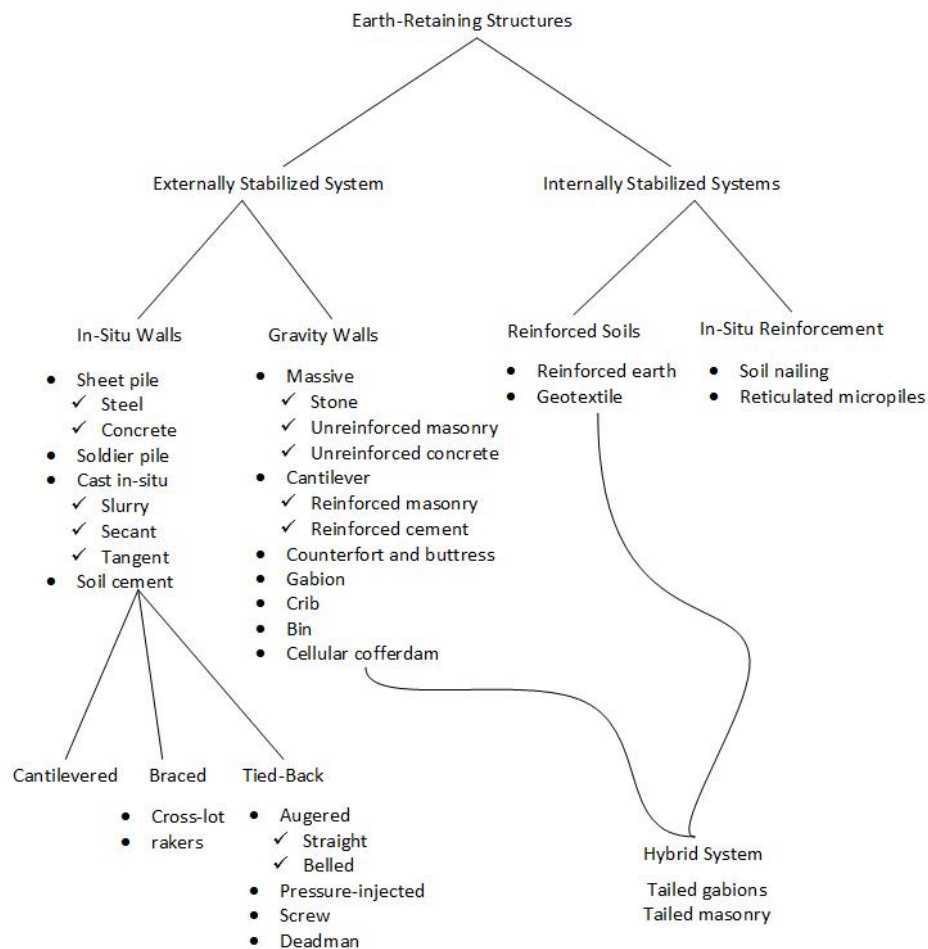


Figure 2.1: Classification of earth-retaining structure (Overview of Earth Retention System: 1970-1990, 1990)

Eurocode 7 (EN 1997-1, 2004) divides retaining structures into 3 categories; gravity walls, embedded walls and composite retaining structures as shown schematically in Figure 2.2. The definition of embedded retaining wall given in Eurocode 7 (EN 1997-1, 2004) is;

“Relatively thin wall of steel, reinforced concrete or timber, supported by anchorages, struts and/or passive earth pressure. The bending capacity of such wall plays a significant role in the support of the retained material while the role of the weight of the wall is insignificant. Example of such walls include cantilever sheet pile wall, anchored or strutted steel or concrete sheet pile wall and diaphragm wall.”

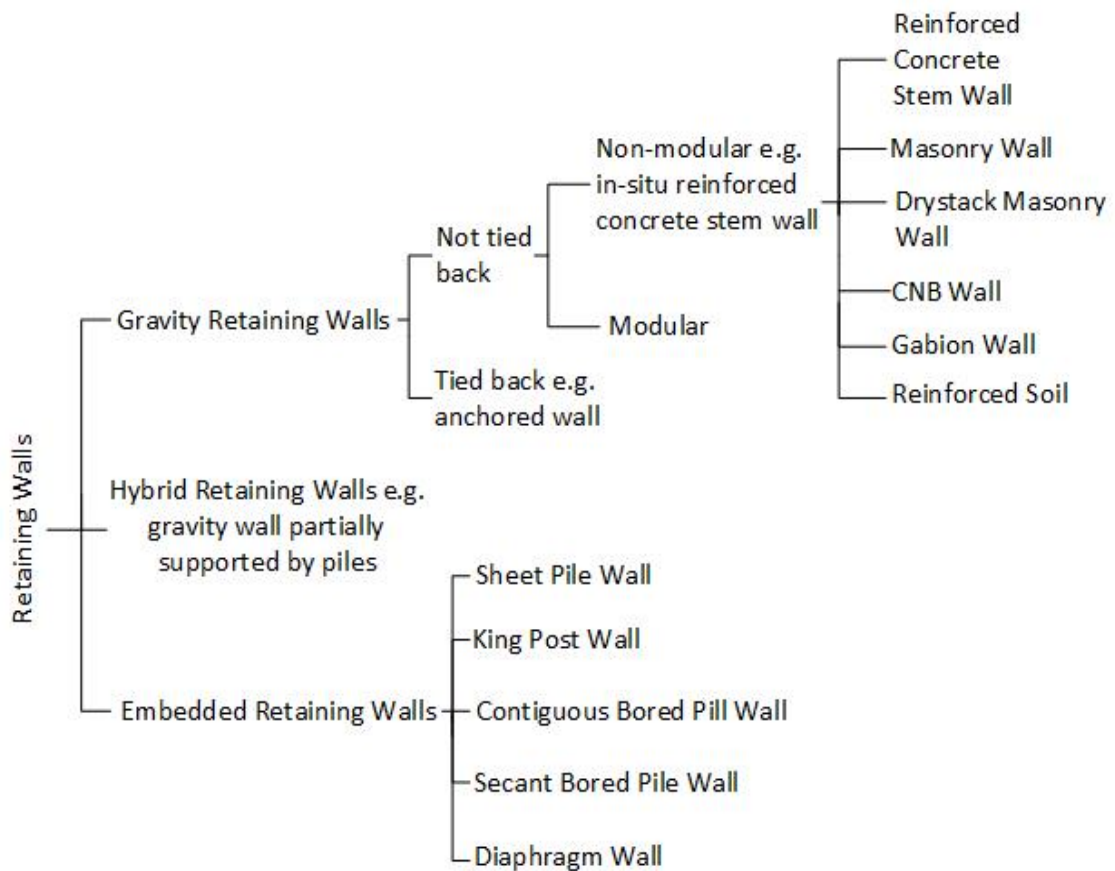


Figure 2.2: Retaining wall types (Adapted after - (EN 1997-1, 2004))

2.2 Sheet Pile Walls

Sheet pile walls consist of driven, vibrated or pushed interlocking pile segments embedded in soils to resist horizontal pressures. They are classified as a flexible retaining system because the stability of these walls is provided through an embedment of the wall on the ground so that it can be subjected to, and tolerate relatively large shear stresses and bending moments. These walls should be designed in order to resist maximum bending moment (Škrabl, 2006). Sheet pile walls are widely used in excavation support systems, slope stabilization, floodwalls and waterfront structures. One of the main benefit is the minimization of used material, in contrast to the needs of rigid retaining structures.

Sheet pile walls are not only able to resist earth pressures and prevent the water inlet, but also to receive vertical loads transmitted by other structural elements. Moreover, sheet pile walls are an efficient solution to limit ground movements associated with the excavation. Thus, there are four main functions that can be carried out by a sheet pile wall (Jiménez Salsa, et al., 1980):

- i. Resist the thrust generated by the excavation.
- ii. Limit the movements in the back of the wall in the unexcavated zone.
- iii. Prevention from water inlet.
- iv. Support vertical loads.

2.2.1 Sheet Pile Wall Type

Sheet pile walls may be cantilever or anchored walls as shown in Figure 2.3. Cantilever walls derive support from adequate embedment below the stream channel or dredge line and are limited to wall heights of about 6m (Craig, 2004). An anchored wall is typically required when the wall height exceeds the one suitable for a cantilever wall. Anchored sheet pile wall derives support from embedment in the soil and the anchor force(s) applied to the piling wall.

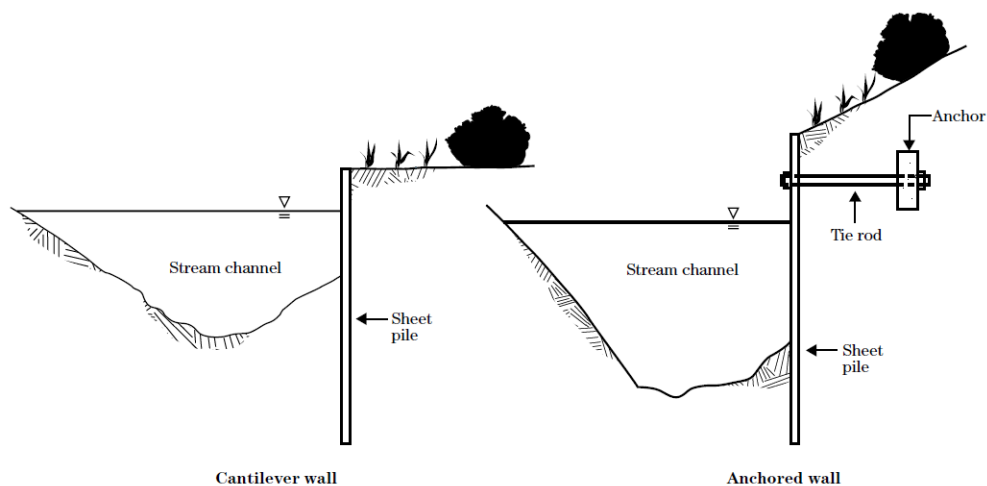


Figure 2.3: Cantilever and Anchored Sheet Pile Wall (*Design and Use of Sheet Pile Walls in Stream Restoration and Stabilization Projects, 2007*)

Cantilever Sheet Pile Wall

Cantilever sheet pile wall is used when the backfill height is 6m or less. These structures can be used either as a permanent or a temporary support system for geotechnical purposes although they are mostly used in the latter situation with the stability of the wall due to the passive pressure that acts on it (Craig, 2004). The mode of failure is by rotation about a point O' near the lower end of the wall as shown in Figure 2.4. Consequently, passive resistance acts in front of the wall above O' and behind the wall below O' as shown in Figure 2.4, thus providing a fixing moment.

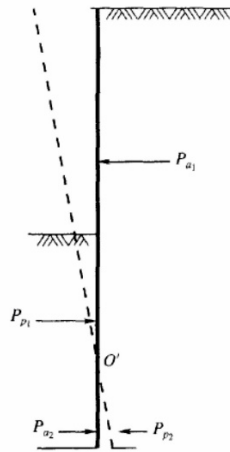


Figure 2.4: Pressure distribution on a cantilever wall (Murthy, 2002)

Anchored Sheet Pile Wall

When the backfill height is greater than 6m, it is economical to use sheet pile walls anchored near the top. This results in a less depth penetration, a lower magnitude of bending moment and consequently a smaller lateral wall deflection of the sheet pile wall. Anchored walls derive stability from the passive resistance acting on the wall and the anchor tie rod installed on the wall, as illustrated in Figure 2.5. These type of walls are broadly used in the support of deep excavations and in waterfront construction.

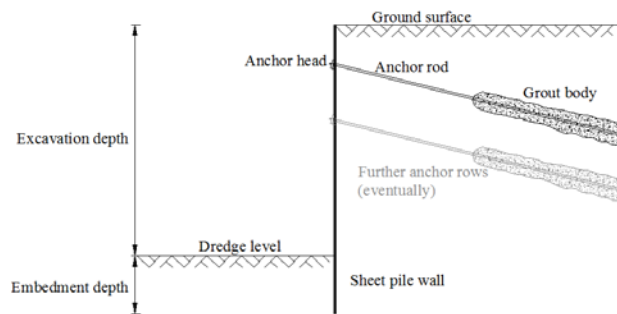


Figure 2.5: Anchored sheet pile wall.

2.2.2 Applications

Sheet piles have been used as an essential element in the construction of various engineering projects such as ports, pile foundations, hydraulic landfills, and containment of contaminated areas and in various types of excavations. Some of the most common uses are listed below.

- Marine and fluvial environments.
 - Bulkheads
 - Seawalls
 - Tide Walls
 - Wave Breaks
 - Erosion Control
 - Retaining Walls
- Flood protection
 - Chemical Containment
 - Seepage Barriers
 - Groundwater Cut Off

- Foundation Protection
- Cut Off and Containment
 - Flood Walls
 - Dam Stabilization
 - Piping Protection
 - Seepage Barrier
- Water Control
 - Baffle walls
 - Weirs
 - Retention Ponds
 - Water Diversion
 - Acid Mine Drainage

2.2.3 Sections, Interlocks and Properties of Steel Sheet Piles

Various steel manufacturers fabricate various sections and interlocks of steel piles based on the design necessity, however, the most common sections normally produced and used in the geotechnical industry are the Z-plates, the U-plates, the straight web piles and the H piles. The names of the sections are based principally on its appearance (See Figure 2.6).

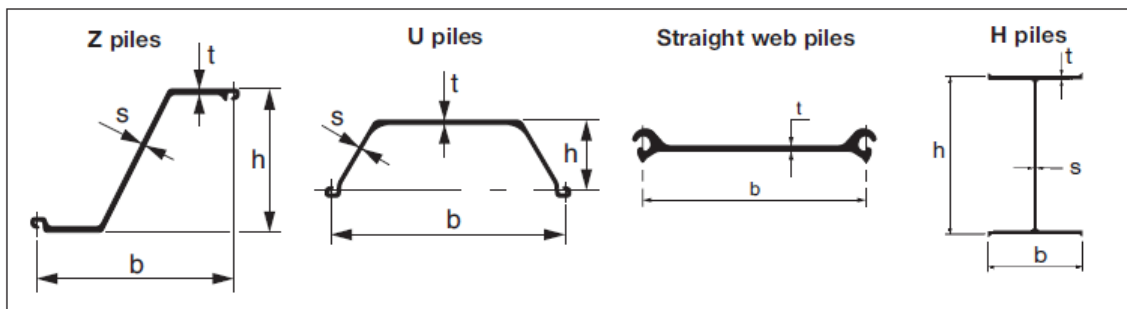


Figure 2.6: Section profiles of steel sheet piles (ArcelorMittal, 2008)

The interlocks of the sheet pile join the individual piles together so as to form a complete wall. This increases the maximum permissible bending moment of the wall. It is important to carefully inspect that the interlocks are firm and secure in order to avoid declutching.

Some examples of steel sheet pile sections with their properties are shown in Table 2.1.

Table 2.1: Steel sheet pile sections and properties (ArcelorMittal, 2008)

Section	Width	Height	Thickness		Sectional Area	Mass		Moment of inertia	Elastic section modulus	Static moment	Plastic section modulus
	b (mm)	h (mm)	t (mm)	s (mm)		cm ² /m	kg/m of single pile				
Z Profile Piles											
AZ 12	670	302	8.5	8.5	126	66.1	99	18140	1200	705	1409
AZ 14	670	304	10.5	10.5	149	78.3	117	21300	1400	825	1651
AZ 19	630	381	10.5	10.5	164	81.0	129	36980	1940	1140	2275
AZ 25	630	426	12.0	11.2	185	91.5	145	52250	2455	1435	2873
AZ 46	580	481	18.0	14.0	291	132.6	229	110450	4595	2650	5295
AZ 50	580	483	20.0	16.0	322	146.7	253	121060	5015	2910	5816
AZ 12-770	770	344	8.5	8.5	120	72.6	94	21430	1245	740	1480
AZ 17-700	700	420	8.5	8.5	133	73.1	104	36230	1730	1015	2027
U Profile Piles											
AU 14	750	408	10.0	8.3	132	77.9	104	28680	1405	820	1663
AU 16	750	411	11.5	9.3	147	86.3	115	32850	1600	935	1891
AU 17	750	412	12.0	9.7	151	89.0	119	34270	1665	975	1968

PU 12	600	360	9.8	9.0	140	66.1	110	21600	1200	715	1457
PU 18	600	430	11.2	9.0	163	76.9	128	38650	1800	1055	2134
PU 22	600	450	11.01	9.5	183	86.1	144	49460	2200	1275	2580
GU 7-600	600	309	7.5	6.4	100	47.0	78	11350	735	435	890
GU 8-600	600	309	8.5	7.1	110	51.8	86	12690	820	485	995
H Piles											
HZ 775A	775.0	460.0	17.0	12.5	20	257.9	202.4	280070	7230	-	-
HZ 775B	779.0	460.0	19.0	12.5	20	276.3	216.9	307930	7905	-	-
HZ 775C	783.0	461.5	21.0	14.0	20	306.8	240.8	342680	8755	-	-
HZ 975A	975.0	460.0	17.0	14.0	20	297.0	233.1	476680	9780	-	-
HZ 975B	979.0	460.0	19.0	14.0	20	315.4	247.6	520700	10635	-	-
HZ 975C	983.0	462.0	21.0	16.0	20	353.9	277.8	582170	11845	-	-
Straight Web Piles											
Section	Normal width	Web thickness	Deviation angle	Section of single pile	Mass per m of a single pile	Mass per m ² wall	Moment of inertia	Section modulus	Coating area		
	b (mm)	t (mm)	δ (°)	cm ²	kg/m	kg/m ²	cm ⁴	cm ³	m ² /m		
AS 500-9.5	500	9.5	4.5	81.3	63.8	128	168	46	0.58		
AS 500-11.0	500	11.0	4.5	90.0	70.6	141	186	49	0.58		
AS 500-12.0	500	12.0	4.5	94.6	74.3	149	196	51	0.58		
AS 500-12.5	500	12.5	4.5	97.2	76.3	153	201	51	0.58		

2.3 Lateral Earth Pressures

2.3.1 Preamble

Lateral earth pressure is the force exerted by the soil mass upon an earth-retaining structure. In order to define the earth pressure at failure conditions, the Rankine states are used. Supposing a horizontal soil surface, with no external loads, the effective horizontal and vertical stress increase linearly with depth, and its relation is known as at-rest coefficient (K_o):

$$K_o = \frac{\sigma'_h}{\sigma'_v} \quad \text{Eq. 2.1}$$

When a sheet pile wall is introduced and an excavation is done, the earth pressure generated can be produced in two ways; the active earth pressure (K_a) of the soil and the passive earth resistance (K_p). The limiting values of both the active earth pressure and passive earth resistance for a given soil depend upon the amount of movement of the structure (Venkatramaiah, 2006). In the case of active pressure, the structure tends to move away from the soil, causing strains in the soil mass, which in turn, mobilize shearing stresses; these stresses help to support the soil mass and thus tend to reduce the pressure exerted by the soil against the structure as indicated in Figure 2.7.

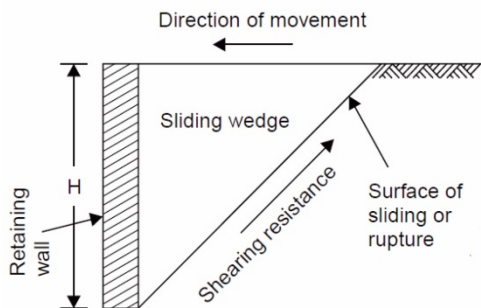


Figure 2.7: Conditions in the case of active earth pressure (Venkatramaiah, 2006)

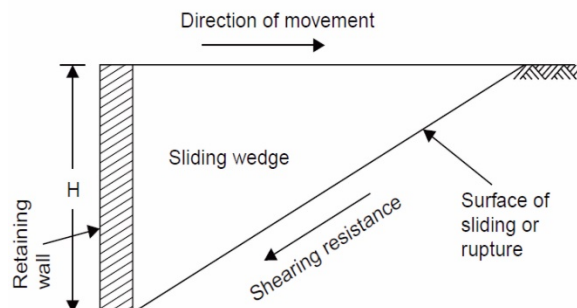


Figure 2.8: Conditions in the case of passive earth resistance (Venkatramaiah, 2006)

In the case of passive earth resistance, internal shearing stresses also develop, but act in the opposite direction to those in the active case and must be overcome by the movement of the structure. This difference in direction of internal stresses accounts for

the difference in magnitude between the active earth pressure and the passive earth resistance. The conditions obtained in the passive case are indicated in Figure 2.8.

Active pressure are accompanied by movements directed away from the soil, and passive resistance are accompanied by movements towards the soil. Logically, therefore, there must be an intermediate situation between the two when the retaining structure is perfectly stationary and does not move in either direction. The pressure which develops in this condition is called 'earth pressure at rest'. Its value is a little larger than the limiting value of active pressure, but is considerably less than the maximum passive resistance (See Figure 2.9).

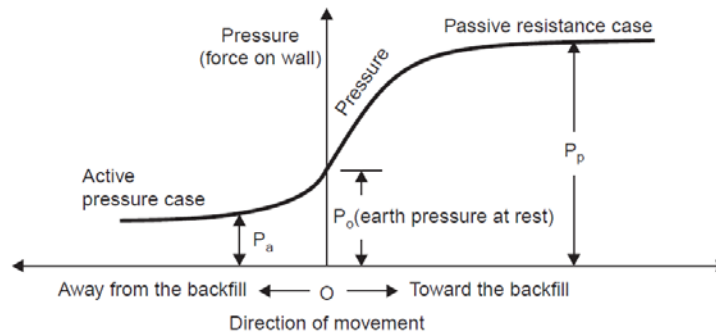


Figure 2.9: Relation between lateral earth pressure and movement of wall (Lambe, et al., 1969)

From Figure 2.9, it can be observed that very little movement is required to mobilize the active pressure; however, relatively much larger movement may be required to mobilize full passive resistance.

The three-dimensional stress state in one point may be represented by Mohr's circle, a two-dimensional graphical representation (see Figure 2.10). The stress state in one point may be broken in two components, the normal stress (ordinate σ_n), and the shear stress (abscissa τ). Principal stresses are σ_I (major) and σ_{III} (minor). The third principal stress σ_{II} , not represented, is assumed to be equal to σ_{III} . The circumference of the circle is the range of points that represent the state of stress on individual planes at all their orientations. The major and minor normal stresses are given when the shear stress is zero. The failure occurs when the linear envelope of Mohr Coulomb is surpassed Eq. 2.2. As seen in Eq. 2.2 and Figure 2.10, the effect of cohesion is always favourable.

$$\tau = c + \sigma \cdot \tan \varphi \quad \text{Eq. 2.2}$$

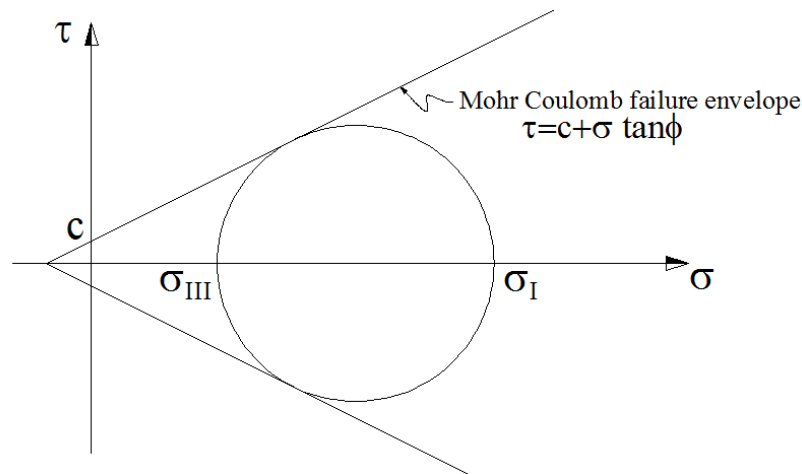


Figure 2.10: Mohr's circle. In this case, the failure criterion of Mohr Coulomb has been reached.

2.3.2 Earth Pressure Theories

The magnitude of the lateral earth pressure is evaluated by the application of one of the so-called 'earth pressure theories'. The theory applied to rigid structures can be applied to sheet pile walls as well. The back of the wall is, in every case, vertical. However, in sheet pile walls the passive pressure is more significant. Over the years, most theories have been proposed by several researchers but, till date the most prominent theories are those proposed by Coulomb and Rankine in 1776 and 1857 respectively. These theories were originally designed to apply to cohesionless soil backfill, although later, researchers gave necessary modification to take into account cohesion, surcharge, submergence etc.

Rankine's Theory

The main hypothesis of this theory is the condition of the soil to be in a Rankine limit state. A Rankine limit state is a stress state of plastic equilibrium, where failure surfaces are found in only two directions. The soil has reached the Mohr-Coulomb failure criterion along these surfaces (Eq. 2.2). The Rankine Theory is based on the assumption that the soil introduces no changes in the shearing stresses at the surface of contact between the wall and the soil (United State Steel, 1984).

As said the failure surfaces in two directions define the size of the wedge produced. In the passive case, the failure involves much more volume of mass than in the active case as seen in Figure 2.7 and Figure 2.8.

Under this criterion, the failure occurs with only two soil friction angles, for respectively active and passive limit state, as shown in Figure 2.11. These angles determine the failure wedge formed, that will be different, as said, for the active and passive limit state. Notice that in the active state, the minor stress σ_{III} corresponds to the horizontal stress σ_h and the major stress σ_I corresponds to the vertical stress σ_v . Accordingly, in the passive state, $\sigma_I = \sigma_h$ and $\sigma_{III} = \sigma_v$. The failure surface in Figure 2.11 is found by drawing a line from the pole to the point where the failure envelope is reached.

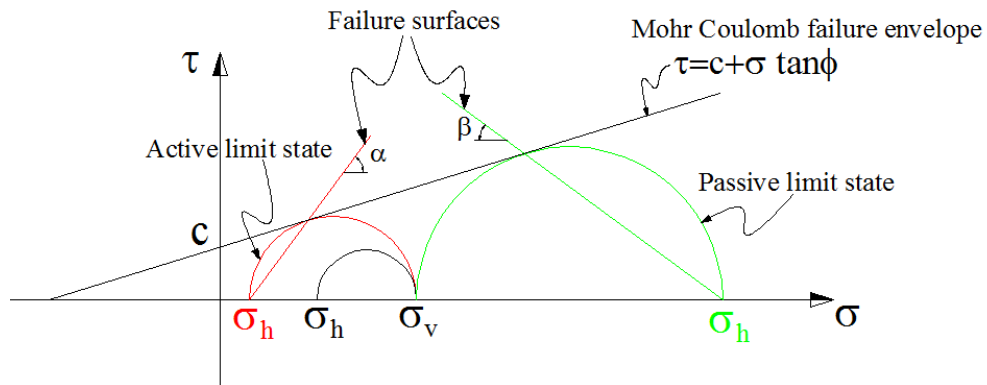


Figure 2.11: Mohr-Coulomb failure criterion. The black circle represents an initial stress state where $\sigma_v > \sigma_h$. A cohesion c has been considered

The failure state can be reached therefore from either active or passive state. The effective stress for each point of the soil, considering a horizontal ground surface, is:

$$\sigma'_H = \sigma'_v K_a - 2c\sqrt{K_a} \quad (\text{Active case}) \quad \text{Eq. 2.3}$$

$$\sigma'_H = \sigma'_v K_p + 2c\sqrt{K_p} \quad (\text{Passive case}) \quad \text{Eq. 2.4}$$

After a geometrical procedure, it can be proved that the angle of the failure surface, in Figure 2.11, depends only on the surface friction angle (ϕ), being $\alpha = \frac{\pi}{4} - \frac{\phi}{2}$ and $\beta = \frac{\pi}{4} +$

$\frac{\varphi}{2}$ for the active and passive limit state respectively. Coefficients K_a and K_p also depend on the soil friction angle (φ). Under conditions of homogenous soil and horizontal surface, their values are:

$$K_a = \tan^2 \left(\frac{\pi}{4} - \frac{\varphi}{2} \right) \quad \text{Eq. 2.5}$$

$$K_p = \tan^2 \left(\frac{\pi}{4} + \frac{\varphi}{2} \right) \quad \text{Eq. 2.6}$$

The Rankine theory is suitable for the active state, and it is known to be slightly conservative. It is nonetheless, inadequate for passive state. Its greatest benefit is the simplification achieved, especially for simple case.

Coulomb's Theory

An inherent assumption of the Rankine Theory is that the presence of the wall does not affect the shearing stresses at the surface of wall contact. However, since the friction between the retaining wall and the soil has a significant effect on the vertical shear stresses in the soil, the lateral stresses on the wall are actually different than those assumed by the Rankine Theory. Most of this error can be avoided by using the Coulomb Theory, which considers the changes in tangential stress along the contact surface due to wall friction (United State Steel, 1984).

As the wall yields, the failure wedge tends to move downward for the active case (see Figure 2.12). For the passive case, where the wall is forced against the soil, the wedge slides upward along the failure plane. These differential movements involve vertical displacements between the wall and backfill and create tangential stresses on the back of the wall due to soil friction and adhesion. The resulting force on the wall is, therefore, inclined at an angle normal to the wall. This angle is known as the angle of wall friction, δ . For the active case, when the active wedge slides downward relative to the wall, δ is taken as positive. For the passive case, when the passive wedge slides upward relative to the wall, δ is taken as negative (United State Steel, 1984). If the angle of wall friction is known, the following analytical expressions for K_a and K_p in the horizontal direction for a vertical wall are given in Eq. 2.7 and Eq. 2.8:

$$K_a = \frac{\cos^2 \varphi}{\cos \delta \left[1 + \sqrt{\frac{\sin(\varphi + \delta) \sin(\varphi - \beta)}{\cos \delta \cos \beta}} \right]^2} \quad \text{Eq. 2.7}$$

$$K_p = \frac{\cos^2 \varphi}{\cos \delta \left[1 - \sqrt{\frac{\sin(\varphi + \delta) \sin(\varphi + \beta)}{\cos \delta \cos \beta}} \right]^2} \quad \text{Eq. 2.8}$$

where:

φ : angle of internal friction of the soil.

β : angle of the backfill with respect to horizontal.

δ : angle of wall friction.

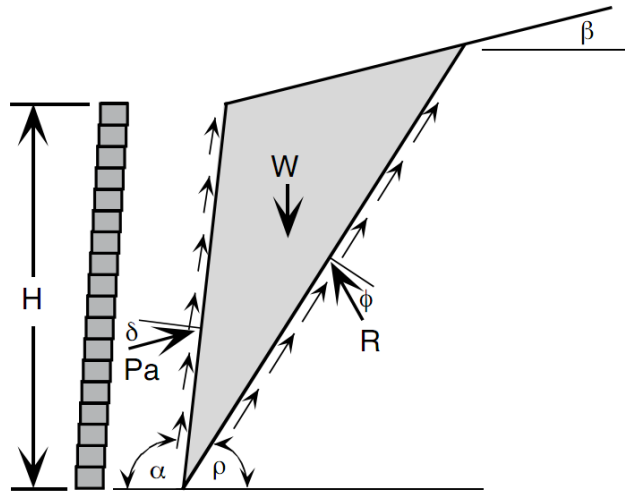


Figure 2.12: Coulomb wedge analysis.

$$\sigma'_H = \sigma'_v K_a - 2c\sqrt{K_a} \cos \delta_a \quad (\text{Active case}) \quad \text{Eq. 2.9}$$

$$\sigma'_H = \sigma'_v K_p + 2c\sqrt{K_p} \cos \delta_p \quad (\text{Passive case}) \quad \text{Eq. 2.10}$$

From Eq. 2.9 and Eq. 2.10, it is seen that the angle of wall friction also affects the cohesive nature of a soil. Notice that the interaction ground-structure promotes stability. The thrust magnitude is calculated through the equilibrium of forces involved at failure, and its direction depends directly on the adopted angle δ . The application point is assumed to be the centre of mass.

Comparison of Coulomb's Theory with Rankine's Theory

- The Coulomb theory considers a retaining wall and the backfill as a system; it takes into account the friction between the wall and the backfill, while Rankine theory does not.
- The backfill surface may be plane or curved in the Coulomb's theory, but the Rankine's theory allows only for a plane surface.
- In the Coulomb's theory, the total earth thrust is first obtained and its position and direction of the earth pressure are assumed to be known; linear variation of pressure with depth is tacitly assumed and the direction is automatically obtained from the concept of wall friction. In the Rankine's theory, plastic equilibrium inside a semi-infinite soil mass is considered, pressures evaluated, a retaining wall is imagined to be interposed later, and the location and magnitude of the total earth thrust are established mathematically.
- The Coulomb's theory is more versatile than the Rankine's considering that it can take into account any shape of the backfill surface, break in the wall face or in the surface of the fill, effect of stratification of the backfill, effect of various kind of surcharge on the earth pressure, and the effects of cohesion, adhesion and wall friction. It lends itself to elegant graphical solutions and gives more reliable results, especially in the determination of the passive earth resistance; this is in spite of the fact that static equilibrium condition does not appear to be satisfied in the analysis.
- Rankine's theory is relatively simple and hence is more commonly used, while Coulomb's theory is more rational and versatile although cumbersome at times; therefore the use of the latter is called for in important geotechnical problems.

Log Spiral Theory

In 1948, an advanced theory that modified Eq. 2.7 and Eq. 2.8 was developed by Caquot and Kerisel. This modification was to account for a non-planar rupture surface (see Figure 2.13). A logarithmic spiral was used in representing the failure surface, rather than a straight line as seen in the Coulomb's theory. Tables are used in analysing the equations for the log spiral theory due to the complexity in utilizing the equation. Figure 2.14 shows values for K_a and K_p for wall with a backfill perpendicular to a vertical pile wall.

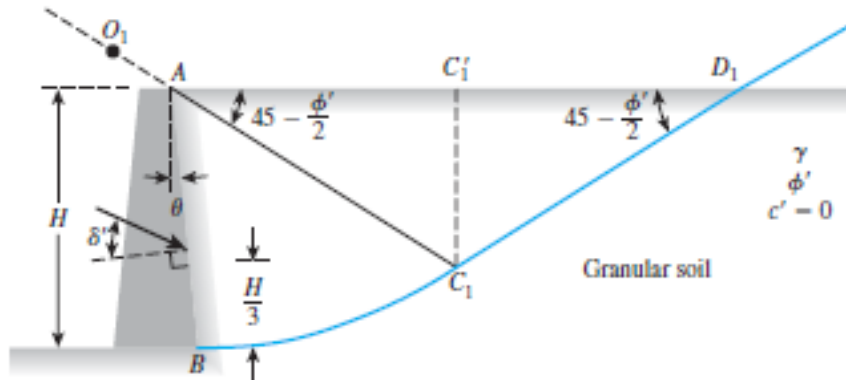


Figure 2.13: Logarithmic spiral surface (Das, 2010)

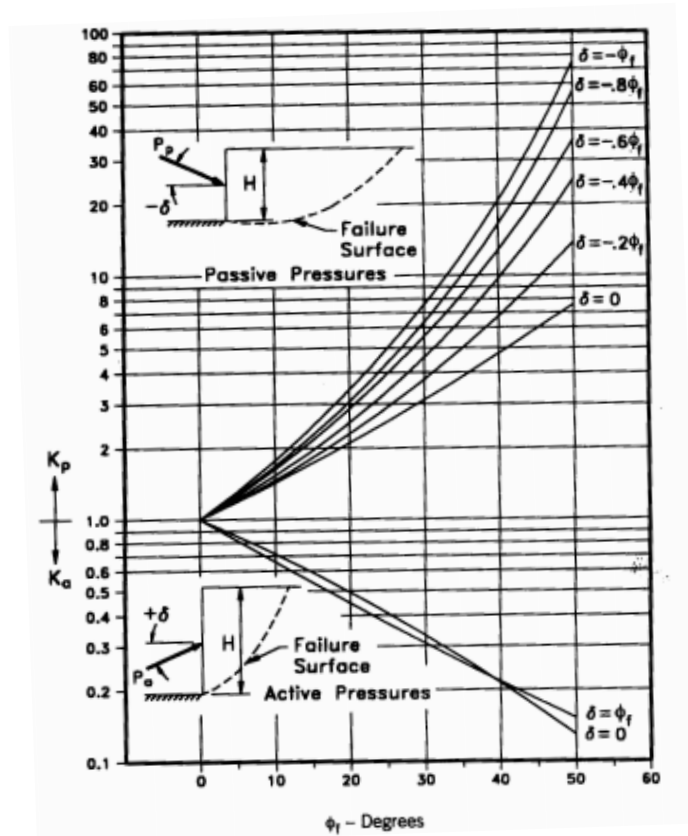


Figure 2.14: Active and passive pressure coefficients for vertical wall and horizontal backfill-based on log spiral failure surfaces [Caquot and Kerisel, 1948]

2.4 Limit Equilibrium Analysis

The limit equilibrium approach depends on estimating the limiting earth pressure coefficients from plastic theories and these values are used to calculate the earth pressure forces on the wall. The equilibrium equations are used to deduce the driven depth of the wall in the limit equilibrium condition. This depth is increased by a certain factor of safety to limit the movement of the wall and to take into consideration the errors in soil parameters and analysis theories.

The basis of the limit equilibrium method is the prediction of the maximum height of the excavation for which static equilibrium is maintained. This is known as the limiting equilibrium situation. It is therefore important to be able to accurately evaluate the earth pressure acting on each side of the wall in the limiting equilibrium condition. The actual distribution and magnitude of earth pressure on the embedded retaining wall is dependent on the complex interaction of the wall and the soil.

The common limit equilibrium design and analysis methods are all based on this general shape. Each method makes different simplifications and assumptions that modify the general shape of the pressure distribution to enable a solution to be found.

2.4.1 Cantilever Walls

In cantilever walls, a reaction force appears at the bottom of the wall, allowing stability as shown in Figure 2.15. When the embedment depth is increased, further reaction appears in the opposite direction but this is strictly unnecessary to guarantee stability.

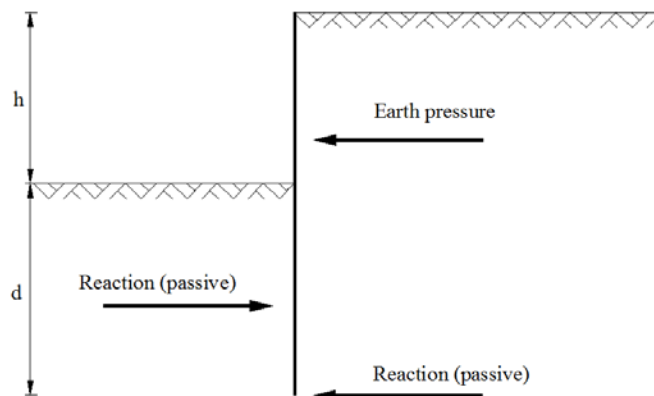


Figure 2.15: Schematic version of the net earth pressure in a cantilever wall.

Stability in cantilever sheet pile walls depends on an adequate embedment below the dredge line. The limit equilibrium methods attempt to model the sheet pile wall at failure conditions, and differ from each other in several assumptions, but being a common feature the reach of the failure state in the whole length of the wall.

The main limit equilibrium methods for cantilever walls are reviewed below.

UK Full Method

This method, shown in Figure 2.16, has been fully described by Padfield, et al., (1984) and gets its name in contrast to the simplified method, described later. The active limit state is assumed to be reached in the back of the wall above the rotation point O , and the passive limit state is assumed to be reached in front of the wall between the dredge line and the rotation point. An overturn in the normal pressure direction is supposed to be produced at the rotation point, below which the full passive pressure is moved behind the wall and the active to the front, so there is a sudden jump in the earth pressure distribution which is needed to prescribe moment equilibrium.

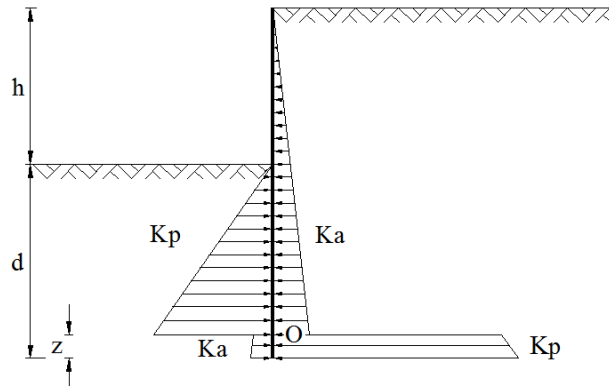


Figure 2.16: Full method of cantilever sheet pile Wall (Craig, 2004).

UK Simplified Method

Due to the complexity of the full method, a simplification is recommended (Padfield, et al., 1984). As shown in Figure 2.17, the earth pressure below the rotation point can be replaced by an equivalent concentrated force acting on point O, represented as R.

The value of the embedment depth (d) calculated is considerably lower than the one calculated from the full method. The common practice is to increase it by about 20% due to the fact that the zone below the rotation point is assumed to receive the passive earth pressure, simplified as the Resultant, and hence an additional length is added so that the total embedment depth coincides with that produced in the full method (Craig, 2004).

The simplified method is slightly more conservative than the other methods, although it leads to appreciably similar results (Padfield, et al., 1984). Its greatest benefit is the simplicity achieved on the traditional system of equations for static equilibrium of forces in horizontal direction and bending moments ($\sum F_H=0, \sum M=0$). A graphical representation of analysing cantilever walls is shown in Figure 2.18.

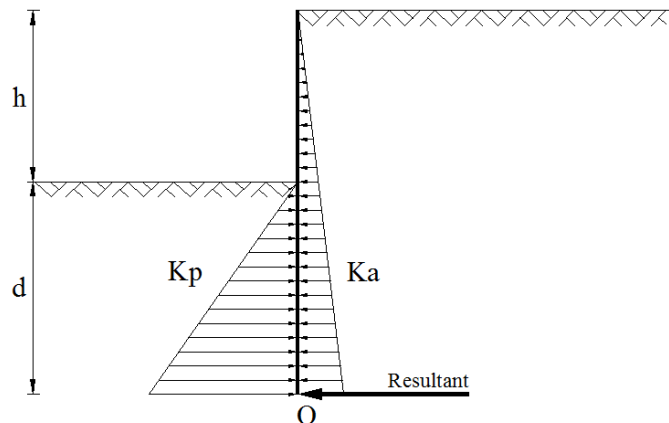


Figure 2.17: Simplified method of the cantilever sheet pile wall (Craig, 2004).

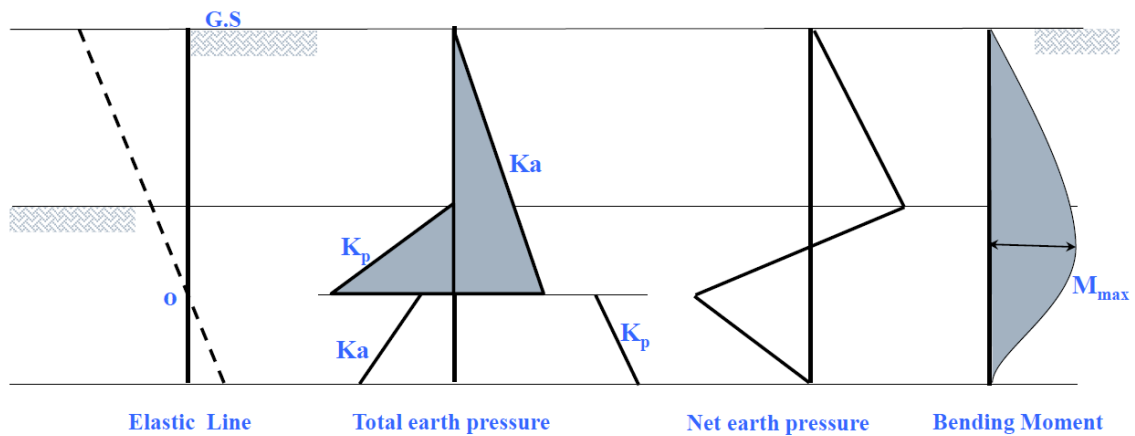


Figure 2.18: Illustration for analysing cantilever sheet pile walls based on the simplified method.

USA Method

The USA method which was first introduced by Krey (1932) and later reviewed by Bowles (1988) assumes a large amount of passive earth resistance occurring at the toe of the sheet pile wall (see Figure 2.19). The resulting earth pressure gradually changes its direction from the passive to the active side of the wall. The change is assumed to be linear (polygonal net pressure distribution) and passes through the point of rotation. With the earth pressure at the bottom of the pile being known, the solution to finding the depth of the embedment is to obtain d_2 , can be easily calculated by using the static equilibrium of forces in horizontal direction and bending moments ($\sum F_H = 0$, $\sum M = 0$) (Škrabl, 2006).

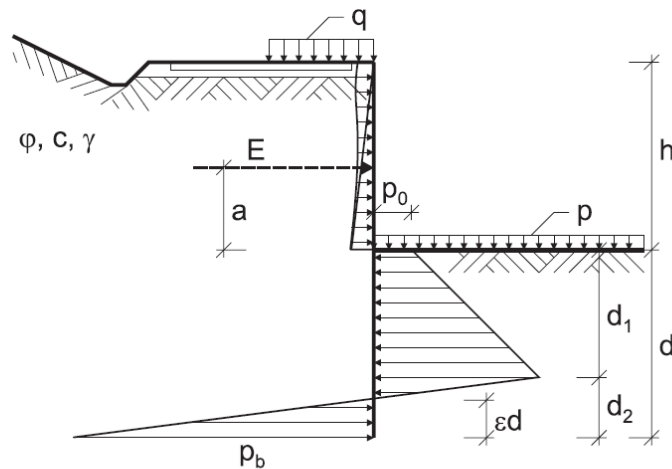


Figure 2.19: Influences and resistance according to the USA Method (Škrabl, 2006)

2.4.2 Anchored or Propped Walls

Anchored walls (or tied-back walls) are able to achieve the equilibrium without considering a passive reaction at the bottom of the back of the wall due to the anchor force, as seen in Figure 2.20. This is because, the earth pressure can be balanced by an increase in the anchor force. The passive reaction is however normally considered when the fixed-earth design method is used in the analyses.

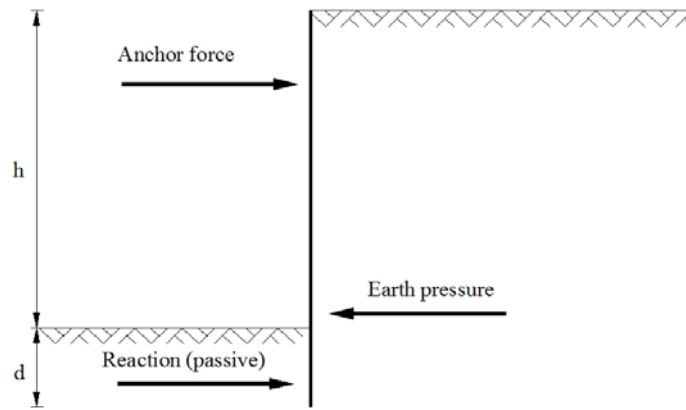


Figure 2.20: Schematic version of the net earth pressure in an anchored wall

The main analytical methods for anchored walls are the free earth support method and the fixed earth support method, which differ on the hypotheses adopted.

Free Earth Support Method

An anchored sheet pile is said to have a free earth support when the embedment depth is small and the wall is considered free to rotate about the base (B). Because the base of the pile is relatively free to move, the passive resistance is mobilized only on one face, that is, no passive resistance develops on the backside of the piling (Figure 2.21). The theoretical depth of embedment (d) is calculated by taking moment about the tie rod at D. Just like the cantilever wall, the actual depth of embedment is calculated by increasing d by about 20% to 40% or the factor of safety for the passive resistance coefficient of 1.5 to 2 is used to allow for design safety.

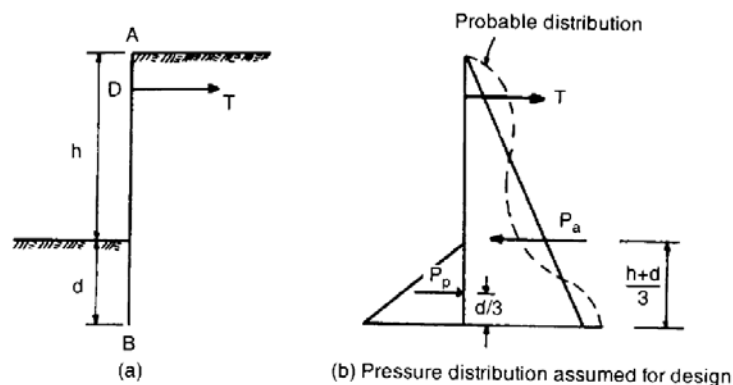


Figure 2.21: Free earth support method for anchored sheet pile wall (Smith, et al., 1998)

Fixed Earth Support Method (Blum Theory)

An anchored sheet pile is said to have a fixed earth support when the embedment depth is large and the base of the pile is fixed against rotation. The pressure distribution assumed for design analyses is shown in Figure 2.22. The deflected shape reverses its curvature at a point of contraflexure, O, is introduced by the assumption of fixity. The Blum's equivalent beam method (see Figure 2.22c) is used in analysing the wall by dividing the wall into two parts. Analysis by the elastic line method (Terzaghi, 1943) gives the following positions for O (depending upon the value of ϕ for the soil) where h is the height of the wall and x is the dimension shown in Figure 2.22a.

Table 2.2: Contraflexure – Wall height relationship based on soil frictional angle

ϕ	20°	25°	30°	35°
x	0.25·h	0.15·h	0.08·h	0.035·h

For most backfills, the average value of ϕ is 30° . Hence if x is assumed to be $0.1h$, little error will generally be involved.

The application of the fixed-end support system is limited to drained soil conditions (i.e. $\phi > 0$).

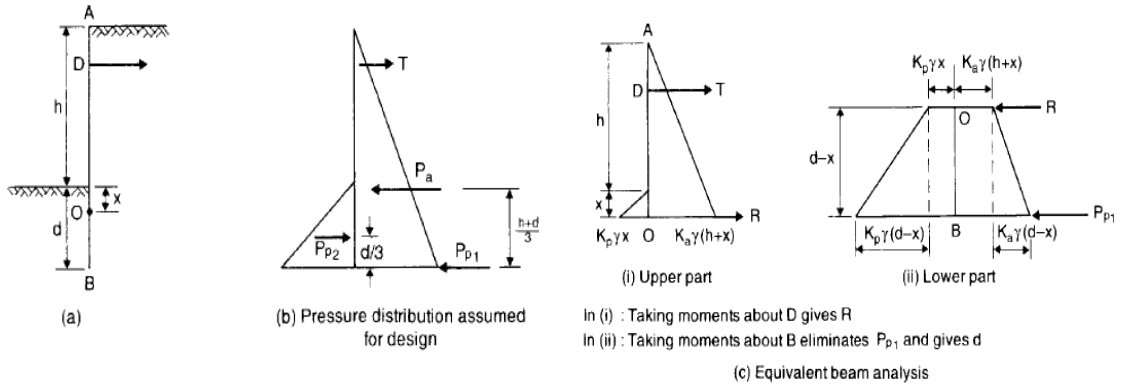


Figure 2.22: Fixed earth support method for anchored sheet pile walls (Smith, et al., 1998)

CHAPTER 3 RESEARCH METHODOLOGY

3.1 Introduction

This chapter presents the methodology used in analysing sheet pile wall as described in the previous chapter. The USA method, as seen in CHAPTER 2, is presented as the main methodology for the stabilization analysis of the sheet pile wall in the cantilever sheet pile wall and the free earth support method of the anchored sheet pile wall while the Blum Theory is employed in analysing the fixed earth support method of the anchored pile walls. Generic equations are developed for the analysis with soils of either granular, cohesive or a combination of both. When the dredge layer in both cantilever and anchored pile analysis is an undrained cohesive soil (i.e. $\phi_u = 0$ and $C_u > 0$) special algorithm is developed due to the fact that the soil behaves in a different manner. The algorithm encompasses situations where groundwater is present or absent and also where there is a surcharge or not. The equations presented in this chapter are subsequently coded into the *GEOWALL* software with the aid of Visual C#.Net programming language.

3.2 Cantilever Sheet Pile Wall in Granular Soils

The basic principles for estimating net lateral pressure distribution on a cantilever sheet pile wall can be explained with the aid of Figure 3.1. Zone A shows the free standing portion above the dredge line with a water table located within the zone. Only the active pressure from the backfill layer is present in this zone. Below the dredge line is Zone B which occurs up to the point of rotation 'O' of the wall. As seen in Figure 3.1a, the lateral pressure acting within the zone is active at the backfill side of the wall and passive at the excavated side of the wall. This is due to the yielding nature of the wall, presented in dotted lines in the same figure. The reverse condition of Zone B occurs in Zone C, and its influence is between the point of rotation 'O' and the toe of the wall. The net actual pressure distribution on the wall is shown in Figure 3.1b. However, for design purposes, Figure 3.1c shows a simplified version.

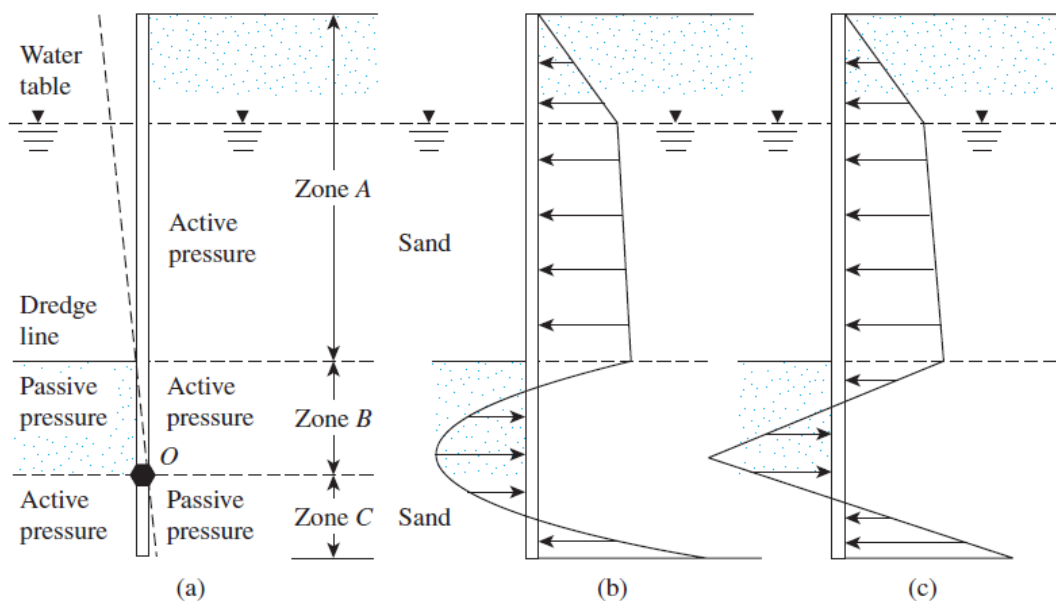


Figure 3.1: Cantilever sheet pile wall in sand (Das, 2011)

Figure 3.2 shows the relationship used to develop a proper depth of embedment of sheet piles driven into a granular soil.

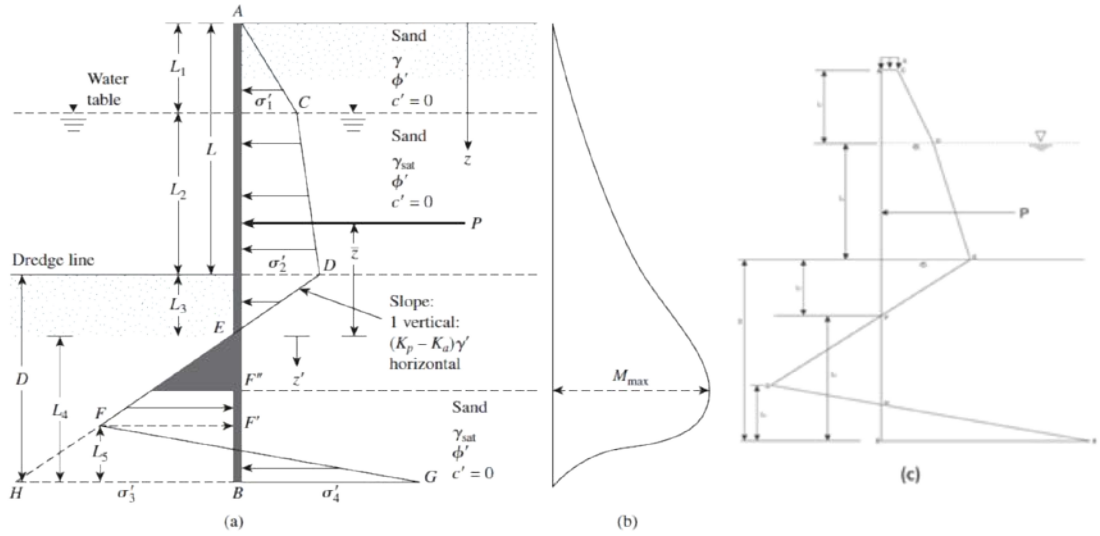


Figure 3.2: Cantilever sheet pile wall in sand: (a) variation of net pressure diagram without surcharge; (b) variation of moment with depth (c) variation of net pressure diagram with depth (surcharge included) (Das, 2011)

A surcharge force (q) exists above the backfill layer as shown in Figure 3.2c. The water table is at a depth L_1 , below the top of the wall with the effective frictional angle of the sand being ϕ' . The intensity of the active pressure at a depth $z = L_1$ is

$$\sigma'_1 = (q + \gamma L_1)K_a - 2c\sqrt{K_a} \cos \delta_a \quad \text{Eq. 3.1}$$

Where;

K_a = Coulomb active pressure coefficient (see Eq. 2.5)

γ = unit weight of soil above the water table

Similarly, the active pressure at a depth $z = L_1 + L_2$ (i.e., at the level of the dredge line) is

$$\sigma'_2 = (q + \gamma L_1 + \gamma' L_2)K_a - 2c\sqrt{K_a} \cos \delta_a \quad \text{Eq. 3.2}$$

Where γ' = effective unit weight of soil = $\gamma_{sat} - \gamma_w$.

Note that, at the level of the dredge line, the hydrostatic pressure from both sides of the wall are the same magnitude and cancel each other.

To determine the net lateral pressure below the dredge line up to the point of rotation, as shown in Figure 3.1a, the passive pressure acting from the water side toward the land side of the wall and also the active pressure acting from the land side to the water side of the wall have to be considered. For such cases, ignoring the hydrostatic pressure from both sides of the wall, the active pressure at depth z is

$$\sigma'_a = [q + \gamma L_1 + \gamma' L_2 + \gamma'(z - L_1 - L_2)]K_a - 2c\sqrt{K_a} \cos \delta_a \quad \text{Eq. 3.3}$$

Also, the passive pressure at depth z is

$$\sigma'_p = \gamma'(z - L_1 - L_2)K_{p(design)} + 2c\sqrt{K_{p(design)}} \cos \delta_p \quad \text{Eq. 3.4}$$

where;

$K_{p(design)}$ = Design Coulomb passive pressure coefficient = $\frac{K_p}{FS}$.

K_p = Coulomb passive pressure coefficient (see Eq. 2.6)

FS = Factor of safety (ranges between 1.5 and 2).

Combining Eq. 3.3 and Eq. 3.4 yields the net lateral pressure, namely,

$$\begin{aligned}\sigma' &= \sigma'_a - \sigma'_p = (q + \gamma L_1 + \gamma' L_2) K_a - \gamma' (z - L_1 - L_2) (K_{p(design)} - K_a) \\ &\quad - 2c \left(\sqrt{K_{p(design)}} \cos \delta_p + \sqrt{K_a} \cos \delta_a \right) \\ \sigma' &= (\sigma'_2 + 2c \sqrt{K_a} \cos \delta_a) - \gamma' (z - L) (K_{p(design)} - K_a) \\ &\quad - 2c \left(\sqrt{K_{p(design)}} \cos \delta_p + \sqrt{K_a} \cos \delta_a \right)\end{aligned}\quad \text{Eq. 3.5}$$

Where $L = L_1 + L_2$.

The net pressure, σ' equals zero at a depth L_3 below the dredge line so

$$\begin{aligned}(\sigma'_2 + 2c \sqrt{K_a} \cos \delta_a) - \gamma' (z - L) (K_{p(design)} - K_a) \\ - 2c \left(\sqrt{K_{p(design)}} \cos \delta_p + \sqrt{K_a} \cos \delta_a \right) = 0\end{aligned}$$

or

$$(z - L) = L_3 = \frac{\sigma'_2 - 2c \sqrt{K_{p(design)}} \cos \delta_p}{\gamma' (K_{p(design)} - K_a)} \quad \text{Eq. 3.6}$$

Inferring from Eq. 3.6 and Figure 3.2;

$$\begin{aligned}\overline{HB} = \sigma'_3 = L_4 (K_{p(design)} - K_a) \gamma' \\ + 2c \left(\sqrt{K_{p(design)}} \cos \delta_p + \sqrt{K_a} \cos \delta_a \right)\end{aligned}\quad \text{Eq. 3.7}$$

At the bottom of the sheet pile, passive pressure, σ'_p , acts from the land side towards the water side while active pressure acts vice versa to the passive pressure of the sheet pile, so at $z = L+D$,

$$\sigma'_p = (q + \gamma L_1 + \gamma' L_2 + \gamma' D) K_{p(design)} + 2c \sqrt{K_{p(design)}} \cos \delta_p \quad \text{Eq. 3.8}$$

At the same depth,

$$\sigma'_a = \gamma' D K_a - 2c \sqrt{K_a} \cos \delta_a \quad \text{Eq. 3.9}$$

Hence, the net lateral pressure at the bottom of the sheet pile is

$$\begin{aligned}\sigma'_p - \sigma'_a &= \sigma'_4 \\ &= (q + \gamma L_1 + \gamma' L_2) K_{p(design)} + \gamma' D (K_{p(design)} - K_a) \\ &\quad + 2c \left(\sqrt{K_{p(design)}} \cos \delta_p + \sqrt{K_a} \cos \delta_a \right) \\ \sigma'_4 &= (q + \gamma L_1 + \gamma' L_2) K_{p(design)} + \gamma' L_3 (K_{p(design)} - K_a) \\ &\quad + \gamma' L_4 (K_{p(design)} - K_a) \\ &\quad + 2c \left(\sqrt{K_{p(design)}} \cos \delta_p + \sqrt{K_a} \cos \delta_a \right) \\ \sigma'_4 &= \sigma'_5 + \gamma' L_4 (K_{p(design)} - K_a) \\ &\quad + 2c \left(\sqrt{K_{p(design)}} \cos \delta_p + \sqrt{K_a} \cos \delta_a \right)\end{aligned}\quad \text{Eq. 3.10}$$

Where

$$\sigma'_5 = (q + \gamma L_1 + \gamma' L_2) K_p + \gamma' L_3 (K_{p(\text{design})} - K_a) \quad \text{Eq. 3.11}$$

$$D = L_3 + L_4 \quad \text{Eq. 3.12}$$

For the stability of the wall the principles of statics can now be applied:

$$\Sigma \text{ horizontal forces per unit length of wall} = 0$$

and

$$\Sigma \text{ moment of the forces per unit length of wall about point B} = 0$$

For the summation of the horizontal forces,

$$\text{Area of the pressure diagram ACDE} - \text{area of EFHB} + \text{area of FHBG} = 0$$

or

$$P - \frac{1}{2} \sigma'_3 L_4 + \frac{1}{2} L_5 (\sigma'_3 + \sigma'_4) = 0 \quad \text{Eq. 3.13}$$

Where P = area of the pressure diagram ACDE.

Summing the moment of all the forces about point B yields

$$P(L_4 - \bar{z}) - \left(\frac{1}{2} L_4 \sigma'_3\right) \left(\frac{L_4}{3}\right) + \frac{1}{2} L_5 (\sigma'_3 + \sigma'_4) \left(\frac{L_5}{3}\right) = 0 \quad \text{Eq. 3.14}$$

From Eq. 3.13,

$$L_5 = \frac{\sigma'_3 L_4 - 2P}{\sigma'_3 + \sigma'_4} \quad \text{Eq. 3.15}$$

Combining Eq. 3.7, Eq. 3.10, Eq. 3.14 and Eq. 3.15 and simplifying them further, we obtain the following fourth-degree equation in terms of L_4 :

$$L_4^4 + A_1 L_4^3 - A_2 L_4^2 - A_3 L_4 - A_4 = 0 \quad \text{Eq. 3.16}$$

where,

$$A_1 = \frac{\sigma'_5 - 24c(\sqrt{K_{p(\text{design})}} \cos \delta_p + \sqrt{K_a} \cos \delta_a)}{\gamma'(K_{p(\text{design})} - K_a)} \quad \text{Eq. 3.17}$$

$$A_2 = \frac{8P}{\gamma'(K_{p(\text{design})} - K_a)} + \frac{2c(\sqrt{K_{p(\text{design})}} \cos \delta_p + \sqrt{K_a} \cos \delta_a)[6\sigma'_5 + 26c(\sqrt{K_{p(\text{design})}} \cos \delta_p + \sqrt{K_a} \cos \delta_a)]}{\gamma'^2(K_{p(\text{design})} - K_a)^2} \quad \text{Eq. 3.18}$$

$$A_3 = \frac{6P[2\bar{z}\gamma'(K_{p(\text{design})} - K_a) + \sigma'_5 + \frac{8}{3}c(\sqrt{K_{p(\text{design})}} \cos \delta_p + \sqrt{K_a} \cos \delta_a)]}{\gamma'^2(K_{p(\text{design})} - K_a)^2} \quad \text{Eq. 3.19}$$

$$A_4 = \frac{P(6\bar{z}\sigma'_5 + 4P - 24\bar{z}c(\sqrt{K_{p(\text{design})}} \cos \delta_p + \sqrt{K_a} \cos \delta_a))}{\gamma'^2(K_{p(\text{design})} - K_a)^2} \quad \text{Eq. 3.20}$$

The theoretical depth of penetration is obtained by summing L_3 and L_4 (see Figure 3.2). The actual depth of penetration is obtained by increasing the theoretical depth ($L_3 + L_4$) of penetration by about 20% to 40% or the factor of safety for passive earth pressure coefficient increased between 1.5 and 2 (Murthy, 2002).

The magnitude of the maximum moment of the wall is

$$M_{max} = P(\bar{z} + z') - \left[\frac{1}{6} \gamma' z'^3 (K_{p(des)} - K_a) \right] \quad \text{Eq. 3.21}$$

where z' is the depth of zero shear force.

$$z' = \sqrt{\frac{2P}{(K_{p(des)} - K_a)\gamma'}} + 2c \left(\sqrt{K_{p(des)} \cos \delta_p} + \sqrt{K_a \cos \delta_a} \right) \quad \text{Eq. 3.22}$$

3.3 Cantilever Sheet Pile Wall in a Cohesive Soil

Two cases of cantilever walls in cohesive soils could occur: (1) sheet pile walls entirely in clay and (2) wall driven in clay and backfilled with sand. Figure 3.3 shows a cantilever sheet pile wall driven into an undrained cohesive soil. The net pressures σ'_1 and σ'_2 are given in Eq. 3.1 and Eq. 3.2. With σ'_7 being known (as seen in Eq. 3.28), the incognita in determining the embedment depth is to determine L_4 .

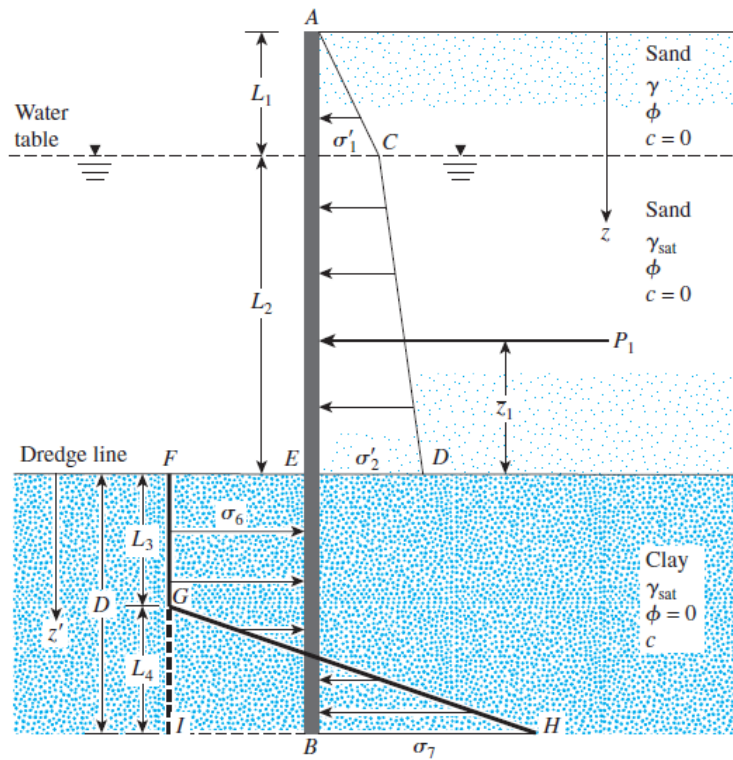


Figure 3.3: Cantilever sheet pile penetrating cohesive soil (Das, 2011)

At any depth greater than $L_1 + L_2$, for $\phi = 0$, the Coulomb active earth pressure coefficient $K_a = 1$. Similarly, for $\phi = 0$, the Coulomb passive earth resistance coefficient $K_p = 1$. Consequently, above the point O in Figure 3.1a, the active pressure becomes

$$\sigma_a = [\gamma L_1 + \gamma' L_2 + \gamma_{sat}(z - L_1 - L_2)] - 2c \quad \text{Eq. 3.23}$$

The passive pressure can be given as

$$\sigma_p = \gamma_{sat}(z - L_1 - L_2) + 2c \quad \text{Eq. 3.24}$$

The net pressure then becomes;

$$\begin{aligned} \sigma_6 = \sigma_p - \sigma_a &= [\gamma_{sat}(z - L_1 - L_2) + 2c] \\ &\quad - [\gamma L_1 + \gamma' L_2 + \gamma_{sat}(z - L_1 - L_2) - 2c] \\ \sigma_6 &= 4c - (\gamma L_1 + \gamma' L_2) \end{aligned} \quad \text{Eq. 3.25}$$

At the bottom of the sheet pile, the passive pressure is

$$\sigma_p = (\gamma L_1 + \gamma' L_2 + \gamma_{sat} D) + 2c \quad \text{Eq. 3.26}$$

Similarly the active pressure is

$$\sigma_a = \gamma_{sat} D - 2c \quad \text{Eq. 3.27}$$

Hence, the net pressure becomes

$$\sigma_7 = \sigma_p - \sigma_a = 4c + (\gamma L_1 + \gamma' L_2) \quad \text{Eq. 3.28}$$

For equilibrium analysis $\Sigma F_H = 0$;

$$\begin{aligned} P - [4c - (q + \gamma L_1 + \gamma' L_2)]D \\ + \frac{1}{2} L_4 [4c - (q + \gamma L_1 + \gamma' L_2) + 4c + (q + \gamma L_1 + \gamma' L_2)] \\ = 0 \end{aligned} \quad \text{Eq. 3.29}$$

where P = area of the pressure diagram ACDE.

Simplifying the preceding equation produces

$$L_4 = \frac{D[4c - (\gamma L_1 + \gamma' L_2)] - P}{4c} \quad \text{Eq. 3.30}$$

Now, taking the moment about point B ($\Sigma M_B = 0$) yields

$$P(D + \bar{z}_1) - [4c - (q + \gamma L_1 + \gamma' L_2)] \frac{D^2}{2} + \frac{1}{2} L_4 (8C) \left(\frac{L_4}{3} \right) = 0 \quad \text{Eq. 3.31}$$

where \bar{z}_1 = distance of the centre of pressure of the pressure diagram ACDE measured from the level of the dredge line.

Combining Eq. 3.30 and Eq. 3.31 yields

$$D^2 [4c - (q + \gamma L_1 + \gamma' L_2)] - 2DP_1 - \frac{P(P + 12c\bar{z}_1)}{(q + \gamma L_1 + \gamma' L_2) + 2c} = 0 \quad \text{Eq. 3.32}$$

The actual depth of penetration is obtained by increasing the theoretical depth of penetration (D), which is obtained by solving Eq. 3.32, by 20% to 40% or the factor of safety for passive earth pressure coefficient increased between 1.5 and 2 (Murthy, 2002).

The magnitude of the maximum moment of the wall is

$$M_{max} = P(\bar{z} + z') - \frac{\sigma_6 z'^2}{2} \quad \text{Eq. 3.33}$$

where z' is the depth of zero shear force.

$$z' = \frac{P}{\sigma_6} \quad \text{Eq. 3.34}$$

3.4 Cantilever sheet pile wall with backfill being a cohesive soil

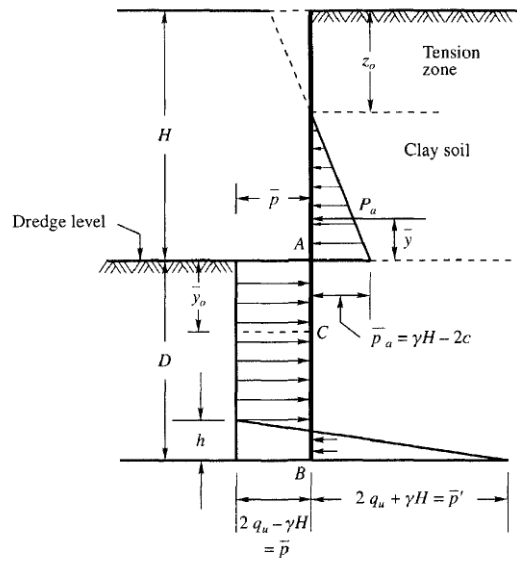


Figure 3.4: Depth of embedment of a cantilever wall in a cohesive soil with a cohesive backfill soil (Murthy, 2002).

The pressure distribution on a sheet pile wall is shown in Figure 3.4. The active pressure P_a , at any depth z may be expressed as

$$P_a = \sigma_v K_A - 2c\sqrt{K_A}$$

where

σ_v = vertical pressure ($\gamma \cdot z$)

z = depth from the surface of the backfill.

The passive pressure P_p at any depth ' y ' and below the dredge line may be expressed as

$$P_p = \sigma_v K_p + 2c\sqrt{K_p}$$

The active pressure distribution on the wall from the backfill surface to the dredge line is shown in Figure 3.4. The soil is supposed to be in tension up to a depth of z_0 and the pressure on the wall is zero at this zone. The net pressure distribution on the wall is shown by the shaded triangle. At the dredge line (at point A);

(a) The active pressure \bar{P}_a acting towards the left is

$$\bar{P}_a = \gamma H K_A - 2c\sqrt{K_A}$$

$$\text{When } \phi = 0 \quad \bar{P}_a = \gamma H - 2c = \gamma H - q_u \quad \text{Eq. 3.35}$$

Where q_u = unconfined compressive strength of the clay soil = $2c$.

(b) The passive pressure acting towards the right at the dredge line is

$$\bar{P}_p = 2c \quad \text{since } \phi = 0 \quad \text{or } \bar{P}_p = q_u$$

The resultant of the passive and active pressures at the dredge line is

$$\bar{P}_p - \bar{P}_a = q_u - (\gamma H - q_u) = 2q_u - \gamma H \quad \text{Eq. 3.36}$$

The resultant of the passive and active pressure at any depth ' y ' below the dredge line is

passive pressure, $P_p = \gamma y + q_u$

active pressure, $P_a = \gamma(H + y) - q_u$

The resultant pressure is

$$P_p - P_a = (\gamma y + q_u) - [\gamma(H + y) - q_u] = 2q_u - \gamma H \quad \text{Eq. 3.37}$$

Eq. 3.36 and Eq. 3.37 indicate that the resultant pressure remains constant at all depths.

If passive pressure is developed on the backfill side at the bottom of the pile (point B), then

$$P_p = \gamma(H + D) + q_u \text{ acting towards the left}$$

$$P_a = \gamma D - q_u \text{ acting towards the right}$$

The resultant is

$$P_p - P_a = (\gamma(H + D) + q_u) - [\gamma D - q_u] = 2q_u + \gamma H \quad \text{Eq. 3.38}$$

For static equilibrium, the sum of all horizontal forces must be equal to zero, that is,

$$P - (2q_u - \gamma H)D + \frac{1}{2}(2q_u + 2q_u)h = 0$$

Simplifying,

$$P + 2q_u h - 2q_u D + \gamma H D = 0, \text{ therefore,}$$

$$h = \frac{D(2q_u - \gamma H) - P_a}{2q_u} \quad \text{Eq. 3.39}$$

Also, for equilibrium, the sum of the moments at any point should be zero. Taking moments about the base,

$$P(\bar{y} + D) + \frac{h^2}{6}(2q_u) - \frac{(2q_u - \gamma H)D^2}{2} = 0 \quad \text{Eq. 3.40}$$

Substituting for h in Eq. 3.40 and simplifying,

$$C_1 D^2 + C_2 D + C_3 = 0 \quad \text{Eq. 3.41}$$

where $C_1 = (2q_u - \gamma H)$

$$C_2 = -2P$$

$$C_3 = -\frac{P(6q_u \bar{y} + P)}{(q_u + \gamma H)}$$

The depth computed from Eq. 3.41 should be increased by 20% to 40% or the factor of safety for passive earth pressure coefficient increased between 1.5 and 2 to ensure a more reliable embedment depth (Murthy, 2002).

The magnitude of the maximum moment of the wall is

$$M_{max} = P(\bar{y}_o + \bar{y}) - \frac{\bar{p}\bar{y}^2}{2} \quad \text{Eq. 3.42}$$

where \bar{y}_o is the depth of zero shear force.

$$\bar{y}_o = \frac{P}{\bar{p}} \quad \text{Eq. 3.43}$$

where $\bar{p} = 2q_u - \gamma H$ as seen in Figure 3.4.

3.5 Analyses of Anchored Sheet Pile Walls

Most sheet pile walls include additional lateral support; using tieback anchor. The additional support reduces the flexural stress and lateral movements in the wall, which permits construction of walls of greater height than it is possible with cantilever designs. Anchors minimize the depth of penetration required by the sheet piles and also reduce the cross-sectional area and weight of the sheet piles needed for construction. However, the tie rods and anchors must be carefully designed.

The two principal design methods for anchored sheet pile walls are:

- The *free earth support method* which permits the bottom of the wall to rotate or translate. This criterion permits shallower depths of embedment, and relies more heavily on the lateral support provided by the anchors.
- The *fixed earth support method* requires a depth of embedment such that the bottom of the sheet pile is fixed against translation and rotation. This is similar to the criterion used in the design of cantilever walls.

It is therefore worth noting that $D_{\text{free-earth}} < D_{\text{fixed-earth}}$. Figure 3.5 shows the assumed nature of deflection of the sheet piles for the two methods.

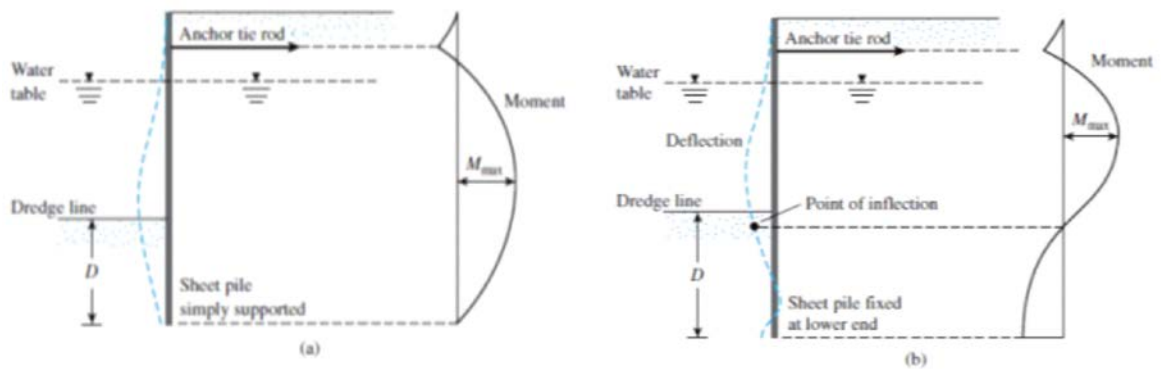


Figure 3.5: Nature of variation of deflection and moment for anchored sheet piles: (a) free earth support method and (b) fixed earth support method (Das, 2011)

3.5.1 Free Earth Support Method

Figure 3.6 shows an anchor sheet pile wall with a backfill. The anchor is located at a depth l_1 below the top of the sheet pile wall.

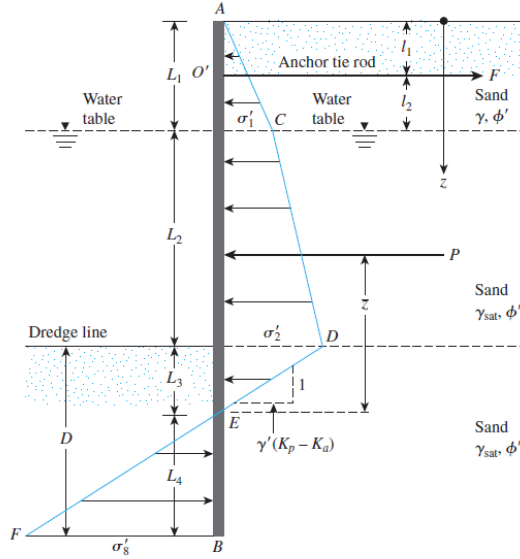


Figure 3.6: Anchored sheet pile wall penetrating drained soil (Das, 2011)

The diagram of the net pressure distribution above the dredge line is similar to that shown in Figure 3.2. Using Eq. 3.1, Eq. 3.2, Eq. 3.6 and Eq. 3.7; where $\sigma'_3 = \sigma'_8$ and applying the static equilibrium equations i.e. $\Sigma F_H = 0$ and $\Sigma \text{Moment about } O' = 0$, where O' is located at the level of the tie rod;

$$P - \frac{1}{2} \sigma'_8 L_4 - F_T = 0$$

or

$$F_T = P - \frac{1}{2} [\gamma' (K_p - K_a)] L_4^2 \quad \text{Eq. 3.44}$$

where

$$F_T = F \cos \theta$$

where θ is the angle of inclination of the anchor with respect to the horizontal axis

and also for moment equation;

$$-P[(L_1 + L_2 + L_3) - (\bar{z} + l_1)] + \frac{1}{2} [\gamma' (K_p - K_a)] L_4^2 \left(l_2 + L_2 + L_3 + \frac{2}{3} L_4 \right) = 0$$

or

$$L_4^3 + A_1 L_4^2 + A_2 L_4 - A_3 = 0 \quad \text{Eq. 3.45}$$

where

$$A_1 = \left[1.5(l_2 + L_2 + L_3) + \frac{(2c\{\sqrt{K_p(\text{design})} + \sqrt{K_a}\})}{\gamma'(K_p - K_a)} \right]$$

$$A_2 = 1.5 \left[\frac{(2c\{\sqrt{K_p(\text{design})} + \sqrt{K_a}\})(l_2 + L_2 + L_3)}{\gamma'(K_p - K_a)} \right]$$

$$A_3 = \frac{3P[(L_1 + L_2 + L_3) - (\bar{z} + l_1)]}{\gamma'(K_p - K_a)}$$

Eq. 3.45 may be solved by trial and error to determine the theoretical depth, L_4 :

$$D_{\text{theoretical}} = L_3 + L_4$$

The theoretical depth is increased by about 30 to 40% or a factor of safety of 1.5 to 2 is employed for actual construction (Murthy, 2002).

The magnitude of the maximum moment of the wall is

$$M_{max} = -\frac{1}{2}\sigma'_1 L_1 \left(z' + \frac{L_1}{3}\right) + F(z' + l_1) - \sigma'_1 \frac{z'^2}{2} - \frac{1}{2}\gamma' K_a z'^2 \left(\frac{z'}{3}\right) \quad \text{Eq. 3.46}$$

where z' is the depth of zero shear force.

$$z' = \frac{-\sigma'_1 \pm \sqrt{(\sigma'_1)^2 - 4 * \frac{1}{2}\gamma' K_a \left(\frac{1}{2}\sigma'_1 l_1\right)}}{\gamma' K_a} \quad \text{Eq. 3.47}$$

3.5.2 Free Earth Support Method for Cohesive Soil

Figure 3.7 shows an anchored sheet pile wall penetrating an undrained clay soil. The diagram of pressure distribution above the dredge line is similar to that shown in Figure 3.3.

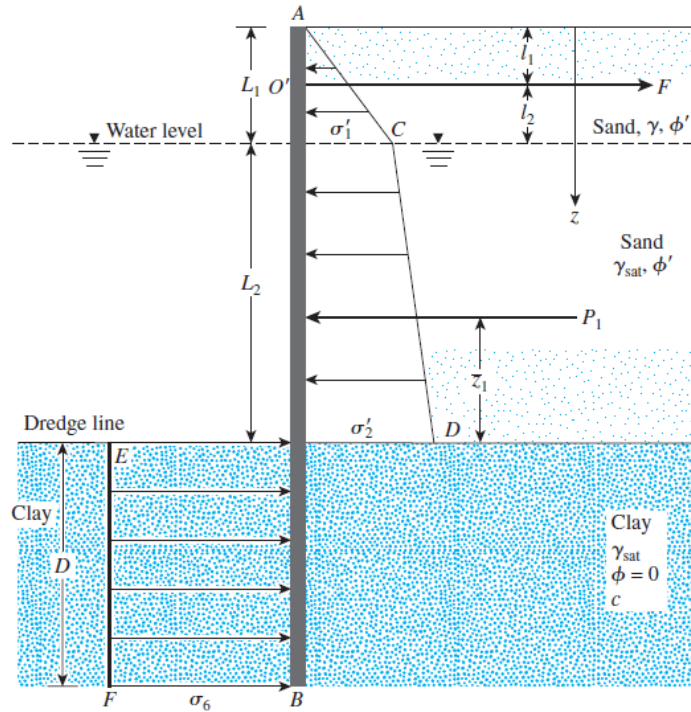


Figure 3.7: Free earth anchored sheet pile wall penetrating undrained cohesive soil (Das, 2011)

From Eq. 3.25 and using the static equilibrium equations i.e. $\Sigma F_H = 0$;

$$F_T = P_1 - \sigma_6 D \quad \text{Eq. 3.48}$$

Again Σ Moment about $O' = 0$, where O' is located at the level of the tie rod;

$$P_1(L_1 + L_2 - l_1 - \bar{z}_1) - \sigma_6 D \left(l_2 + L_2 + \frac{D}{2}\right) = 0$$

Simplification yields

$$\sigma_6 D^2 + 2\sigma_6 D(L_1 + L_2 - l_1) - 2P_1(L_1 + L_2 - l_1 - \bar{z}_1) = 0 \quad \text{Eq. 3.49}$$

Eq. 3.49 gives the theoretical depth of penetration D that should be increased by about 30 to 40% for actual construction or using a factor of safety of 1.5 to 2 (Murthy, 2002).

The magnitude of the maximum moment of the wall is

$$M_{max} = Fz' - \frac{1}{6}\gamma K_a(z' + L_1)^3 \quad \text{Eq. 3.50}$$

where z' is the depth of zero shear force given by;

$$z' = \sqrt{\frac{2F}{\gamma K_a}} - L_1 \quad \text{Eq. 3.51}$$

Section 3.5.1 can be applied in anchored sheet pile wall (i.e. when the backfill is a cohesive soil) and as a result, detailed analysis on cohesive backfill for the free end method is not explained.

3.5.3 Fixed Earth Support Method for Penetrating Granular Soil

In the fixed earth support method, the toe of the pile is assumed to be restrained from rotating, as shown in Figure 3.8a. A simplified method called the equivalent beam solution which is attributed to Blum (1931) is generally used to calculate L_3 , and thus, D . (Das, 2011).

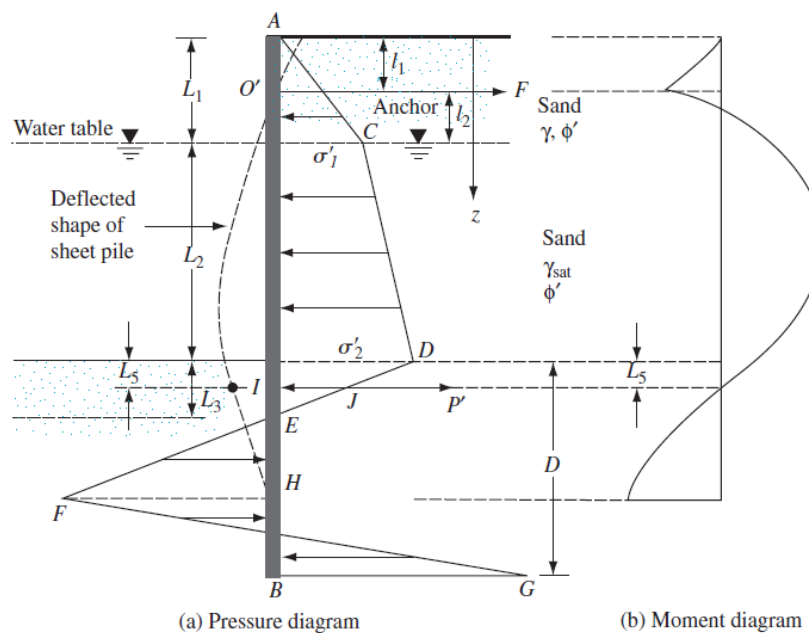


Figure 3.8: Fixed earth support method penetrating drained soil (Das, 2011)

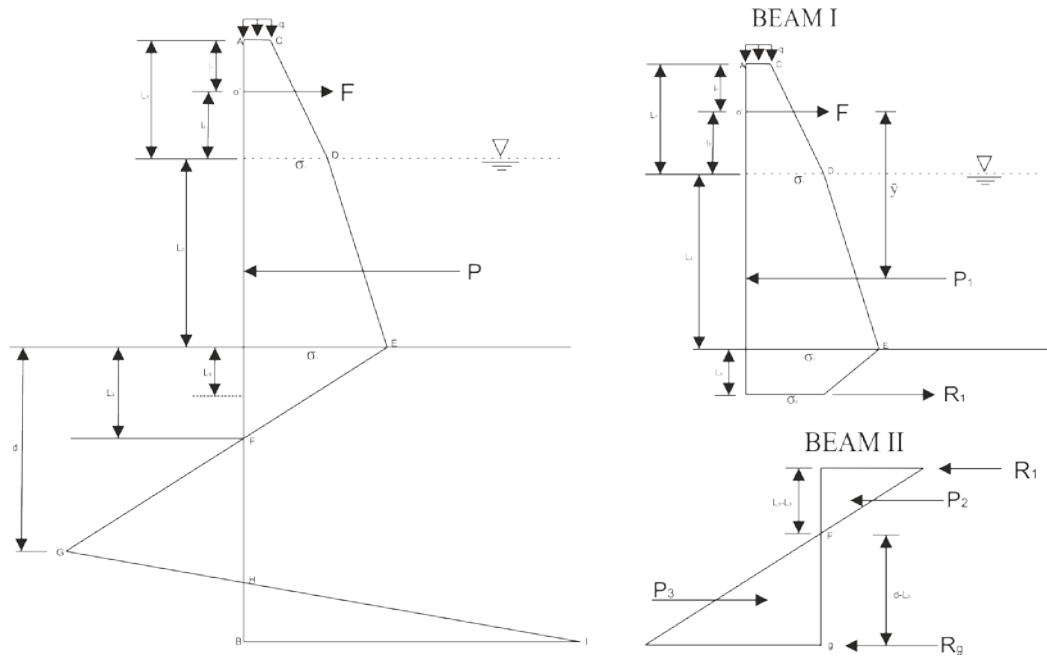


Figure 3.9: Analysing Fixed earth support method

The analysis is achieved by considering Figure 3.8a as two beams as shown in Figure 3.9. Beam I is taken from point A to Point I and Beam II being Point I to Point F.

Considering Beam I:

Σ moment of the forces per unit length of wall about point O' = 0

$$P_1 \bar{y} = R_1 (H - l_1 + L_5)$$

$$R_1 = \frac{P_1 \bar{y}}{(H - l_1 + L_5)} \quad \text{Eq. 3.52}$$

where L_5 can be obtained from Table 2.2.

Also,

$$\frac{\sigma_2}{L_3} = \frac{\sigma_0}{L_3 - L_5}$$

$$\sigma_0 = \frac{\sigma_2}{L_3} (L_3 - L_5) \quad \text{Eq. 3.53}$$

Where σ_2 is shown in Eq. 3.2 and L_3 is shown in Eq. 3.6.

Considering Beam II:

Σ moment of the forces per unit length of wall about point H = 0

$$\frac{1}{2} \sigma_2 (d - L_3) \left(\frac{d - L_3}{3} \right) - R_1 (d - L_5) - P_2 \left\{ (d - L_3) + \frac{2}{3} (L_3 - L_5) \right\} = 0 \quad \text{Eq. 3.54}$$

with;

$$P_2 = \frac{1}{2} \sigma_0 (L_3 - L_5)$$

$$P_3 = \frac{1}{2} \sigma_2 (d - L_3)$$

putting σ_2 into Eq. 3.54;

$$\frac{1}{2}\gamma(K_p - K_a)\left(\frac{d - L_3}{3}\right)^3 + \frac{1}{2}\left[2c\left(\sqrt{K_{p(design)}} + \sqrt{K_a}\right)\right]\left(\frac{d - L_3}{3}\right)^3 - R_1(d - L_5) - \frac{1}{3}P_2(3d - L_3 - 2L_5) = 0 \quad \text{Eq. 3.55}$$

Simplifying Eq. 3.55 in terms of d, we obtain

$$d^3 - A_1d^3 - A_2d^3 - A_3 = 0 \quad \text{Eq. 3.56}$$

where,

$$A_1 = L_3 \quad \text{Eq. 3.57}$$

$$A_2 = 18 \left\{ \frac{R_1 + P_2 - \frac{1}{2}\gamma'(K_{p(design)} - K_a) - \frac{1}{2}2c(\sqrt{K_{p(design)}} + \sqrt{K_a})}{\gamma'(K_{p(design)} - K_a) + 2c(\sqrt{K_{p(design)}} + \sqrt{K_a})} \right\} \quad \text{Eq. 3.58}$$

$$A_3 = \frac{\left\{ L_3^3 \left[\frac{1}{3}\gamma'(K_{p(design)} - K_a) + \frac{1}{3}2c(\sqrt{K_{p(design)}} + \sqrt{K_a}) \right] \right\} - 6P_2(2 + L_3) - 18R_1L_5}{\gamma'(K_{p(design)} - K_a) + 2c(\sqrt{K_{p(design)}} + \sqrt{K_a})} \quad \text{Eq. 3.59}$$

The actual depth of penetration (D) is obtained by increasing d by about 20% to 40% or using a factor of safety of 1.5 to 2 (Murthy, 2002).

$$F_T = P_1 - R_1 \quad \text{Eq. 3.60}$$

The magnitude of the maximum moment of the wall is

$$M_{max} = \frac{P(l_2 + L_2 + z')}{8} \quad \text{Eq. 3.61}$$

where z' is the depth of zero shear force given by;

$$z' = \frac{\gamma HK_a}{(P_p - P_a)} \quad \text{Eq. 3.62}$$

CHAPTER 4 ANALYTICAL AND NUMERICAL MODELLING

4.1 Introduction

This chapter aims at introducing a general scheme of usage of both software's employed in the analytical and numerical modelling. The chapter only gives a summary in using the various software's presented to model a sheet pile wall with special emphases on the most relevant information necessary for the current study. This is because detailed information on the entire modelling technique can be obtained in the various software manuals.

4.2 GEOWALL Software

The software *GEOWALL* is a beta version developed using Microsoft Visual C#.Net 2013, as the programming tool, and Microsoft XNA Game Studio 4.0 framework; with the database handled with Microsoft Access. The software allows installation on recent versions of Windows Operating System (Windows 7 and latest versions). It consist of a splash screen and a main window.

4.2.1 Splash Screen and User Login

The splash screen is the start-up page of the software which welcomes users, giving them a brief idea about the software as shown in Figure 4.1. The splash screen has been set to 5 second after which it disappears, giving way to the login window.



Figure 4.1: Splash screen

The main window of the software is made active when the username and password of an existent user is correctly introduced or an account for a new user is correctly created (see Figure 4.2).

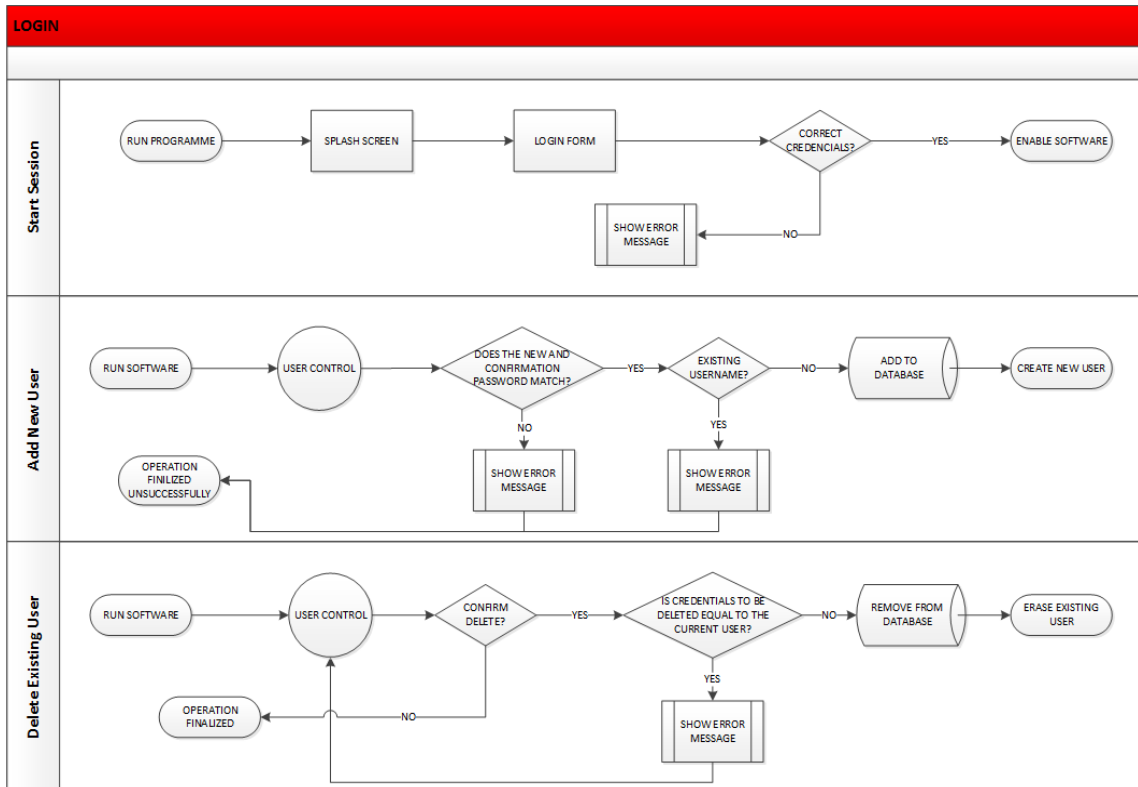


Figure 4.2: Flowchart showing user login functionality

4.2.2 Project Creation

GEOWALL has a main window and several sub windows for defining various parameters necessary for modelling a specific project. On the initialization of the software, after the user credentials have been correctly validated, all buttons are inactive. In order to start modelling a specific task, the user would have to create a new project (see Figure 4.3 and Figure 4.4). This is done by clicking on the 'New' button located in the 'File' Tab. The buttons are made active, after the user confirms the creation of the project.

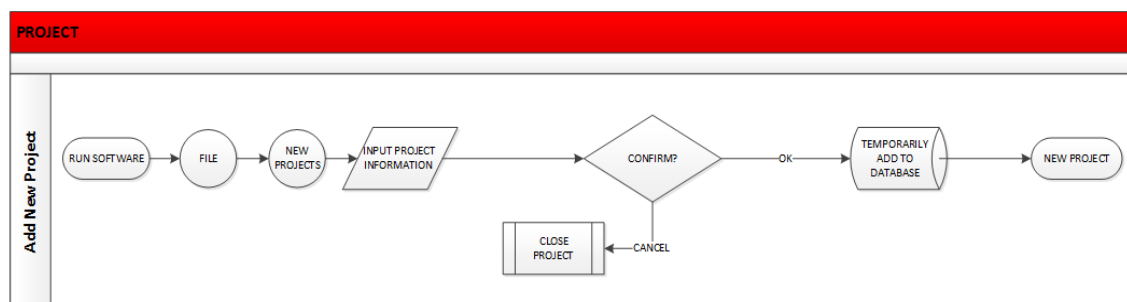


Figure 4.3: Flowchart showing project creation

New Project

Project

Project Name: Jäger Project

Date Created: jueves, 4 de junio de 2015

Project Designer: Sergio Garcia Giner

Locality: Berlin, Germany

Description: Anchored sheet pile wall design for the north-east section of the Jäger Project. The soil stratum is uniform in nature and surcharge force of 65kN is present

Wall Type

Cantilever Sheet Pile

Anchored Sheet Pile

Metric System

SI Unit

Imperial Unit

Passive Pressure

Factor of Safety: 1.0

Geometry

Excavation Height: 9 [m]

GroundWater

Yes No

OK Cancel

Figure 4.4: Project creation window

4.2.3 Project Modelling

Modelling can be started after a successful project has been created. All models necessary for modelling are found in the 'Data' tab of the software. The first step is the generation of a soil structure. This is done, clicking on the 'Soil Stratum' button. A dialog box appears where the user selects sample soils implemented into the software or simulates a different soil material. After the material creation is done and confirmed, the pile wall is then created. This is achieved by clicking on the 'Wall' button and following the same procedure as stated above for the generation of the material model. Other properties such as anchor, groundwater and surcharge can then be introduced added to the project, if necessary, by clicking on 'Anchor', 'Groundwater' and 'Surcharge' buttons respectively (refer to Figure 4.5 and Figure 4.6).

After the material and wall are successfully generated, the analyses can begin by clicking on the 'Run' button located in the 'Computation' tab.

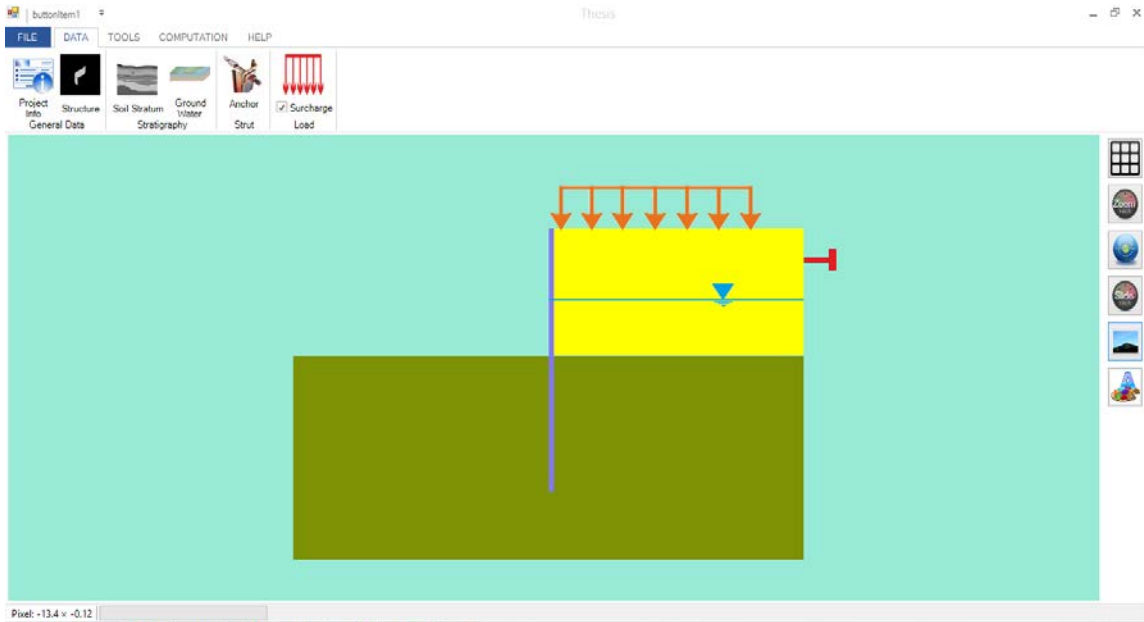


Figure 4.5: Main window showing a completed generated project

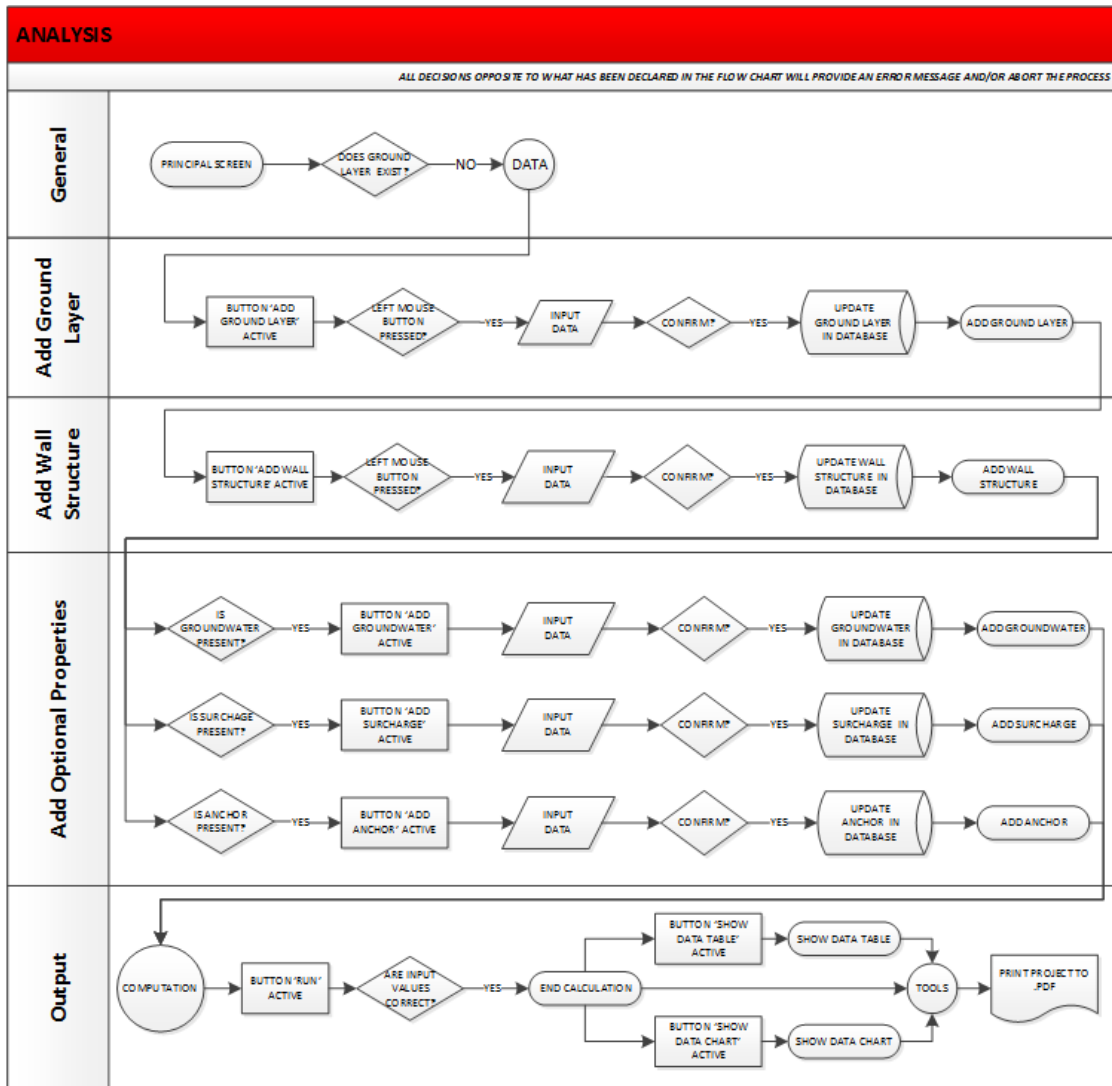


Figure 4.6: Flowchart of software simulation

4.2.4 Output

Results obtained from the project analyses can be viewed in the form of graphs and tables by clicking on the 'Results' and 'Stability Diagram' buttons located in the 'Computation' tab as shown in Figure 4.7. The entire project can also be exported into a PDF file for archiving and future reference.

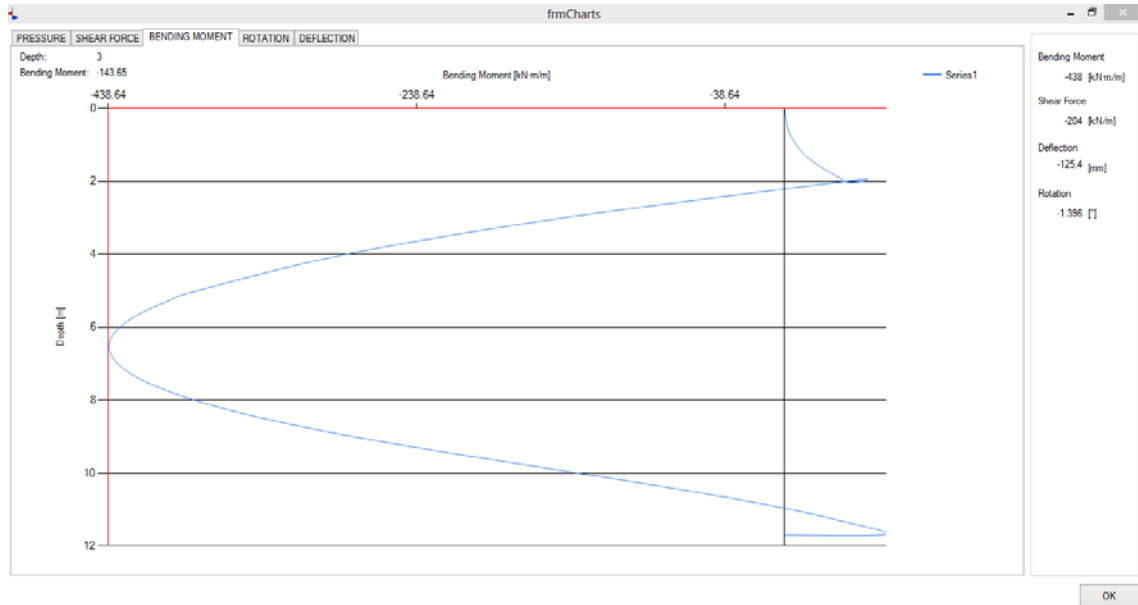


Figure 4.7: Maximum Bending Moment of the analyses

The software also includes additional events such as grid view, background colour selection, distance measurement, etc. that don't influence the pile wall analyses but enhances the manipulation of the software.

4.3 PROSHEET Software

PROSHEET is a commercial software developed in collaboration with ARCELOR COMMERCIAL RPS which employs the limit equilibrium method in its analyses. It uses the Logarithmic spiral theory, described in CHAPTER 2, in estimating the lateral earth pressure of the soil. Three static systems are possible in this software namely, cantilever, free earth support with one layer of anchor and fixed earth support with one layer of anchor, analysed with the Blum theory. Figure 4.5 to Figure 4.14 presented below shows a step-by-step procedure in analysing a sheet pile wall using *PROSHEET*.

- Start PROSHEET
- Set options:
 - Units
 - Project information
 - Configuration

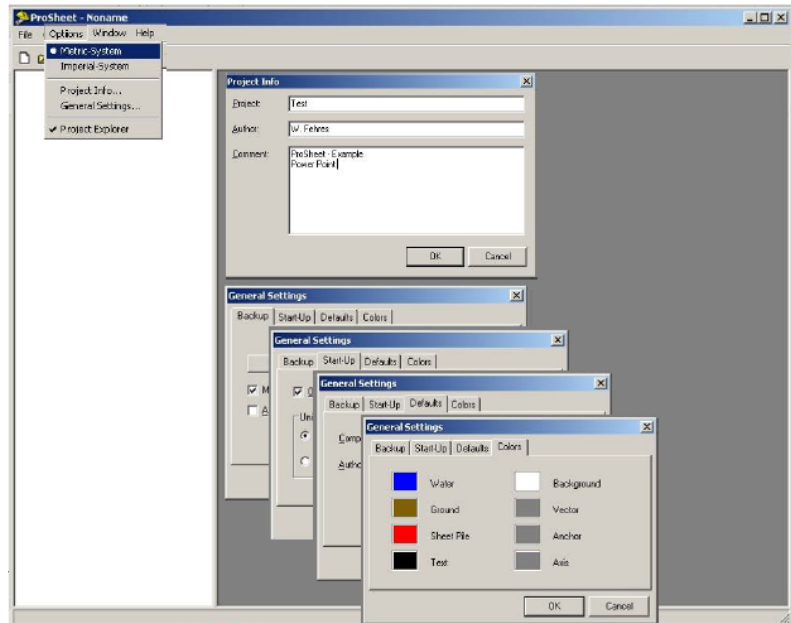


Figure 4.8: Units, configuration and Project information

- Fill in at least:
 - Geodata
 - Soil layers
 - Pile Section
- Don't click on OK until all the design data has been correctly filled in.

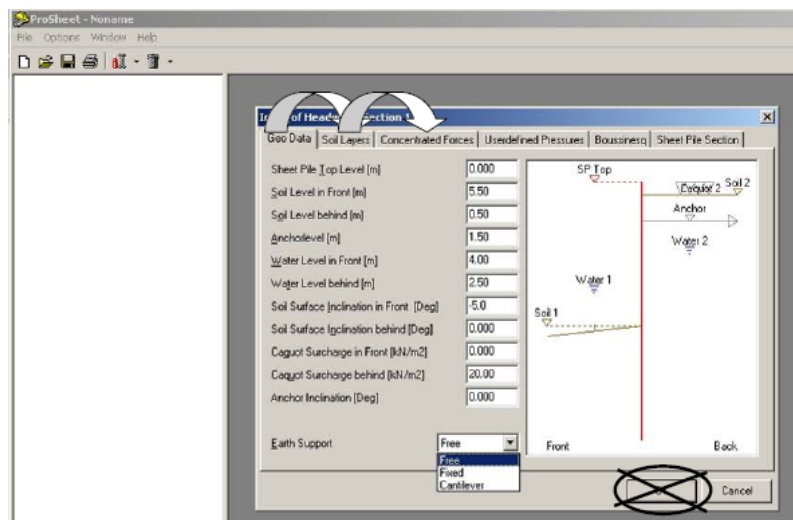


Figure 4.9: Design data

- Soil layers can be added or deleted and edited
- Check 'Automatic K_{ph} Value' and 'Automatic K_{ah} Values' checkboxes to automatically calculate the earth pressure coefficients
- For layer in Front soil-wall friction angle (Delta) should be negative and for layer behind Delta should be positive.

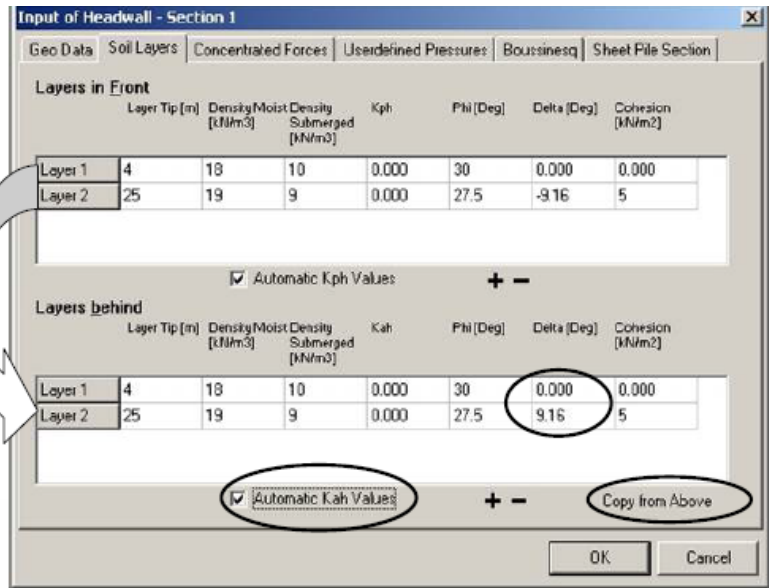


Figure 4.10: Soil layers

- Select the appropriate sheet pile necessary for the analyses
- Click on OK to begin the analyses.

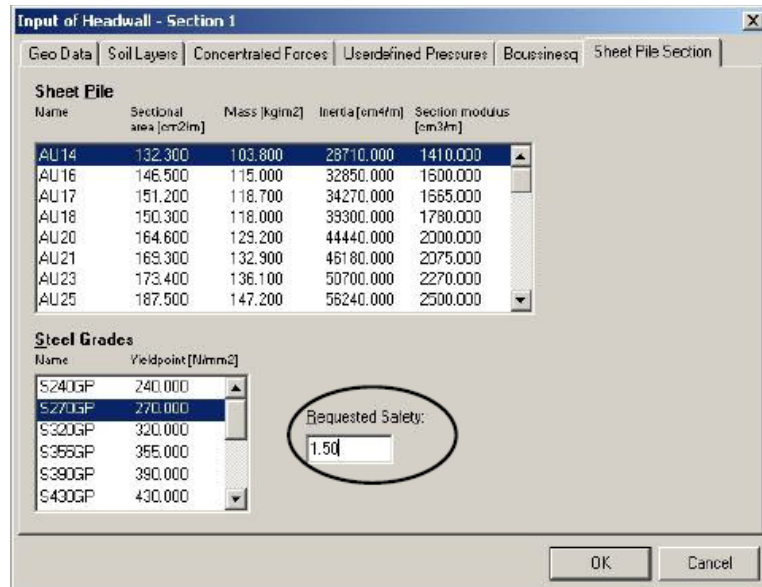


Figure 4.11: Sheet pile section

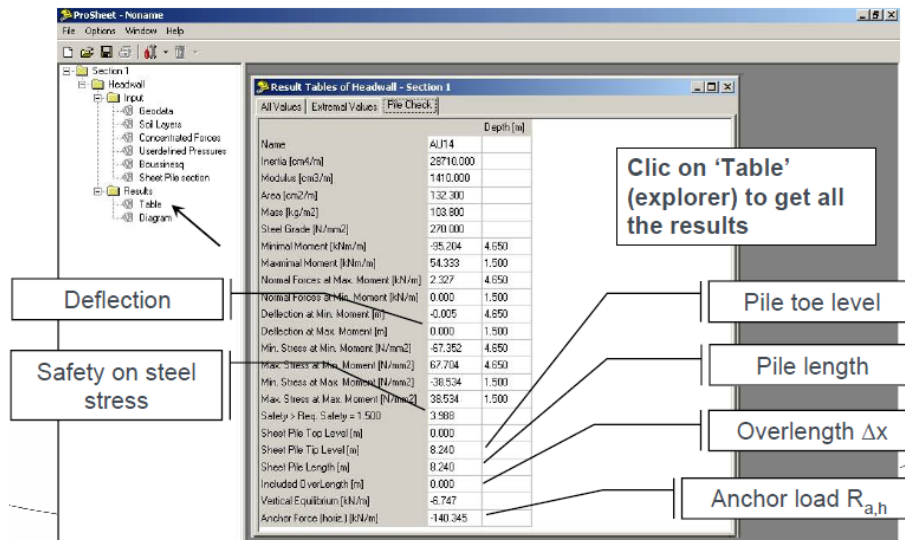


Figure 4.12: Results: Pile check values

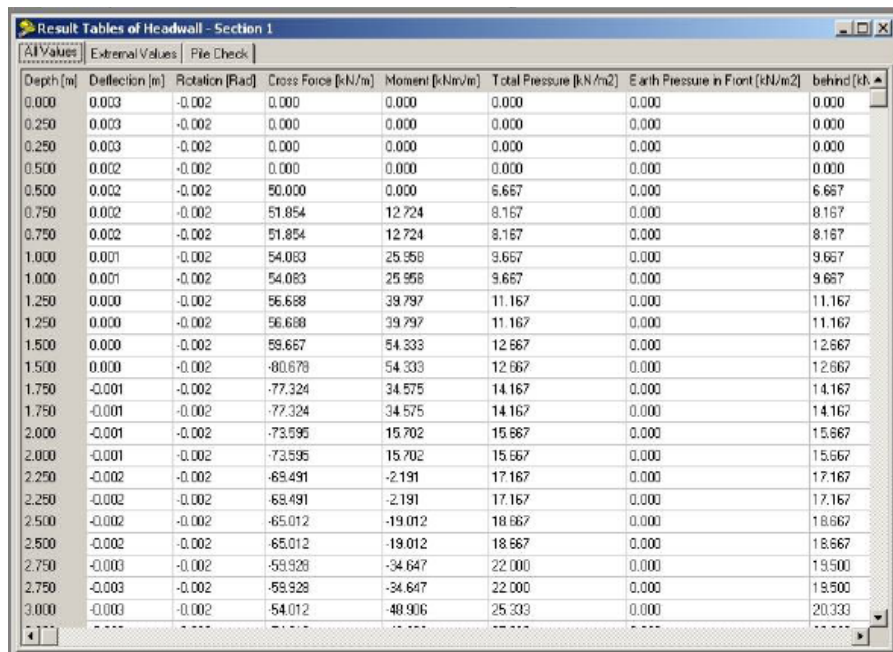


Figure 4.13: Results: All values

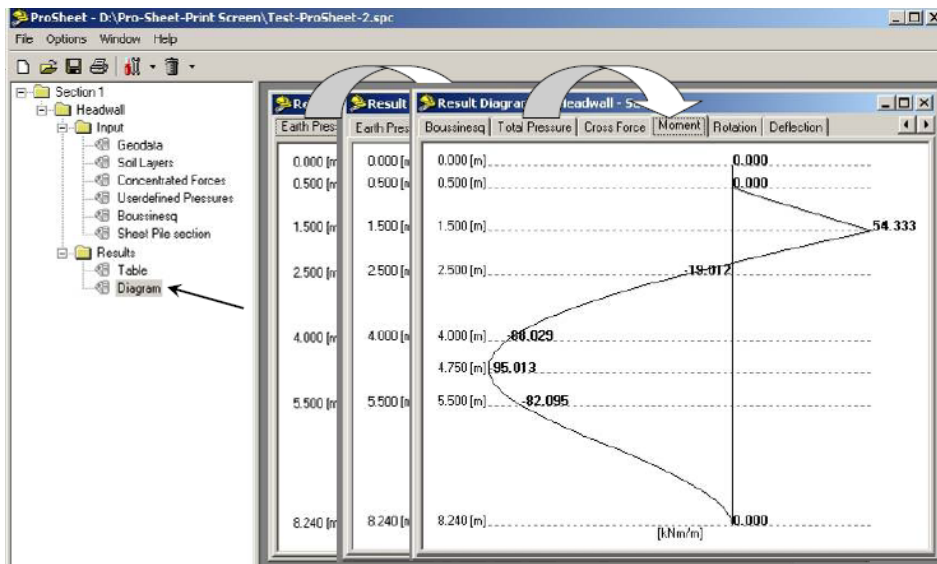


Figure 4.14: Result: Diagrams

4.4 Excel Macros Application

An Excel application is developed based on the principles of sheet pile wall design presented in Das (2011). It employs the Rankine theory in calculating the lateral earth pressure (i.e. wall friction angle is not considered). Unlike examples presented in the Das (2011), the Excel Application, models a sheet pile wall considering the soil's cohesion and surcharge forces, when present. The methodology used in developing the Excel Macros Application is presented in CHAPTER 3. However, the only difference in the methodology is that, K_a and K_p values used in the analyses are the Rankine coefficient of active earth pressure and passive earth resistance respectively as presented in Eq. 2.5 and Eq. 2.6 and not the Coulomb coefficient for lateral earth pressure as presented in CHAPTER 3. The setback in the Excel Application is that it doesn't calculate the maximum wall deflection. That is, only the bending moment and shear force distributions are calculated.

4.5 PLAXIS Software

4.5.1 Preamble

PLAXIS is a finite element software for analysing deformation, stresses and stability validation that occurs in constructions in the field of geotechnical engineering employing a loading analyses method (staged construction, total multipliers or incremental multipliers). There are different versions of PLAXIS software, each version analyse different type of structure/problem, namely PLAXIS 2D Foundation, PLAXIS 2D Tunnel, PLAXIS 3D Foundation and PLAXIS 3D Tunnel. The PLAXIS 2D Foundation, hereafter PLAXIS 2D, is used in this research.

PLAXIS 2D provides two different types of modelling:

- **Plane strain model** which is used for geometries with a (more or less) uniform cross section and corresponding stress state and loading scheme over a certain length perpendicular to the cross-section. Displacements and strains in the longitudinal direction are assumed to be zero, however normal stresses in the longitudinal direction are fully taken into account.
- **Axisymmetric model** which is used for circular structures with a (more or less) uniform radial cross section and loading scheme around to be identical in any

radial direction. Since the x-coordinate represents the radius and the y-coordinate corresponds to the axial line of symmetry, a negative x-coordinate cannot be used in an axisymmetric modelling.

The flow chart as shown below gives a summary of the general procedure of analysis employed by PLAXIS 2D.

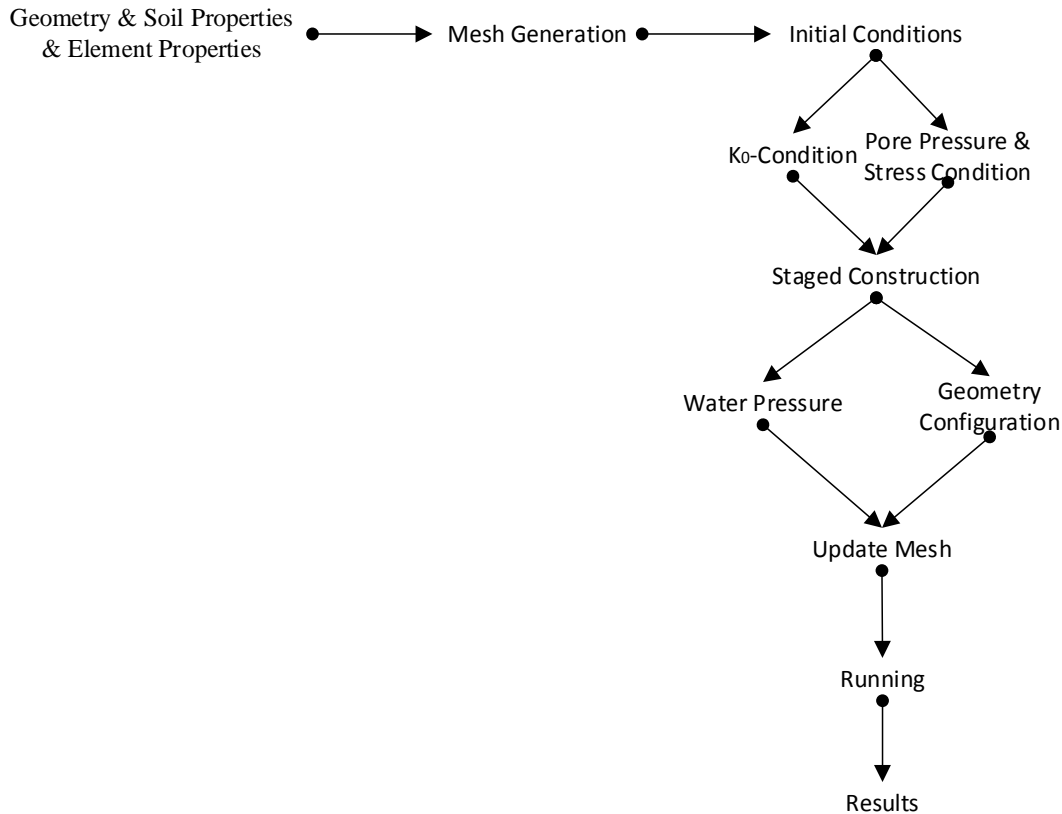


Figure 4.15: Flowchart for general analysis procedure in PLAXIS 2D

4.5.2 Modelling Sheet Pile Wall

The PLAXIS 2D program consists of four main interfaces; namely the Input, Calculations, Output and Curves, which are used successively in performing a geotechnical modelling. This section describes how a sheet pile wall is modelled using PLAXIS 2D in a methodological manner; from the Input to the Curve interface. An anchored sheet pile wall with a uniform distributed surcharge is used in the modelling procedure. The detailed modelling procedure can be found in the PLAXIS 2D user manual via www.plaxis.com; consequently, only a summary of the procedure would be introduced in this section.

Geometry

The first step consists of the creation of the geometry of the model. On the general settings window, shown in Figure 4.16, the user can select the general model used (plane strain), the element type (15-node triangle) and the dimensions.

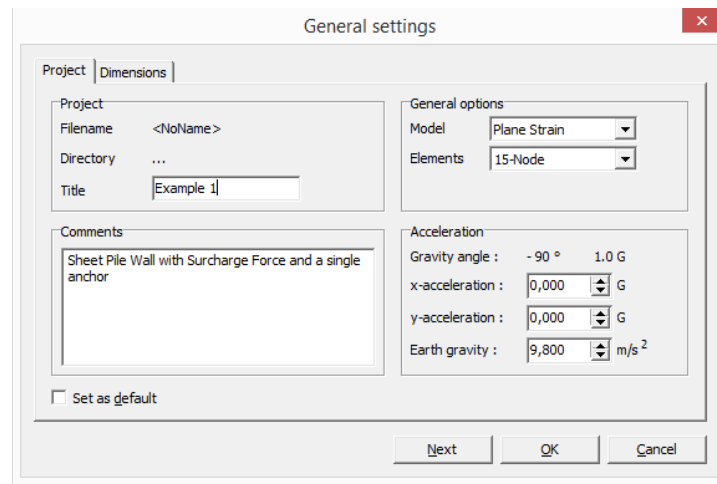


Figure 4.16: General setting window

A finite element mesh related to a given problem in geomechanics must always have dimensions that are sufficient for representing the problem. The mesh should be wide enough to include not only the stress changes in the soil mass beneath the wall, but also the potential development of long term active and passive stress failures, as well as the possibility of a deep circular failure. For the analysis of diaphragm and sheet pile walls, the dimensions of the mesh must be taken as in Figure 4.17 (Azizi, 1999).

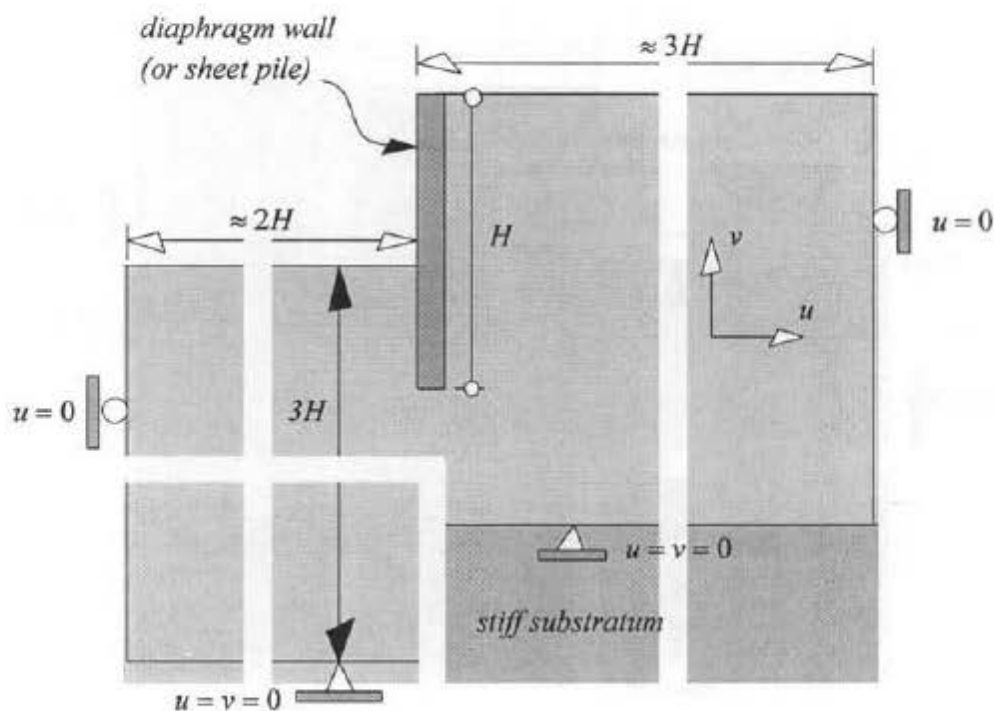


Figure 4.17: Typical mesh dimensions for a sheet pile wall retaining an isotropic homogenous soil (Azizi, 1999).

Modelling soil and structural behaviours and elements

The geometry can be represented by a set of independent lines. When these lines form a closed polygon, an independent cluster is created, where the soil properties can be applied. Diverse cluster can be created in order to model stratified soil or excavation levels. A standard fixity is applied on the boundary to ensure a non-zero prescribed displacement (displacement could occur on the soil surface).

Various material models are defined in the PLAXIS 2D software, however, the Mohr-Coulomb model is utilized in this research analysis. It represents a first order and fast

approximation, especially when detailed input parameters are not present. It is defined by five input parameters namely;

- Young Modulus and Poison Ratio; for soil elasticity
- Cohesion and Frictional Angle ; for soil plasticity
- Angle of Dilatancy.

Sheet pile walls are modelled through the element “Plate”. The software allows for elastic or elastoplastic behaviour in plate elements. The elastic behaviour, which is considered in the research, is defined by two parameters:

- Normal stiffness
- Bending stiffness

These parameters are used in calculating the equivalent plate thickness.

The soil-structure relationship, also known as interface is defined based on the soil material being used and the type of sheet pile wall. The interface is placed on both sides of the structure. The roughness of the interaction is modelled by choosing a suitable value for the strength reduction factor. This factor relates the wall friction and adhesion to the friction and cohesion of the soil. It has a significant effect on the output values of the sheet pile wall analysis, as will be seen in the next chapter. U.S. Army Corps of Engineers (1994) gives the relationship between the angle of internal friction (ϕ) and the wall friction angle (δ) and the values of wall friction angle for various interface as shown in Table 4.1 and Table 4.2 respectively.

Table 4.1: Ratio of δ/ϕ (Design of Sheet Pile Walls, 1994)

Soil Type	Steel	Wood	Concrete
Sand	$\delta/\phi = 0.54$	$\delta/\phi = 0.76$	$\delta/\phi = 0.76$
Silt & Clay	$\delta/\phi = 0.54$	$\delta/\phi = 0.55$	$\delta/\phi = 0.50$

Table 4.2: Values of δ for various interface (Design of Sheet Pile Walls, 1994)

Soil Type	δ (deg.)
(a) Steel sheet piles	
Clean gravel, gravel sand mixtures, well-graded rockfill with spalls	22
Clean sand, silty sand-gravel mixture, single size hard rockfill	17
Silty sand, gravel or sand mixed with silt or clay	14
Fine sandy silt, nonplastic silt	11
(b) Concrete Sheet piles	
Clean gravel, gravel sand mixtures, well-graded rockfill with spalls	22-26
Clean sand, silty sand-gravel mixture, single size hard rockfill	17-22
Silty sand, gravel or sand mixed with silt or clay	17
Fine sandy silt, nonplastic silt	14

In modelling the anchor element, the fixed anchor is used. These could also exhibit elastic or elastoplastic behaviour. Elastic behaviour is considered in this research but unlike plates, fixed anchor is defined solely by the bending stiffness. Distributed load is used to show the effect of surcharge force on the soil and sheet pile wall being analysed. The figure below shows a fully modelled sheet pile wall.

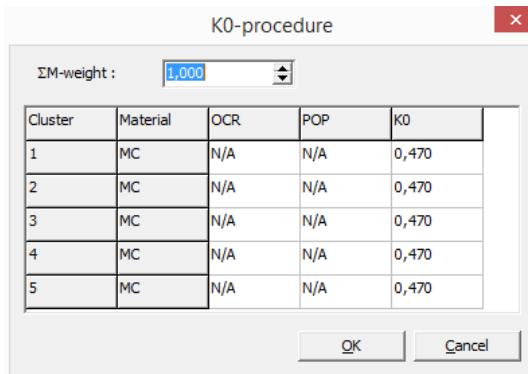


Figure 4.21: Window for entering K_0

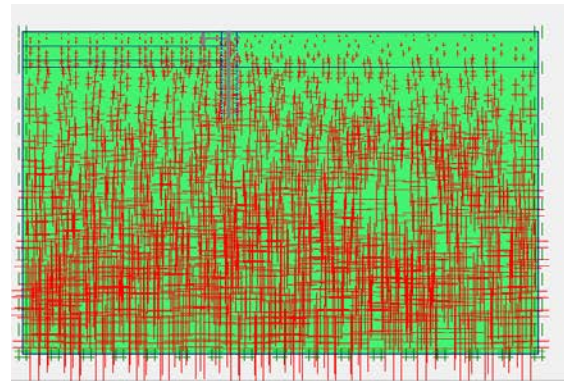


Figure 4.22: Initial effective stresses

Calculation module

The calculation module of the software is the part where analysis methods, numerical analysis parameters, construction stages, change of material properties and water levels are presented. The input method can be incremental multipliers, total multipliers or staged construction whereas the calculation types are defined as plastic analysis, consolidation analysis, phi/c reduction or dynamic analysis. The staged construction method and the plastic analysis are used in the current research. This is achieved by individually defining the construction stages for each step as shown below. The calculate button is then clicked after a point of maximum stress has been selected, to begin the simulation (see Figure 4.23).

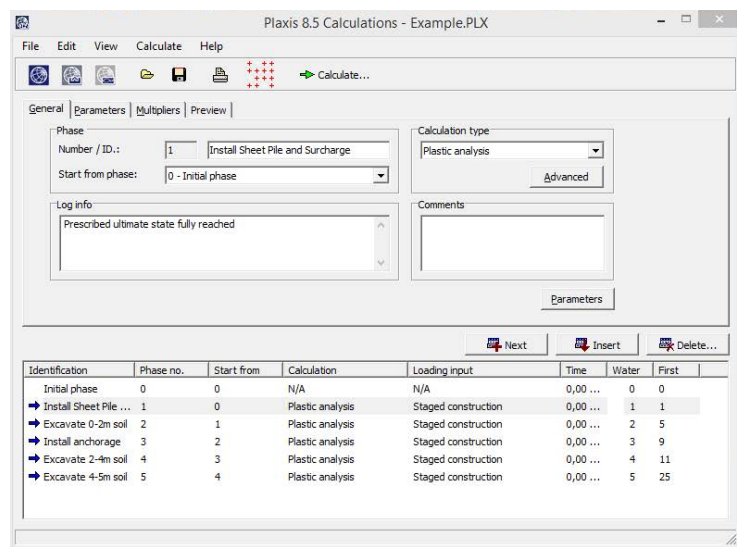


Figure 4.23: Calculation module

Output and Curve module

The main output quantities of the calculation are the displacements and the stresses. In addition, when the finite element model involves structural elements, such as sheet pile wall, the structural forces and bending moments in the elements are calculated as well. Also strain and pore-pressures are visualized for every phase of the calculation. Some curves, such as load-displacement and safety factor analysis curves, could be plotted. In addition, the shear forces and bending moments in the wall, showing their respective maximum values (see Figure 4.24, Figure 4.25 and Figure 4.26).

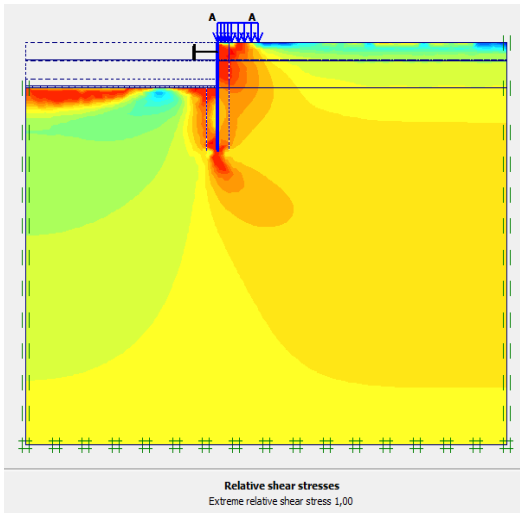


Figure 4.24: Stress diagram of an analysis

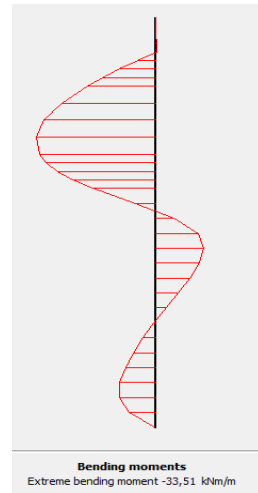


Figure 4.25: Bending Moment

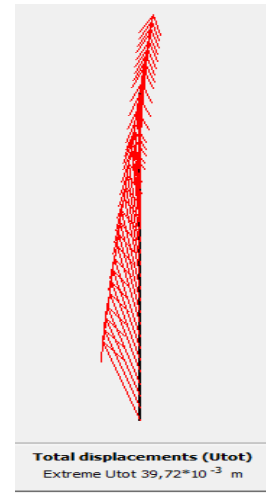


Figure 4.26: Displacement

CHAPTER 5 DATA ANALYSIS

5.1 Introduction

This chapter presents results of different examples analysed using *GEOWALL*, *PLAXIS 2D*, *Excel Macros Application* and *PROSHEET* and the variation in the output result for the various software carefully studied.

The chapter starts by studying the effect of the Rankine, the Coulomb and the Caquot and Kerisel earth pressure theories on the coefficient of passive earth resistance. A sensitivity analysis of the *PLAXIS 2D* is then undertaken in order to investigate the influence of different input parameters on the output values since the use of numerical methods requires a lot of input parameters compared to the analytical methods.

It follows up to present the data used in the analysis. The limit equilibrium methods (*GEOWALL*, *PROSHEET* and *Excel Macros Application*) are used in calculating the wall height necessary for stability and then. Since the final dredge depth obtained from the various limit equilibrium methods varies between each other, the wall height obtained from the *Excel Macros Application* used in *PLAXIS 2D* for the finite element modelling. Finally a regression analysis is presented to determine the variation each software presents with respect to its counterpart.

5.2 Lateral Earth Pressure Theories

Coulomb theory

Soil's frictional angle (φ) (from 25° to 40°) was varied with soil-wall frictional angle (δ) (from 0° to 25°) and the coefficient of passive earth resistance (K_p) (see Eq. 2.8) is obtained as shown in Table 5.1. As seen in CHAPTER 2, the Rankine value for the passive earth resistance is obtained when δ is 0° (compare Eq. 2.6 with Eq. 2.8). The inclination of the backfill soil (β) with respect to the sheet pile wall is considered to be 90° (or 0° with respect to the horizontal). *GEOWALL* was used in obtaining the values presented in Table 5.1 and the *Excel Macros Application* is also used to compare the values of K_p obtained when δ is 0°.

Table 5.1: Coulombs K_p values with varying φ and δ

Coefficient of Passive Earth Resistance Values						
φ	δ					
	0	5	10	15	20	25
25	2.464	2.833	3.285	3.855	4.597	5.599
28	2.77	3.215	3.77	4.484	5.436	6.757
30	3	3.505	4.143	4.977	6.105	7.704
32	3.255	3.829	4.565	5.541	6.886	8.833
35	3.691	4.391	5.309	6.555	8.324	10.98
40	4.599	5.593	6.946	8.872	11.771	16.473

A 3D graph plotted for the values presented in the table above (see Figure 5.1) shows an exponential rise in the value of the coefficient of passive earth resistance (K_p), when both φ and δ are increased. It is observed that the Rankine theory gave a much lower value in the K_p value than the Coulomb theory. The use of the Rankine theory is seen to exponentially underestimate the K_p value when the δ value is gradually increased.

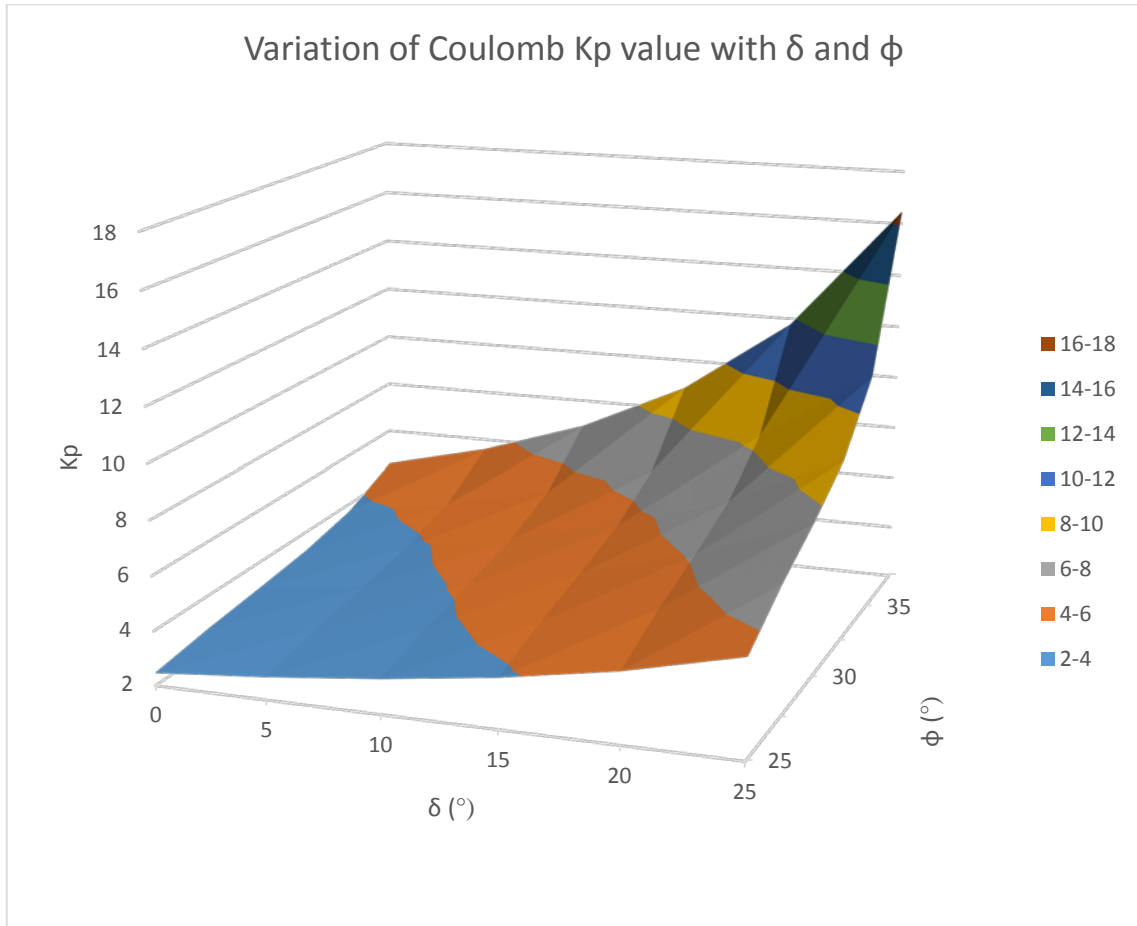


Figure 5.1: Variation of K_p value with δ and ϕ using the Coulomb theory

From the values obtained and the graph presented above, a relation between the K_p value for the Rankine and Coulomb theory is deduced.

$$K_{pCoulomb} = K_{pRankine} \cdot e^{\frac{\delta\phi \cdot \tan \beta}{100}} \quad \text{Eq. 5.1}$$

where;

$K_{pCoulomb}$ = Coulomb's coefficient of passive earth resistance

$K_{pRankine}$ = Rankine's coefficient of passive earth resistance

δ = Soil-Wall friction angle (Interface angle)

ϕ = Soil's friction angle

β = Angle of inclination of backfill soil with respect to the sheet pile wall (**vertical**)

β , as stated earlier in this section, is considered to be 90° . However, due to mathematical constraints, a value of 89.925° has been used. This simplifies Eq. 5.1 Figure 5.1 to Eq. 5.2.

$$K_{pCoulomb} = K_{pRankine} \cdot e^{\frac{0.13\delta\phi}{100}} \quad \text{Eq. 5.2}$$

Logarithmic spiral theory

Just like the Coulomb analyses performed as shown in Table 5.1, Table 5.2 shows the analyses performed with the log spiral theory as presented in CHAPTER 2. *PROSHEET* was used in obtaining the values presented in Table 5.2 and the *Excel Macros Application* is also used to compare the values of K_p obtained when δ is 0° .

Table 5.2: Log spiral K_p values with varying ϕ and δ

Coefficient of Passive Earth Resistance Values						
ϕ	δ					
	0	5	10	15	20	25
25	2.46	2.862	3.266	3.698	4.046	4.34
28	2.776	3.273	3.777	4.334	4.874	5.28
30	3	3.58	4.16	4.8	5.51	6.005
32	3.256	3.938	4.621	5.381	6.23	6.926
35	3.69	4.556	5.421	6.384	7.477	8.56
40	4.6	5.92	7.24	8.69	10.4	12.485

Figure 5.2 shows a 3D graph plotted based on values in Table 5.2. The figure shows a linear increment in the K_p values as the ϕ and δ values increases. Comparing K_p values in Table 5.2 with Table 5.1 when $\delta=0$, it is observed that, Rankine K_p value obtained is equal in both Coulomb and Log spiral theories.

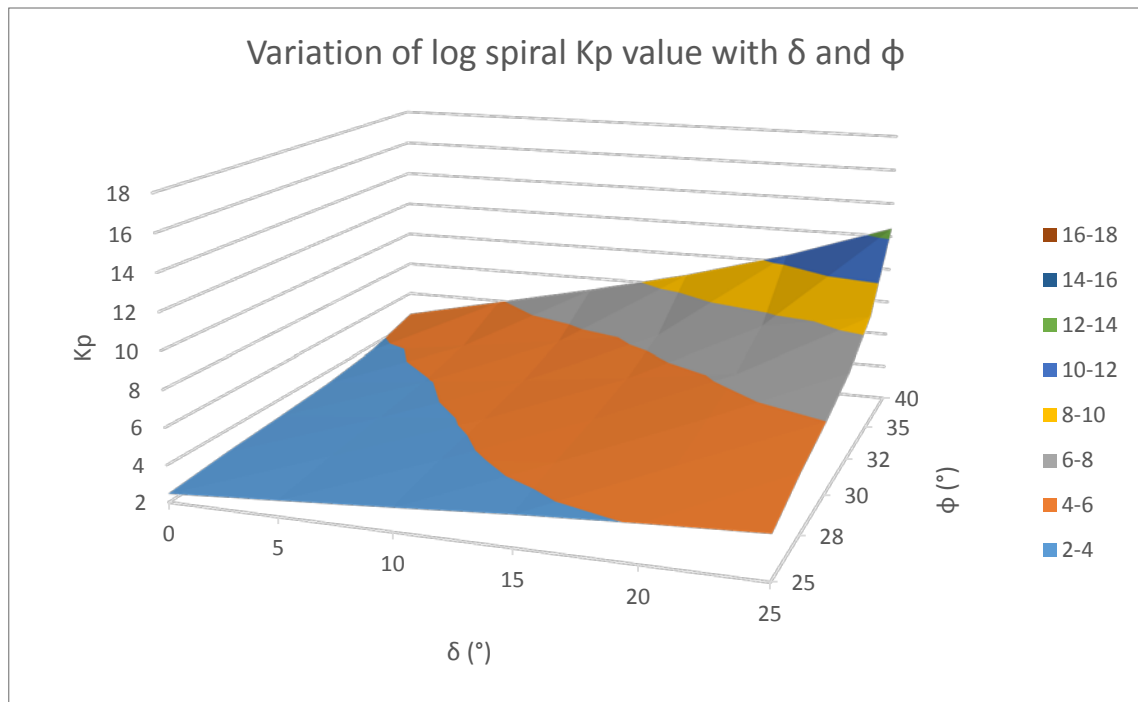


Figure 5.2: Variation of K_p value with δ and ϕ using the log spiral theory

A relationship between the K_p values for the log spiral theory and the Rankine theory is deduced based on the values obtained and is represented below.

$$K_{p_{\log\text{spiral}}} = K_{p_{\text{Rankine}}} + 0.0075\delta e^{0.0931\phi} \quad \text{Eq. 5.3}$$

Comparison of the Coulomb and logarithmic spiral theory

Table 5.3 is obtained by subtracting the values of Table 5.2 from Table 5.1. The Table 5.3 shows an increase in ΔK_p values when the δ and ϕ values increases. According to Das (2010), this phenomenon is due to the fact that the Coulomb theory assumes that the potential failure surface in the backfill is planar instead of curved, as seen in the log spiral theory. The curvature becomes more concave as the frictional angle increases, increasing the difference in the K_p value. Das (2010) concludes that unsafe results may be obtained when the Coulomb theory is employed for higher frictional angles (normally when $\frac{\delta}{\phi} > 0.5$), and as a correction to this, the log spiral theory could be employed since it is less conservative.

Table 5.3: Difference in K_p Values between Coulomb and log spiral theories

Difference in K_p Values between Coulomb and log spiral theories						
ϕ	δ					
	0	5	10	15	20	25
25	0.0	0.0	0.0	0.2	0.6	1.3
28	0.0	0.1	0.0	0.2	0.6	1.5
30	0.0	0.1	0.0	0.2	0.6	1.7
32	0.0	0.1	0.1	0.2	0.7	1.9
35	0.0	0.2	0.1	0.2	0.8	2.4
40	0.0	0.3	0.3	0.2	1.4	4.0

5.3 Sensitivity Analysis of PLAXIS 2D

The main purpose of this section is to review the extent to which the input parameters used in analysing a sheet pile wall affects the output results. Input values that have been considered in this analysis includes the soil-wall interface, the Poisson ratio of the soil and the normal and bending stiffness's of the wall. It is obvious that the unit weight of the soil, the soils cohesion and the soil's frictional angle have a significant effect on the analysis results and also, because the limit equilibrium method takes into consideration these parameters, and as such the research does not undertake sensitivity analyses for the above mentioned parameters. The input data used in the analyses are given in Figure 5.3 and Table 5.4. Table 5.5 shows the output values obtained by varying the soil's Poisson ratio (ν) from 0.2 to 0.4 and the soil's elastic modulus (E_{ref}) from 1.3MPa to 1300MPa and Table 5.6 shows the output values obtained after varying the soil-wall interface value (from 0.34 to 1), the normal stiffness of the wall (EA) (from 100 MNm²/m to 50000 MNm²/m) and the flexural stiffness of the wall (EI) (from 500 MN/m to 750000 MN/m).

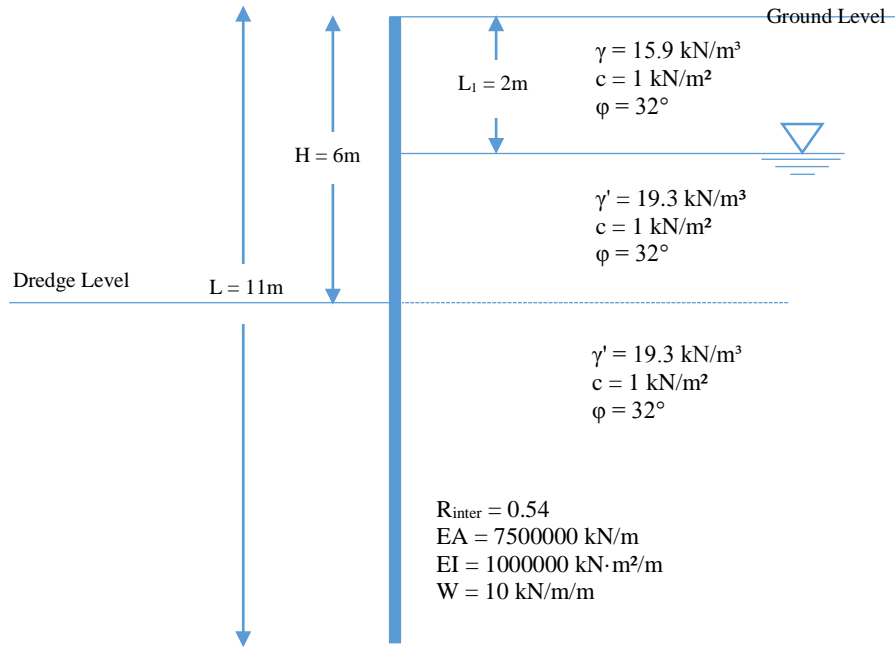


Figure 5.3: Geometrical and geotechnical parameters for sensitivity analyses

Table 5.4: Input Parameters for Sensitivity Analysis

General Properties		
Parameter	Drained	
Material model	Elastic	
Type of material behaviour	Mohr-Coulomb	
Element	15-Node	
Mesh	Medium	
Total Length of Sheet pile wall	11	m
Groundwater level	2	m
Soil Properties		
Soil unsaturated unit weight (γ_{unsat})	15.9	kN/m ³
Soil saturated unit weight (γ_{sat})	19.33	kN/m ³
Permeability in horizontal direction (K_x)	1	m/day
Permeability in vertical direction (K_y)	1	m/day
Young's modulus (E)	13000	kN/m ²
Poisson's ratio (u)	0.3	-
Cohesion (C)	1	kN/m ²
Friction angle (ϕ)	32	°
Dilatancy angle (ψ)	0	°
Soil-wall interface strength (R_{inter})	0.54	-
Wall Properties		
Normal Stiffness (EA)	7500000	kN/m
Bending Stiffness (EI)	1000000	kN·m ² /m
Equivalent thickness (d)	1.265	m
Weight (W)	10	kN/m/m
Poisson's ratio (u)	0	-

Table 5.5: Output values (maximum displacement, maximum shear force and maximum bending moment) for different Poisson Ratio and E_{ref} values

Poisson Output Values			E_{ref} Output Values			Units
u = 0.2	Displacement	0.02704	$E_{ref} = 1.3\text{MPa}$	Displacement	0.02704	m
	Max. SF	42.92		Max. SF	42.92	kN/m
	Max. BM	116.47		Max. BM	116.47	kN·m/m
u = 0.3	Displacement	0.02875	$E_{ref} = 13\text{MPa}$	Displacement	0.02875	m
	Max. SF	43.48		Max. SF	43.48	kN/m
	Max. BM	121.15		Max. BM	121.15	kN·m/m
u = 0.4	Displacement	0.0268	$E_{ref} = 130\text{MPa}$	Displacement	0.0268	m
	Max. SF	44.21		Max. SF	44.21	kN/m
	Max. BM	123.12		Max. BM	123.12	kN·m/m

Table 5.6: Output values (maximum displacement, maximum shear force and maximum bending moment) for different Interface, EI and EA values

Interface Output Values			EI Output Values			EA Output Values			Units
Interface = 0.34	Displacement	0.04338	EI = 100 MNm ² /m	Displacement	0.04931	EA = 500 MN/m	Displacement	0.02965	m
	Max. SF	46.44		Max. SF	40.84		Max. SF	43.4	kN/m
	Max. BM	136.15		Max. BM	117.04		Max. BM	121.68	kN·m/m
Interface = 0.54	Displacement	0.02875	EI = 1000 MNm ² /m	Displacement	0.02857	EA = 4500 MN/m	Displacement	0.02856	m
	Max. SF	43.48		Max. SF	43.48		Max. SF	43.48	kN/m
	Max. BM	121.15		Max. BM	120.91		Max. BM	120.91	kN·m/m
Interface = 0.67	Displacement	0.02688	EI = 10000 MNm ² /m	Displacement	0.02663	EA = 6500 MN/m	Displacement	0.02855	m
	Max. SF	41.95		Max. SF	43.95		Max. SF	43.54	kN/m
	Max. BM	110.6		Max. BM	121.34		Max. BM	121.01	kN·m/m
Interface = 1	Displacement	0.02692	EI = 50000 MNm ² /m	Displacement	0.02651	EA = 7500 MN/m	Displacement	0.02875	m
	Max. SF	38.45		Max. SF	44.02		Max. SF	43.48	kN/m
	Max. BM	98.15		Max. BM	121.6		Max. BM	121.15	kN·m/m
						EA = 75000 MN/m	Displacement	0.02881	m
							Max. SF	43.59	kN/m
							Max. BM	122.21	kN·m/m
						EA = 750000 MN/m	Displacement	0.02855	m
							Max. SF	43.54	kN/m
							Max. BM	121.01	kN·m/m

The following conclusions can be made based on results from tables and figures given above:

- The interface value is seen to have a significant effect on the various output parameters of the sheet pile wall analyses with the difference in the various output values ranging between 25% - 40%. That is the finite element method shows the important role played by the wall friction angle on the output results. This support discussions made in CHAPTER 2 in relation to the lateral earth pressure theories. That is, from the results obtained in Figure 5.4, and from the Lateral Earth Pressure Theories seen in this current chapter, it can be inferred that the use of the Rankine earth pressure theory underestimates to a great extent the output results (bending moment, shear force and wall deflection) obtained from the analyses because it fails in considering the soil-wall frictional angle. This shortcoming is however corrected when the Coulomb or the log spiral theory is employed in sheet pile wall analyses.

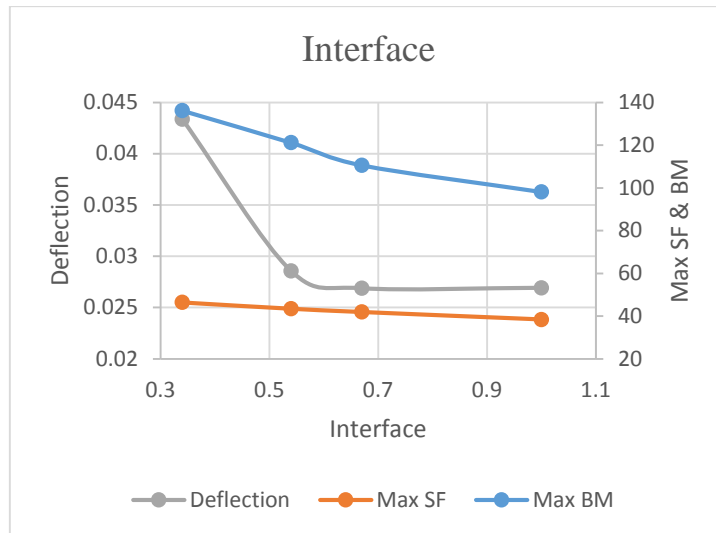


Figure 5.4: Correlation between the maximum shear force, the maximum bending moment and the wall deflection with different interface values

- Both the Poisson's ratio of the soil and the normal stiffness of the sheet pile wall had a little effect (less than 5% variation) on the wall displacement value, the maximum shear force and the maximum bending moment values (see Figure 5.5 and Figure 5.6). As a result, omitting these input parameters in the limit equilibrium analyses of the sheet pile wall, as presented in CHAPTER 3, does not significantly affect its output results.

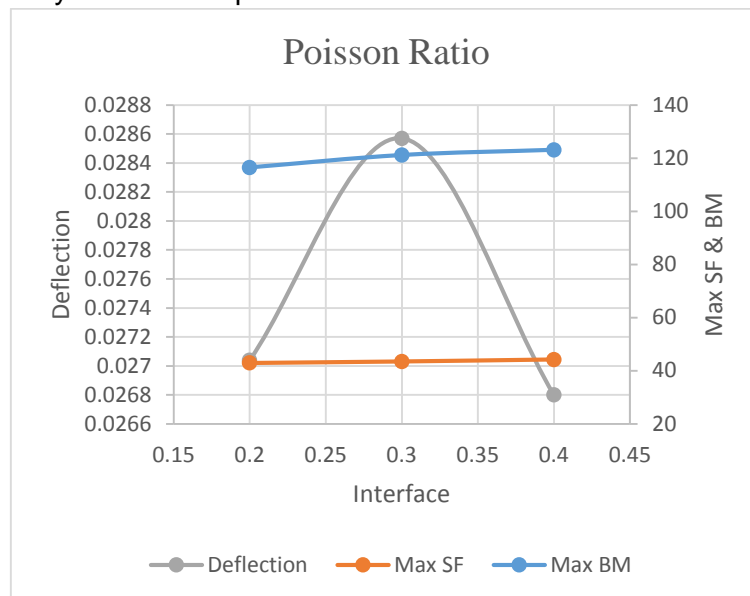


Figure 5.5: Relationship between the maximum shear force, the maximum bending moment and the wall deflection with the different Poisson's ratio values

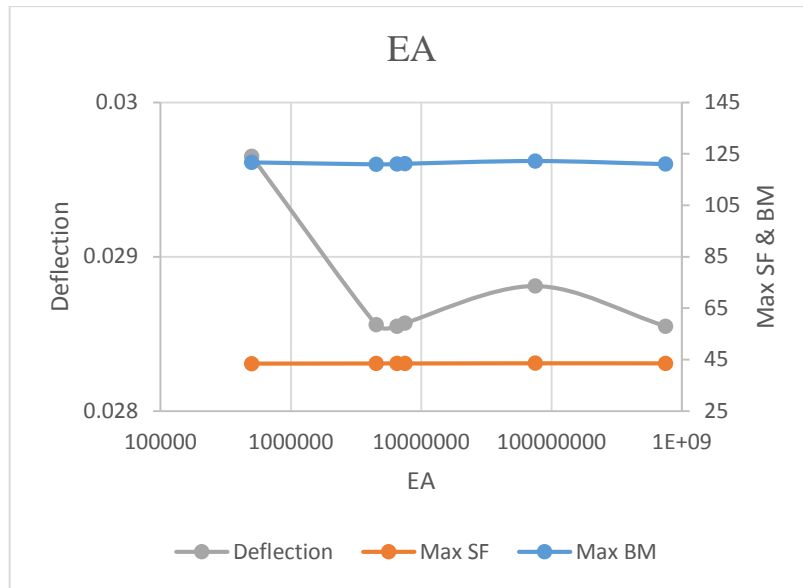


Figure 5.6: Correlation between the maximum shear force, the maximum bending moment and the wall deflection with varying wall normal stiffness values

- There exists a little variation in the bending moment and shear force values but a rather larger variation in the deflection value with respect to changes in the E_{ref} of the soil as indicated in Figure 5.7. An increase in the E_{ref} value increases the stiffness of the soil and hence increasing the soil's resistance to bending. This consequently decreases the ease with which the sheet pile wall deflects. The vice versa occurs when the E_{ref} value decreases. The limit equilibrium method, as presented in CHAPTER 2, falls short in mathematically representing the explained hypotheses.

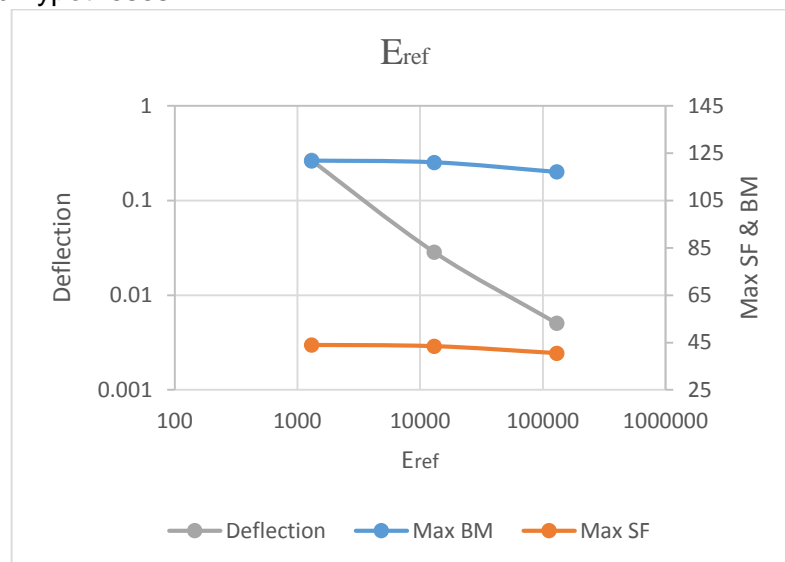


Figure 5.7: Relationship between the maximum shear force, the maximum bending moment and the wall deflection with varying soil elastic modulus values

- The bending stiffness presented a very low influence on variation in the bending moment and shear force values, but showed a significant effect on the wall displacement as seen in Figure 5.8. This can be supported with the beam curvature theory as explained in (Hulse, et al., 2000) which states that the vertical

deflection of the wall (y) is given by the double integration of the ratio of the Moment (M) and the bending stiffness (EI) of the wall ($y = \iint \frac{M}{EI}$).

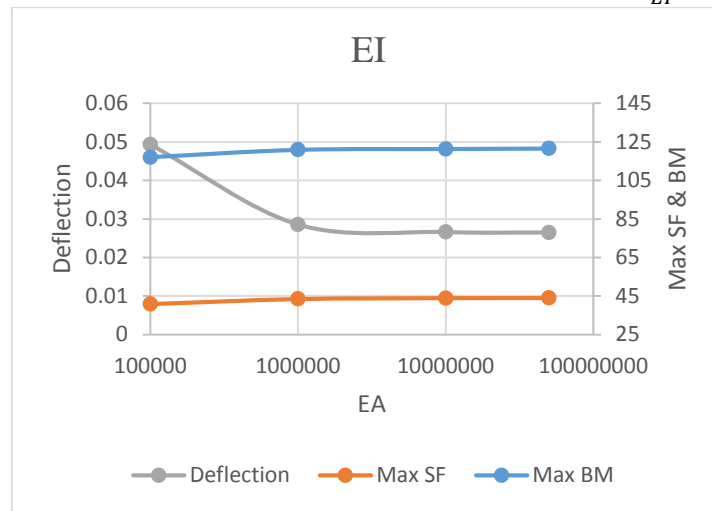


Figure 5.8: Correlation between the maximum shear force, the maximum bending moment and the wall deflection with varying wall bending stiffness values

Table 5.7 presents a summary of the discussion explained from the sensitivity analyses represented above.

Table 5.7: Percentage difference in extreme values

Output Values	Interface	EA	EI	u	E_{ref}
Displacement	38%	<5%	46%	<5%	98%
Maximum Shear Force	17%	<5%	8%	<5%	8%
Maximum Bending Moment	28%	<5%	<5%	5%	<5%

Based on the results presented above, a sensitivity analyses was carried out in order to ascertain the influence of the various input parameters on the output parameters of the sheet pile wall.

The maximum shear force tornado plot (see Figure 5.9) shows that the interface is the input parameter that largely affects the output results and the normal stiffness has the lowest influence on the output value. This same trend can be observed in the maximum bending moment tornado plot as shown in Figure 5.10. It can be seen from Figure 5.9 and Figure 5.10 that the Poisson's ratio, the E_{ref} value and the bending stiffness have a rather significant effect on the shear force but have a low effect on the bending moment.

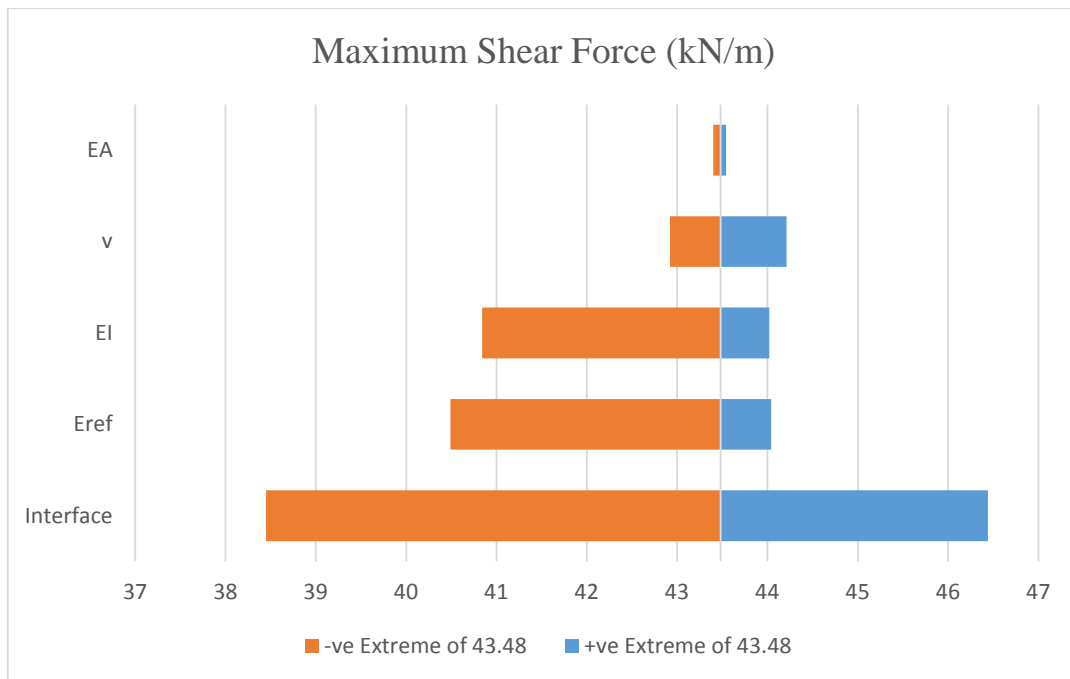


Figure 5.9: Tornado plot for maximum shear force parameter

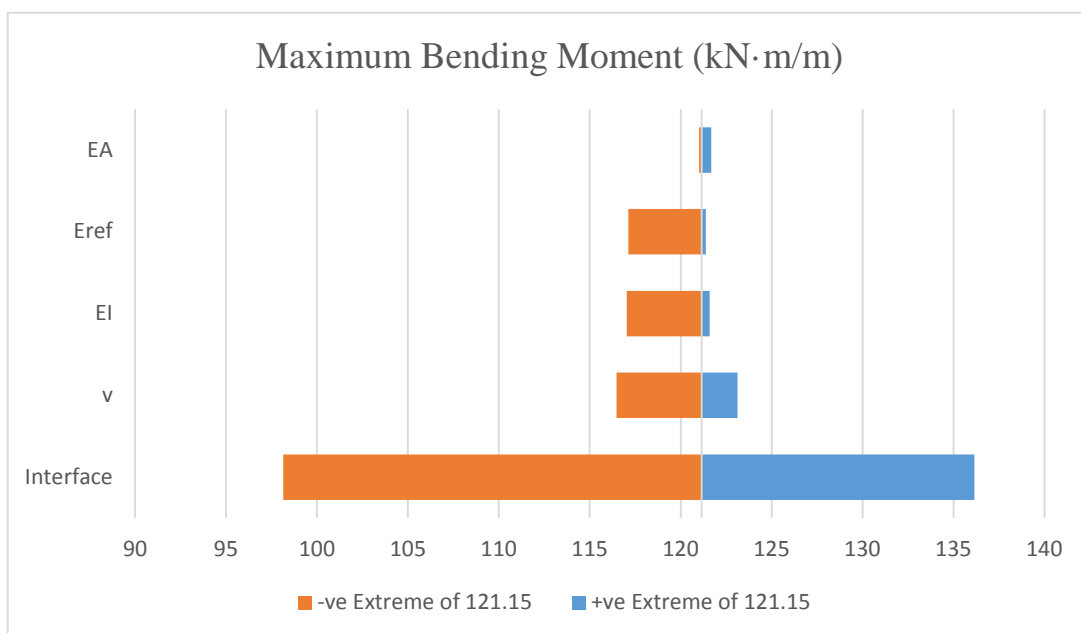


Figure 5.10: Tornado plot for maximum bending moment parameter

Figure 5.11 shows that the E_{ref} value of the soil has a great effect on the wall deflection. This phenomenon, as explained above, is due to the soil stiffness characteristics. It can be concluded that the limit equilibrium gives a major shortcoming in failing to implement the effect of the E_{ref} on the deflection of the sheet pile wall. From Figure 5.11, it can be concluded that the bending stiffness input parameter has a greater influence on the displacement of the sheet pile wall. This is attributed to the fact that, as explained above, the moment parameter is very sensitive to change in the interface value. This is supported by the equation of the beam theory (Hulse, et al., 2000). The interface is also seen to have a somewhat significant effect on the wall deflection.

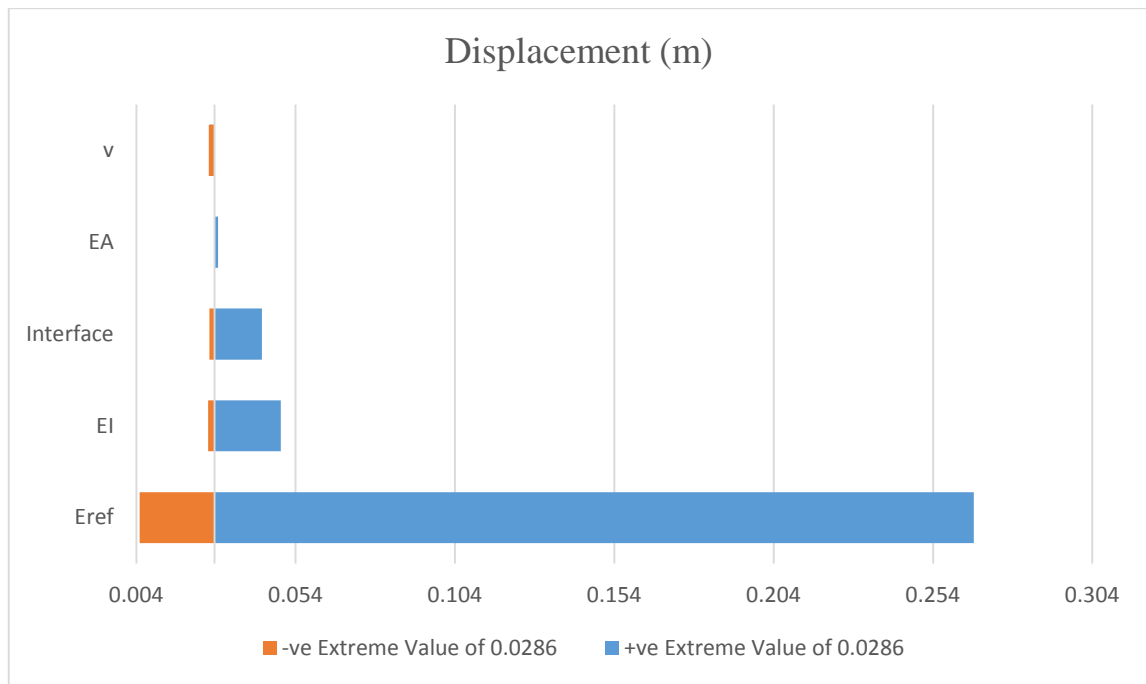


Figure 5.11: Tornado plot for displacement parameter

5.4 Data Analyses and Results

5.4.1 Cantilever Wall

Figure 5.12, Table 5.8 and Table 5.10 show the material and wall properties used in the cantilever analyses. *GEOWALL* is used to first and foremost analyse the data presented below. The total depth obtained from the *GEOWALL* analyses is then introduced into *PLAXIS 2D* for the numerical analyses. *PROSHEET* and the *Excel Macros Application* are also used in modelling the same problem for comparison and constructive analyses.

From the sensitivity analyses presented previously in Section 3 of CHAPTER 5, some of the analysed parameters necessary solely for *PLAXIS 2D* modelling are presented in Table 5.9. These values are used because they are considered to be the average values for sand, which is the material considered in the analyses.

Table 5.8: Material property of the sheet pile wall

Parameter	Wall 1	Unit
Normal Stiffness (EA)	7.5×10^6	kN/m
Bending Stiffness (EI)	1.0×10^6	kN·m ² /m
Equivalent thickness (d)	1.265	m

Table 5.9: Constant properties used in *PLAXIS 2D* throughout the analyses

Parameter	Property/Value	Unit
Material		
Material model	M-C	-
Type of material behaviour	Drained	-
Permeability in x-direction (k_x)	1	m/day
Permeability in y-direction (k_y)	1	m/day
Modulus of elasticity (E_{ref})	13	MPa
Poisson ratio (ν)	0.3	-
Dilatancy angle (ψ)	0	°
Plate		
Material type	Elastic	-
Weight (w)	10	kN/m/m
Poisson ratio (ν)	0	-
Rayleigh (α)	0	-

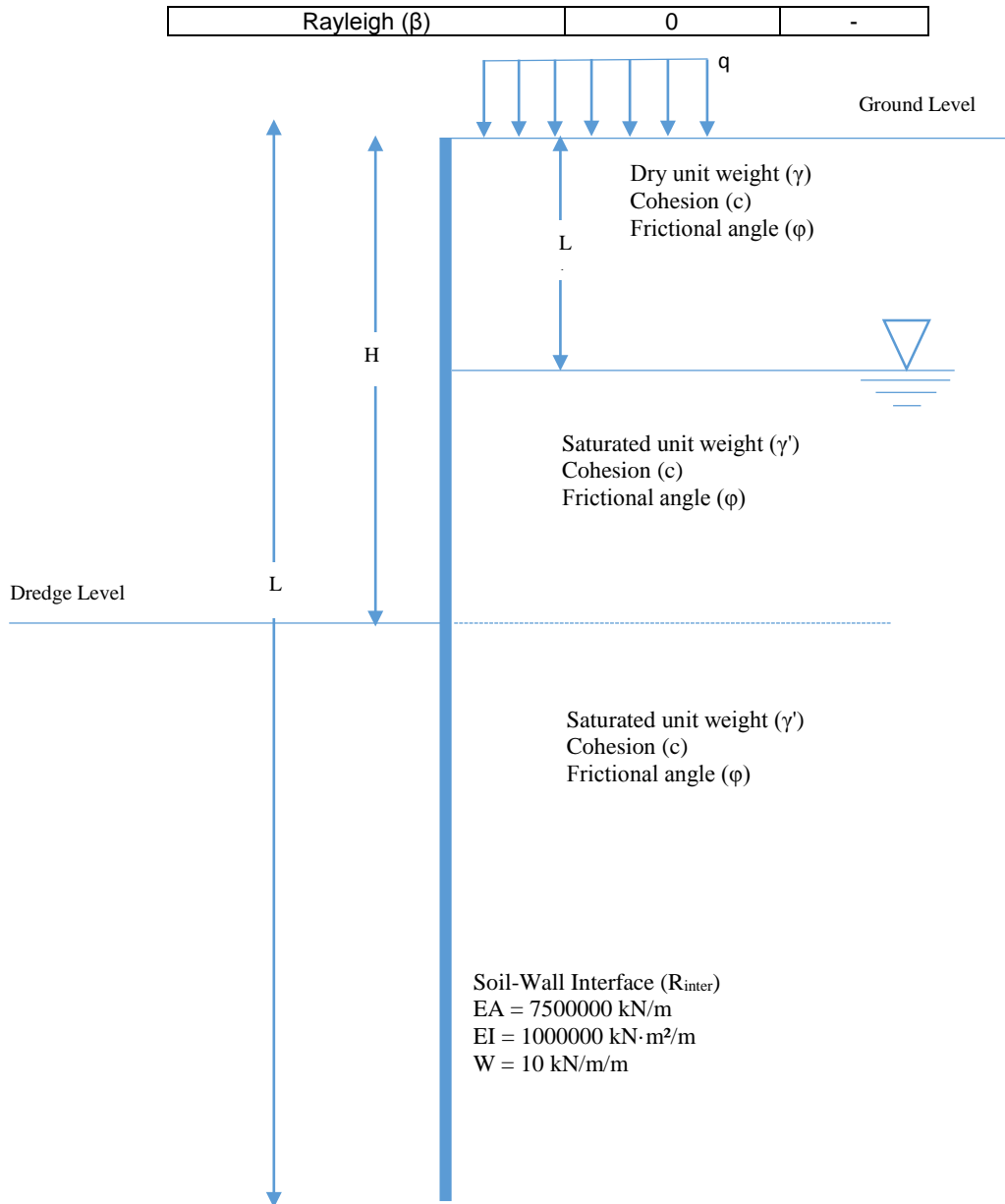


Figure 5.12: Geometrical and geotechnical parameters for cantilever analyses

Table 5.10: Material properties of the soil type studied for the cantilever wall analyses.

Parameter	Mat. 1	Mat. 2	Mat. 3	Mat. 4	Mat. 5	Mat. 6	Mat. 7	Mat. 8	Mat. 9	Mat. 10	Unit
Excavation height (H)	5	4	6	6	5	4	5	5	6	6	m
Groundwater level (L_1)	2	0	2	3	1	1	3	2	2	0	m
Soil saturated unit weight (γ_{sat})	19.33	16	19	20	18	19.04	20.5	18	19.5	21	kN/m ³
Soil unsaturated unit weight (γ_{unsat})	15.9	16	17	18	16	14.8	16	14.5	15.9	21	kN/m ³
Cohesion (C)	1	1	1	3	1	0.3	0.5	0.6	1	0	kN/m ²
Friction angle (ϕ)	32	30	36	42	25	28	32	35	30	28	°
Soil-wall interface strength (R_{inter})	0.54	0.67	0.54	0.63	0.5	0.67	0.63	0.6	0.54	0.67	-
Surcharge (q)	0	0	0	0	0	40	22.5	30	20	25	kN/m ²

Table 5.11: Output result obtained from cantilever wall analyses using various software's

Cantilevered Wall Output Properties	Mat. 1	Mat. 2	Mat. 3	Mat. 4	Mat. 5	Mat. 6	Mat. 7	Mat. 8	Mat. 9	Mat. 10	Unit
GEOWALL SOFTWARE											
Total Wall Length Obtained	9	7	9	8	11	9	9	9	12	11	m
Maximum Shear Force	45	37	54	41	52	88	86	75	109	181	kN/m
Maximum Bending Moment	123	75	164	92	183	310	281	248	461	700	kN·m/m
Maximum Horizontal Deflection of Wall	138	47	203	50	38	60	43	37	125	156	mm
PROSHEET SOFTWARE											
Total Wall Length Obtained	8	7	9	8	10	9	9	9	11	12	m
Maximum Shear Force	56	32	67	44	75	95	94	81	127	171.8	kN/m
Maximum Bending Moment	144	63	185	94	236	298	289	242	482	667	kN·m/m
Maximum Horizontal Deflection of Wall	69	32	93	41	150	138	114	119	215	423	mm
EXCEL MACROS APPLICATION											
Total Wall Length Obtained	9	8	10	9	11	11	11	10	13	14	m
Maximum Shear Force	69	41	82	54	91	123	119	101	156	220	kN/m
Maximum Bending Moment	216	103	275	143	348	510	470	381	731	1093	kN·m/m
PLAXIS 2D SOFTWARE											
Total Wall Length Used	10	8	11	9	13	11	10	10	13	12	m
Maximum Shear Force	51	33	60	35	46	85	90	85	139	181	kN/m
Maximum Bending Moment	120	64	152	77	160	313	294	255	439	729	kN·m/m
Maximum Horizontal Deflection of Wall	55	59	74	66	33	88	89	134	213	135	Mm

Table 5.11 shows the output results (maximum shear force, maximum bending moment and maximum wall deflection) obtained from the analyses by different methods applied in this research. The results are discussed below based on the output values studied. The table shows slight variations in the total wall length amongst the analytical software's. The difference is largely due to approximation in the calculation of the sheet pile wall height and the difference in algorithm used by these software's. The total wall height used in *PLAXIS 2D*, as can be seen in Table 5.11, is obtained from the *Excel Macros Application* wall height calculated. Table 5.12 shows the percentage difference in the wall height employed for each material the various software.

Table 5.12: Percentage difference in cantilever sheet pile wall height for the various software

Depth Variation	Mat. 1	Mat. 2	Mat. 3	Mat. 4	Mat. 5	Mat. 6	Mat. 7	Mat. 8	Mat. 9	Mat. 10
GEOWALL – PLAXIS 2D	10%	13%	18%	11%	15%	18%	10%	10%	8%	8%
PROSHEET – PLAXIS 2D	20%	13%	18%	11%	23%	18%	10%	10%	15%	0%
Excel – PLAXIS 2D	0%	0%	0%	0%	0%	0%	0%	0%	0%	0%
GEOWALL – PROSHEET	11%	0%	0%	0%	9%	0%	0%	0%	8%	8%

Maximum Bending Moment

An average of 7% increase in value obtained from *GEOWALL* software and a 12% increase in value obtained from *PROSHEET* software were observed with respect to the values obtained with *PLAXIS 2D*. Conversely, a 41% increase in maximum bending moment was obtained from *Excel Macros Application* as compared to *PLAXIS 2D*. Although, the latter value ascertains research observations made by Fourie & Potts (1989) that the limit equilibrium methods overestimates the maximum bending moment by about 50% with respect to the numerical methods, the current research showed that this overestimation was largely due to the material-plate frictional angle that is omitted in most limit equilibrium analyses (Rankine theory) as presented in the sensitivity analyses discussed previously in Section 3 of CHAPTER 5. The 7% and 12% increase in *GEOWALL* and *PROSHEET* respectively can be explained as due to the shortcoming in the analytical methods in establishing a mathematical relationship that shows the influence of the soil's elastic modulus and walls flexural stiffness on the bending moment. Figure 5.13 shows a histogram representing the variation in bending moment with respect to each soil material analysed by various software. The bending moment graphs for the analyses as presented in Annex A show a similar distribution in the bending moment of the software with the maximum bending moment occurring at almost the same depth. Also the small variation in the wall heights for the various software as presented in Table 5.12 affects the maximum bending moment by less than 1% and as the result, the height variation does not present a problem in the analyses.

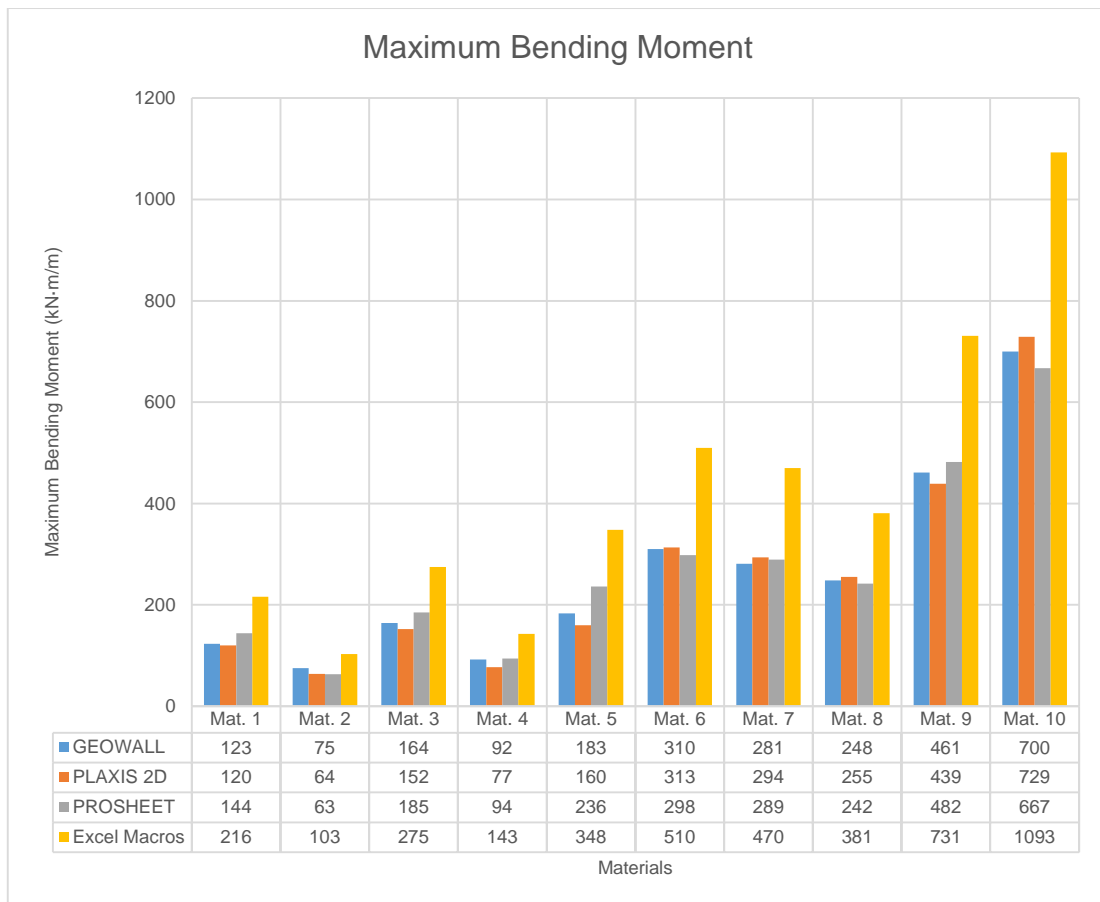


Figure 5.13: Histogram of maximum bending moment obtained from different software analyses for the cantilever sheet pile wall

Maximum Shear Force

An average of 10% increase in the maximum shear force value obtained from the *GEOWALL* software was observed with respect to the value obtained with *PLAXIS 2D*. The increase occurs as a result of the analytical method unable to represent the effect of the wall flexural stiffness, the soil's elastic modulus and the soil's Poisson ratio on the shear force. *PROSHEET* showed a 11% increase in the maximum shear force value obtained with respect to the maximum shear force values from *PLAXIS 2D*. *Excel Macros Application* however recorded a much higher average difference (26%) in comparison to values obtained using *PLAXIS 2D*. This fairly high variation in the result obtained from the *Excel Macros Application* is attributed, as presented in the simulation analyses, to the lapse in use of interface value in the Rankine theory analyses. Figure 5.14 shows a summary of the shear force analyses. The shear force graphs for the analyses as presented in Annex A show a similar distribution in the shear force of the software with the maximum shear force occurring at almost the same depth. Also the variation in the wall heights for the various software as presented in Table 5.12 shows an insignificant change in maximum shear force and as the result, the height variation does not present a problem in the analyses.

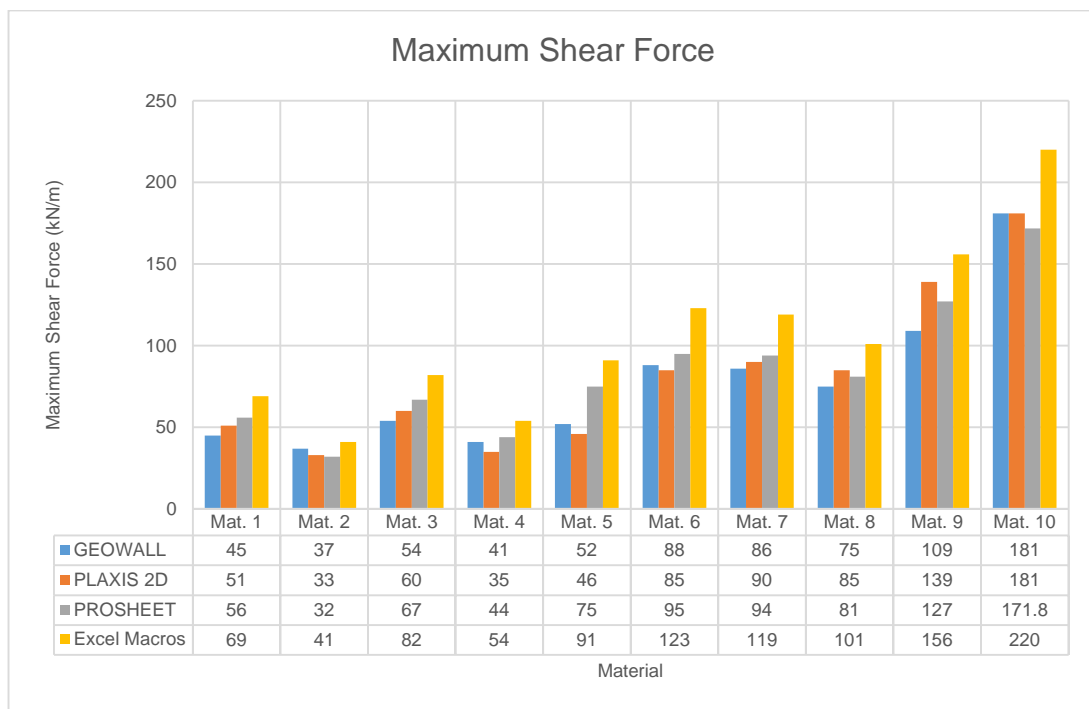


Figure 5.14: Histogram of maximum shear force obtained from different software analyses for the cantilever sheet pile wall

Maximum Wall Deflection

A larger variation in the wall deflection values were obtained after the analyses. The *GEOWALL-PLAXIS 2D* recorded a 39% increase in value while the *PROSHEET-PLAXIS 2D* recorded a 34% increase in value. Based on the sensitivity analyses presented above in the current chapter, and precisely referring to Figure 5.11, the soil's elastic modulus is the parameter that largely influences the wall displacement. It is evident, that the shortcoming of the analytical method in omitting the elastic modulus during the wall deflection was the major factor in the huge incremental values obtained.

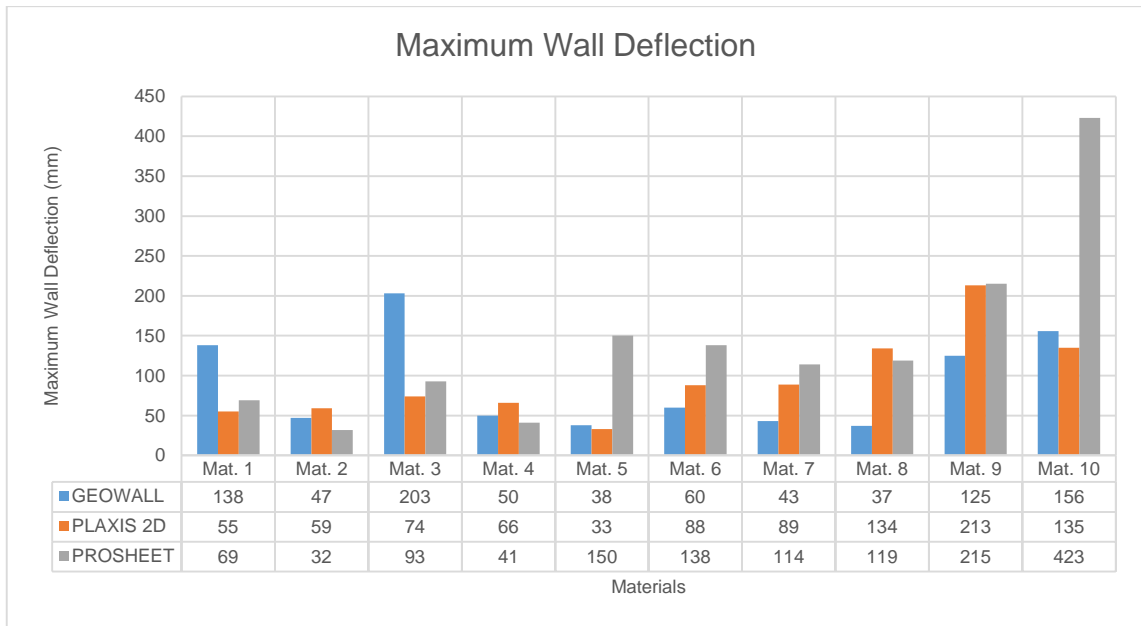


Figure 5.15: Histogram of maximum wall deflection obtained from different software analyses for the cantilevered sheet pile wall

5.4.2 Anchored Wall

Figure 5.16, Table 5.10 and Table 5.13 Table 5.8 shows the wall and material properties used in the anchored wall analyses. The *Excel Macros Application* is used to first and foremost analyse the data presented below. The total depth obtained from the *Excel Macros Application* analyses is then introduced into *PLAXIS 2D* for the numerical analyses. *GEOWALL* and *PROSHEET* are then used in modelling the same problem for the analyses.

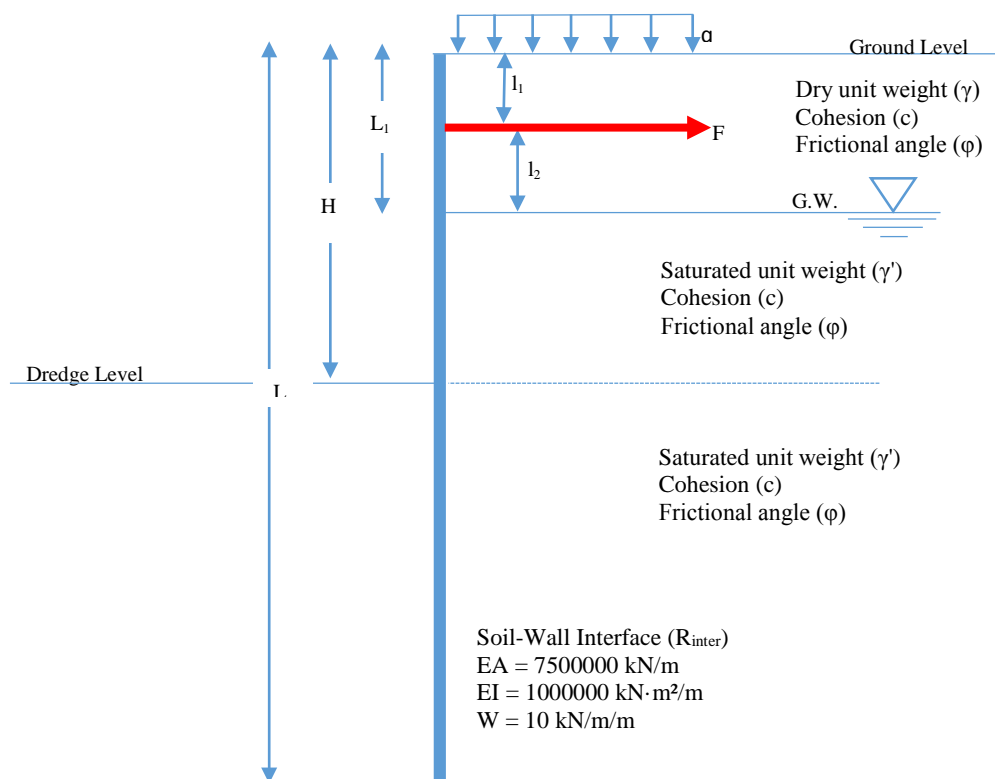


Figure 5.16: Geometrical and geotechnical parameters for anchored analyses

Table 5.13: Material properties of the soil studied for the anchored wall analyses

Parameter	Mat. 1	Mat. 2	Mat. 3	Mat. 4	Mat. 5	Mat. 6	Mat. 7	Mat. 8	Mat. 9	Mat. 10	Unit
Excavation height (H)	9.15	9	12	7	9	7	8	9	9	7	m
Groundwater level (L_1)	3.05	4	0	3	5	3	4	4	3	3	m
Anchor level	1.53	2	3	2	2	1	2	2	1	2	m
Anchor angle	0	15	5	10	0	0	30	10	20	0	°
Soil saturated unit weight (γ_{sat})	19.5	19	20	18	20	19.04	20.5	18	19.5	21	kN/m ³
Soil unsaturated unit weight (γ_{unsat})	16	17.5	20	16	18	14.8	16	14.5	15.9	16.5	kN/m ³
Cohesion (C)	1	0.2	5	0.5	3	1	0.6	0.3	10	5	kN/m ²
Friction angle (ϕ)	30	27	28	25	42	28	32	35	30	28	°
Soil-wall interface strength (R_{inter})	0.67	0.54	0.60	0.5	0.67	0.67	0.63	0.6	0.54	0.67	-
Surcharge (q)	0	0	0	0	0	15	10	17	13	20	kN/m ²

Table 5.14 shows results obtained from the analyses. The results are discussed below based on the output results obtained.

Table 5.14: Output result obtained from anchored wall analyses using the various software's

Anchored Wall Output Properties	Mat. 1	Mat. 2	Mat. 3	Mat. 4	Mat. 5	Mat. 6	Mat. 7	Mat. 8	Mat. 9	Mat. 10	Unit
GEO WALL SOFTWARE											
Total Wall Length Obtained	11	12	15	10	10	9	10	11	12	9	m
Maximum Shear Force	83	123	204	76	60	77	94	91	84	72	kN/m
Maximum Bending Moment	250	360	724	154	163	166	228	258	279	142	kN-m/m
Maximum Horizontal Deflection of Wall	78	125	281	32	31	37	43	62	102	23	mm
PROSHEET SOFTWARE											
Total Wall Length Obtained	11	12	15	11	10	9	10	11	11	9	m
Maximum Shear Force	107	123	195	69	62	78	82	89	90	64	kN/m
Maximum Bending Moment	286	359	649	164	111	185	179	210	207	125	kN-m/m
Maximum Horizontal Deflection of Wall	67	84	221	22	17	30	26	38	46	13	mm
EXCEL MACROS APPLICATION											
Total Wall Length Obtained	13	13	16	11	11	11	11	12	11	10	m
Maximum Shear Force	126	142	225	79	71	92	96	92	100	74	kN/m
Maximum Bending Moment	438	521	958	235	160	288	275	307	290	193	kN-m/m
PLAXIS 2D SOFTWARE											
Total Wall Length Used	13	13	16	11	11	11	11	12	11	10	m
Maximum Shear Force	87	123	199	75	67	71	73	83	85	61	kN/m
Maximum Bending Moment	246	350	727	151	149	168	147	206	194	111	kN-m/m
Maximum Horizontal Deflection of Wall	66	73	164	59	78	41	105	49	67	56	mm

Table 5.15 shows the wall height variation for each material the various software.

Table 5.15: Percentage difference in anchored sheet pile wall height for the various software

Depth Variation	Mat. 1	Mat. 2	Mat. 3	Mat. 4	Mat. 5	Mat. 6	Mat. 7	Mat. 8	Mat. 9	Mat. 10
GEO WALL – PLAXIS 2D	10%	13%	18%	11%	15%	18%	10%	10%	8%	8%
PROSHEET – PLAXIS 2D	20%	13%	18%	11%	23%	18%	10%	10%	15%	0%
Excel – PLAXIS 2D	0%	0%	0%	0%	0%	0%	0%	0%	0%	0%
GEO WALL – PROSHEET	11%	0%	0%	0%	9%	0%	0%	0%	8%	8%

Maximum Bending Moment

An average of 12% increase in value obtained from *GEO WALL* software was observed with respect to the values obtained with *PLAXIS 2D* with a 11% increase in the value of the maximum bending moment obtained between *PROSHEET* and *PLAXIS 2D*. A 34% increase in bending moment value was obtained from the *Excel Macros Application* as compared to *PLAXIS 2D* (see Figure 5.17). The large variation presented by the *Excel Macros Application* is due to the fact that the Rankine theory doesn't consider the effect of the wall friction angle in its analyses. From the sensitivity analyses previously presented in CHAPTER 5 and specifically referring to Figure 5.4, it is seen that the wall friction angle largely affects the maximum bending moment value. Also, the variation in the values obtained from the analyses performed with *GEO WALL* and *PROSHEET* is largely due to the omission of the soil's elastic modulus in estimating the bending moment with the limit equilibrium method. The bending moment graphs for the analyses as presented in Annex A show a similar distribution in the bending moment of the software with the maximum bending moment occurring at almost the same depth. Also the variation in the wall heights for the various software as presented in Table 5.15 shows an insignificant change in maximum bending moment and as the result, the height variation does not present a problem in the analyses.

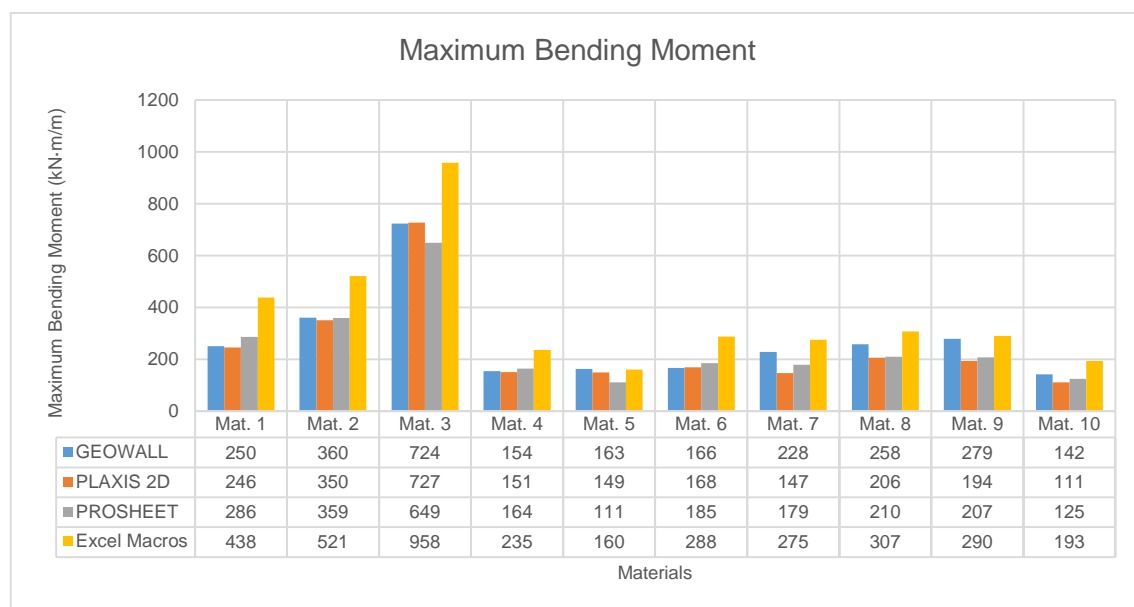


Figure 5.17: Histogram of maximum bending force obtained from different software analyses for the anchored sheet pile wall

Maximum Shear Force

An average of 7% increase in the maximum shear force value was obtained with both *GEO WALL* and *PROSHEET* with respect to the values obtained with *PLAXIS 2D*. However, a 16% increase recorded in shear force values obtained between the *Excel Macros Application* and *PLAXIS 2D* (see Figure 5.18). These percentage increment in value is a result of the inability of the limit equilibrium method in representing the effect of the wall flexural stiffness and the soil's Poisson ratio on the shear force. The larger difference in the *Excel Macros Application-PLAXIS 2D* value over *GEO WALL-PLAXIS 2D* and *PROSHEET-PLAXIS 2D* values is attributed to the absence in the wall friction angle in the Rankine theory for the limit earth pressure analyses. The shear force graphs for the analyses as presented in Annex A show a similar distribution in the shear force of the software with the maximum shear force occurring at almost the same depth. Also the variation in the wall heights for the various software as presented in Table 5.15 shows

an insignificant change in maximum shear force and as the result, the height variation does not present a problem in the analyses.

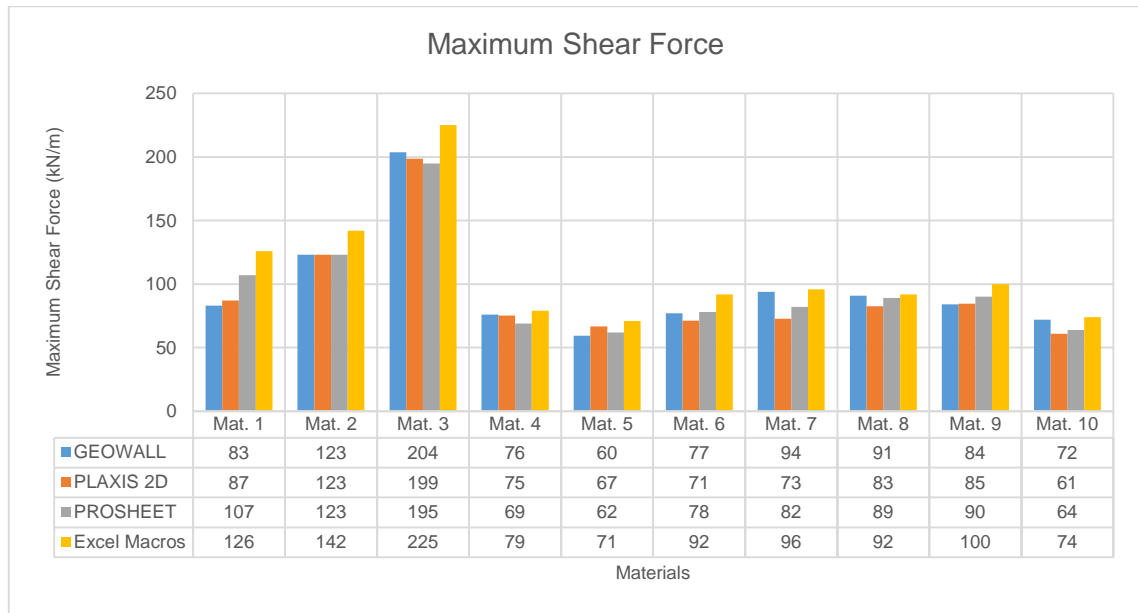


Figure 5.18: Histogram of maximum shear force obtained from different software analyses for the anchored sheet pile wall

Maximum Wall Deflection

The *GEOWALL-PLAXIS 2D* analyses recorded a 39% increase in value while the *PROSHEET- PLAXIS 2D* showed a 41% increase in value. Based on the sensitivity analyses presented in Section 3 of the current chapter, and precisely referring to Figure 5.11, the soil's elastic modulus is parameter that largely influences the wall displacement. It is evident, that the shortcoming of the analytical method in omitting the elastic modulus during the wall deflection was the major factor in the huge incremental values obtained. Figure 5.19 shows a histogram of the maximum wall deflection for the various soil materials.

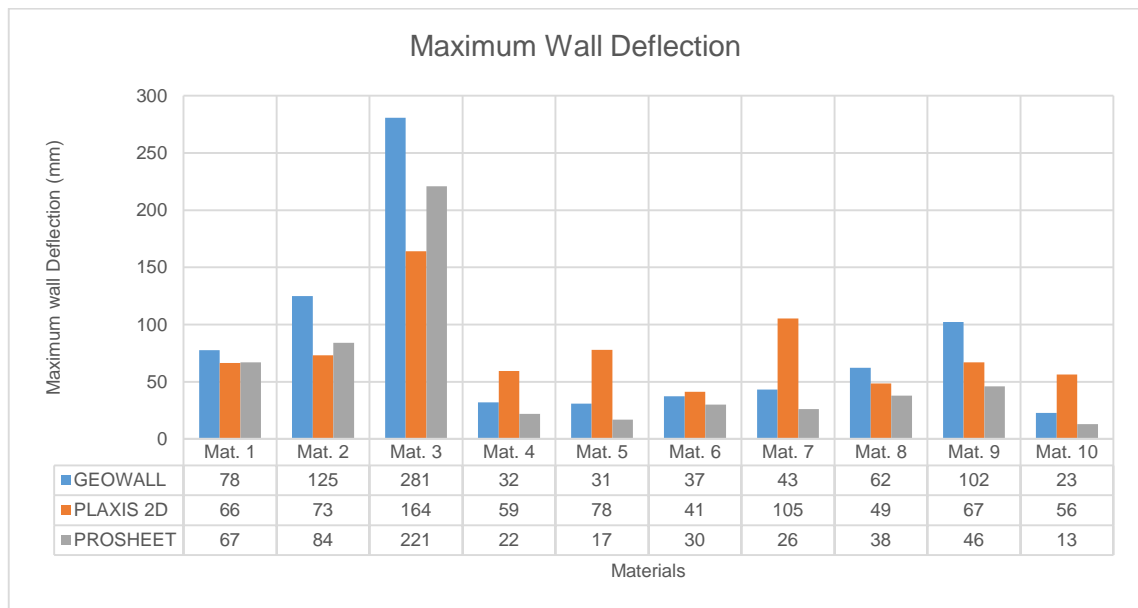


Figure 5.19: Histogram of maximum wall deflection obtained from different software analyses for the anchored sheet pile wall

CHAPTER 6 CONCLUSIONS AND RECOMMENDATIONS

6.1 Conclusions

The study of the stability of the sheet pile wall has been carried out. It involved analytical and numerical modelling methods for cantilever and anchored sheet pile wall. In order to carry out the analyses, 20 different soil materials have been studied. Ten of these materials have been used in the cantilever wall analyses and the other ten used in the anchored wall analyses. A unique wall property has been used in undertaking all the analyses. In the case of the numerical modelling, a finite element program; *PLAXIS 2D*, has been used to carry out the analyses. *GEO WALL*, a software developed to carry out sheet pile wall analyses by using the Coulomb theory for lateral earth pressure and the USA method of analytical modelling has also used. An analytical commercial software namely, *PROSHEET*, which employs the log spiral theory for estimating the lateral earth pressure has also been used in the research. Finally, an *Excel Macros Application*, developed based on the book by Das (2011), and which employs the Rankine theory in calculating the lateral earth pressure is used as well in this study.

From the analyses carried out and the data results obtained, with supporting literatures reviewed during the study, the following conclusions have been reached.

Lateral Earth Pressure Theories

There is an underestimation in the coefficient of passive earth resistance when the Rankine theory is used as a result of the omission made by the theory in soil-wall friction angle. This underestimation increases exponentially with an increase in the frictional angle of the soil-wall interface, and this error is corrected using the Coulomb theory. An exponential relation is found to exist between the coefficient of passive earth resistance (K_p) for both the Rankine and Coulomb theories, and is represented by;

$$K_{p_{Coulomb}} = K_{p_{Rankine}} \cdot e^{\frac{0.13\delta\phi}{100}}$$

The log spiral theory shows a linear relationship of its coefficient of passive earth resistance with the Rankine's coefficient of passive earth resistance represented by;

$$K_{p_{log\ spiral}} = K_{p_{Rankine}} + 0.0075e^{0.0931\delta\phi}$$

As the soils friction angle and the wall friction angle gradually increased, the Coulomb's coefficient of passive earth resistance increased with respect to the log spiral coefficient of passive earth resistance as a result of the planar failure surface introduced as a hypothesis in the Coulomb theory. The difference in the K_p did not however cause significant variations in the maximum bending moments and maximum shear forces for the *GEO WALL* and *PROSHEET* software's and as a conclusion, dispute the conclusion made by Das (2010) that the Coulomb theory grossly overestimates the K_p when the relationship between the wall's friction angle and the soil's friction angle is greater than 0.5 ($\delta/\phi > 0.5$).

Bending Moment and Shear Force

Both the maximum bending moment and shear force showed a positive correlation with the total length of sheet pile wall and the values of the maximum bending moment and the maximum shear force were largely affected by the soil-wall interface. As a result, and comparing the limit equilibrium method with the finite element method, the use of the Coulomb theory or the log spiral theory in calculating the lateral earth pressures gave a much more acceptable value than the use of the Rankine theory. This was observed in the results obtained after the data analyses, where an increase of 7% in the maximum

bending moment was observed for the *GEOWALL-PLAXIS 2D* analyses and an increase of 12% in the maximum bending moment of the *PROSHEET-PLAXIS 2D* was obtained as compared to the 40% increase in the *Excel Macros Application-PLAXIS 2D* analyses for the cantilever analyses. However, in the anchored wall analyses, 12% and a 11% differences in the values obtained between *GEOWALL-PLAXIS 2D* and *GEOWALL-PLAXIS 2D* respectively are obtained, and a 34% difference in the maximum bending moment value was observed in the *Excel Macros Application-PLAXIS 2D*. Recurrently, the difference in maximum shear force observed between *GEOWALL-PLAXIS 2D* for the cantilever analyses was 10% while 7% was observed in the anchored analyses. The *PROSHEET-PLAXIS 2D* analyses also showed a variation of 11% increase in the cantilevered wall analyses and a 7% variation in the values obtained in the anchored wall analyses. However, the *Excel Macros Application-PLAXIS 2D* showed a 26% variation in the maximum shear force value obtained in the cantilever analyses and a 16% variation for the anchored analyses. Generally, a drop in the bending moment and shear force values between the cantilever and anchored wall analyses is observed and this occurs as a result of two basic phenomenon:

- The dredge depth for cantilever walls are much deeper than for the anchored walls. This reduces the amount of passive lateral earth resistance and hence reduces the maximum bending moment.
- The presence of the anchor force increases the stability of the wall, hence reducing the amount of passive earth resistance necessary for wall stability. This in turns reduces the maximum bending moment.

Wall Deflection

The maximum wall deflection presented a close variation in values obtained between the cantilever and anchored sheet pile wall analyses and between the *GEOWALL-PLAXIS 2D* and the *PROSHEET-PLAXIS 2D*. For the cantilever wall analyses, the *GEOWALL-PLAXIS 2D* presented a 39% increase in maximum wall deflection value while the *PROSHEET-PLAXIS 2D* presented a 34% increase in the maximum wall deflection value and for the anchored wall analyses, the *GEOWALL-PLAXIS 2D* presented a 39% increase in the maximum wall deflection value while the *PROSHEET-PLAXIS 2D* presented a 41% increase in the maximum wall deflection value. From the sensitivity analyses carried out, and considering the large variation in the analytical-numerical values obtained in the wall deflection, it was observed that the variation was momentarily due to the absence in the soil's elastic modulus in the analytical analyses of the sheet pile wall.

From the values obtained from this research, it can be concluded that the use of the Coulomb and the log spiral theories for the analyses of a sheet pile wall gave very acceptable values in the calculation of the maximum bending moment and shear force. They however, lagged in estimating an adequate value of horizontal wall deflection.

6.2 Recommendations for Future Study

The objectives of the research has been successfully achieved after the study. However, as a future study, the limitations presented in this current study can be implemented in studying the soil-wall behaviour. Also, the introduction of the soil and wall properties absent in the classical method for sheet pile wall analyses would be a big advancement in the limit equilibrium method, with emphasis especially on the soil's elastic modulus, so as to reduce the overestimation of the wall deflection.

REFERENCES

A new design method for retaining walls in clay. **Osman, Ashraf S. and Bolton, Malcolm D. 2004.** s.l. : NRC Resaerch Press, 2004, Canadian Geotechnical Journal, Vol. 41, pp. 451-466.

ArcelorMittal. 2008. *Piling Handbook.* 8th. Luxembourg : ArcelorMittal Commerial RPS, 2008. p. 368.

Azizi, Fethi. 1999. *Applied Analyses in Geotechnics.* London : E & FN Spom, 1999.

Bowles, Joseph E. 1997. *Foundation Analysis and Design.* 5th. Singapore : McGraw-Hill, 1997. p. 1170.

Coduto, Donald P. 2001. *Foundation Design: Principles and Practices.* 2nd. New Jersey : Prentice Hall, 2001. p. 883.

Comparison of a finite element and limiting equilibrium analyses for an embedded cantiveler retaining wall. **Fourie, A. B. and Potts, D. M. 1989.** 1989, Géotechnique 39, Vol. No. 2, pp. 175-188.

Craig, Robert F. 2004. *Craig's Soil Mechanics.* 7th. London : Spon Press, 2004. p. 447.

Das, Braja M. 2011. *Principles of Foundation Engineering.* [ed.] 7th. Stamford CT : CENGAGE Learning, 2011. p. 815.

Das, Braja M. 2010. *Principles of Geotechnical Engineering.* 7th. Stamford CT : CENGAGE Learning, 2010. p. 683.

Design and Use of Sheet Pile Walls in Stream Restoration and Stabilization Projects. **Technical Supplement 14R. 2007.** 2007, National Engineering Handbook, Vol. Part 654, pp. TS14R-1-TS14R-31.

Design of Sheet Pile Walls. **U.S. Army Corps of Engineers. 1994.** Washington : s.n., 1994, Engineering and Design, p. 75.

Embedded retaining walls: theory, practice and understanding. **Simpson, Brian and Powrie, William. 2001.** Istanbul : s.n., 2001. Prespective Lecture: 15th International Conference on Soil Mechanics and Geotechnical Engineering. p. 22.

EN 1997-1. 2004. *Eurocode 7: Geotechnical design - Part 1: General rules.* Brussels : CEN, 2004. p. 168.

Hulse, Ray and Cain, Jack. 2000. *Structural Mechanics.* Second. London : Palgrave Macmillan, 2000. p. 592.

Jiménez Salsa, J. A., et al. 1980. *Geotecnia y Cimientos III.* Madrid : Editorial Rueda, 1980.

Lambe, T. W. and Whitman, R. V. 1969. *Soil Mechanics.* New York : John Wiley & Sons, 1969.

Murthy, V. N. S. 2002. *Geotechnical Engineering: Principles and Practices of Soil Mechanics and Foundation Engineering.* New York : Marcel Dekker, 2002. p. 1029.

Overview of Earth Retention System: 1970-1990. **O'Rourke, T. D. and Jones, C. J.F.P. 1990.** s.l. : P.C. Lambe and L.A. Hansen, 1990, Design and Performance of Earth Retaining Structures, pp. 22-51.

Padfield, C. J. and Mair, R. J. 1984. *Design of propped cantilever walls embedded in stiff clay.* Construction Industry Research and Information Association (CIRIA) Report 104. London : s.n., 1984.

Škrabl, Stanislav. 2006. *Interactional Approach of Cantilever Pile Wall Analysis.* Slovenia : ACTA Geotechnica, 2006. pp. 47-59.

Smith, Geoffrey N. and Smith, Ian G. N. 1998. *Element of Soil Mechanics.* Cambridge : Blackwell Science, 1998. p. 494. Vol. 7th.

Terzaghi, Karl. 1943. *Theoretical soil mechanics.* London and New York : John Wiley, 1943.

United State Steel. 1984. *Steel Sheet Piling Design Manual.* Washington : FHWA, 1984. p. 133.

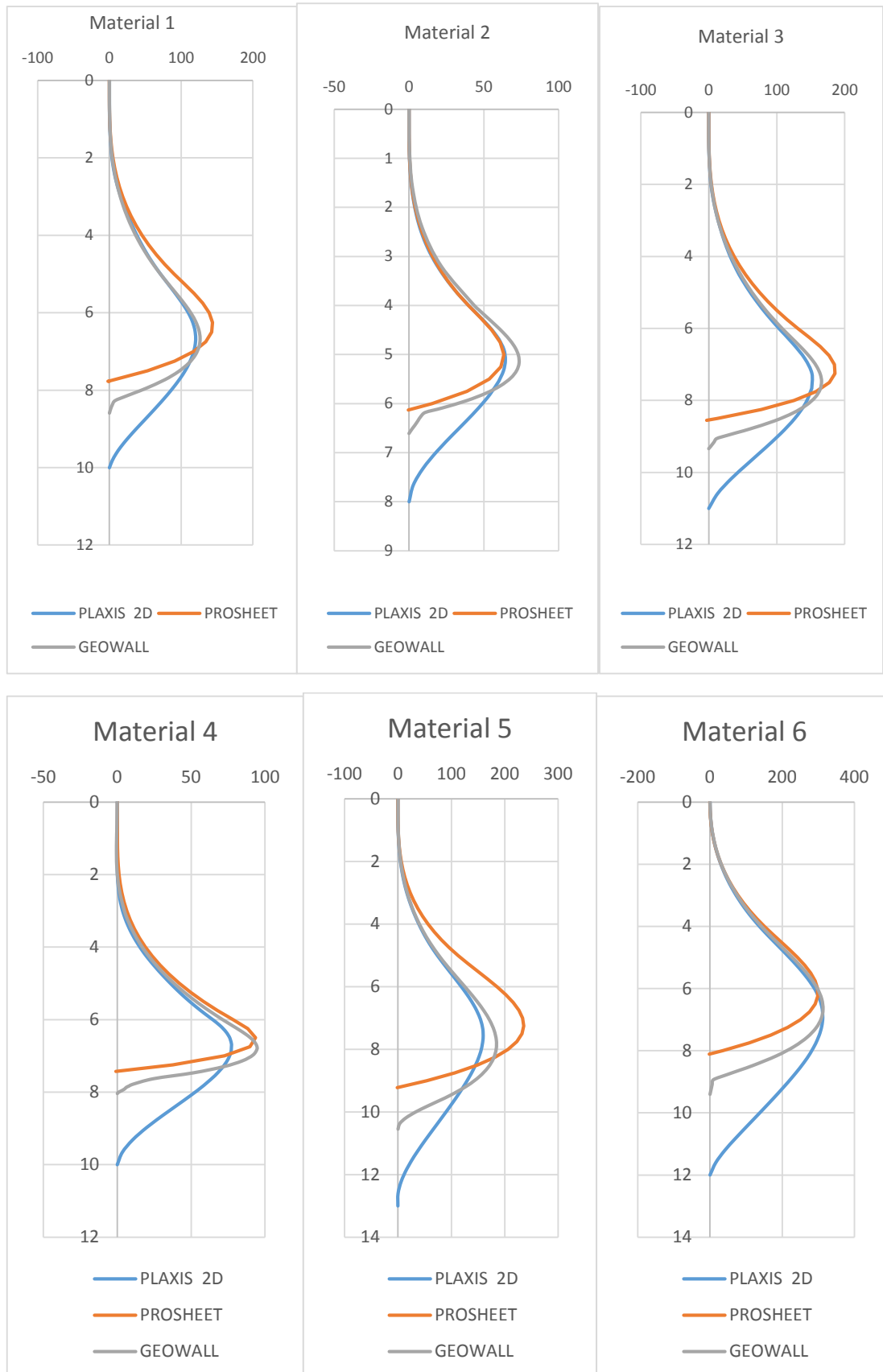
Venkatramaiah, C. 2006. *Geotechnical Engineering.* 3rd. New Delhi : New Age International, 2006. p. 824.

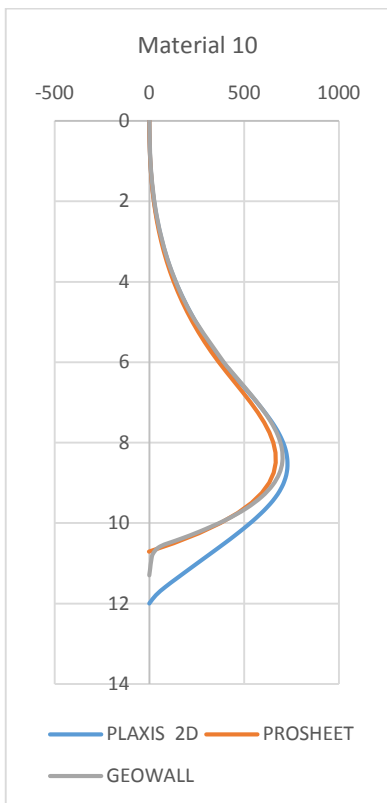
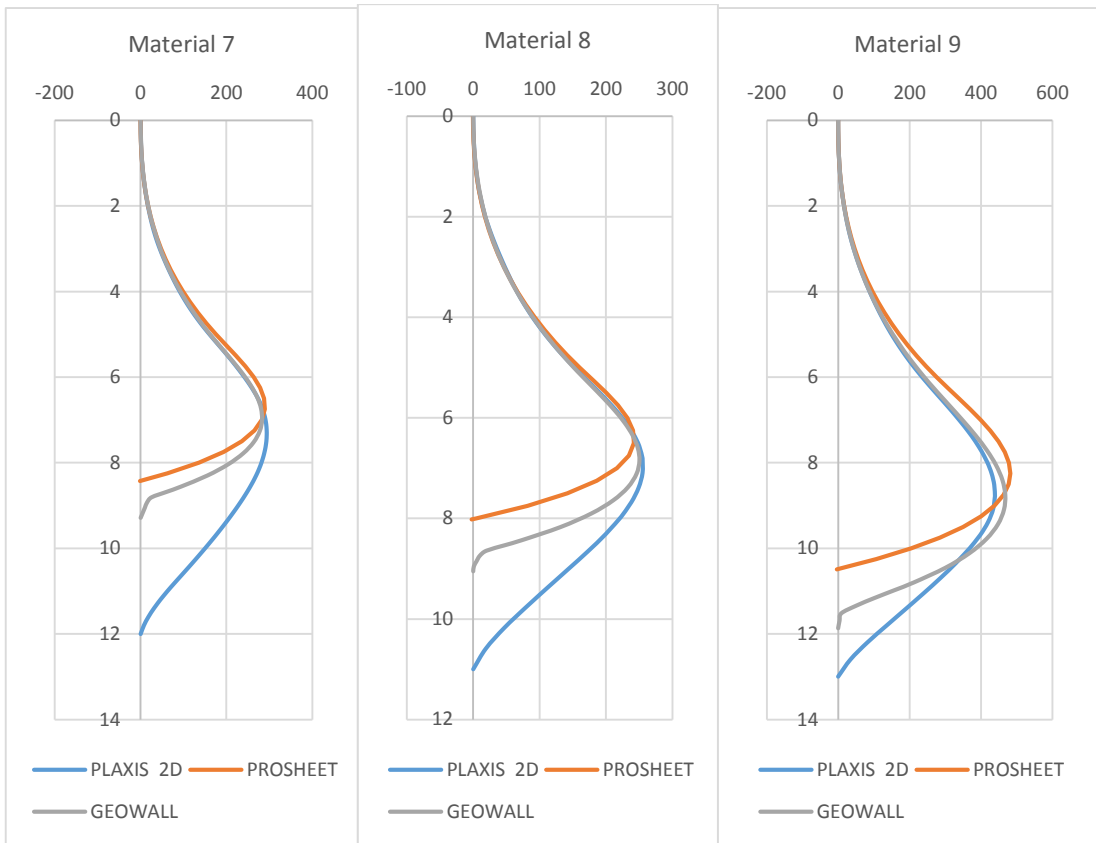
ANNEX A BENDING MOMENT AND SHEAR FORCE DISTRIBUTION CURVES

Cantilever Sheet Pile Wall

Bending Moment Distribution

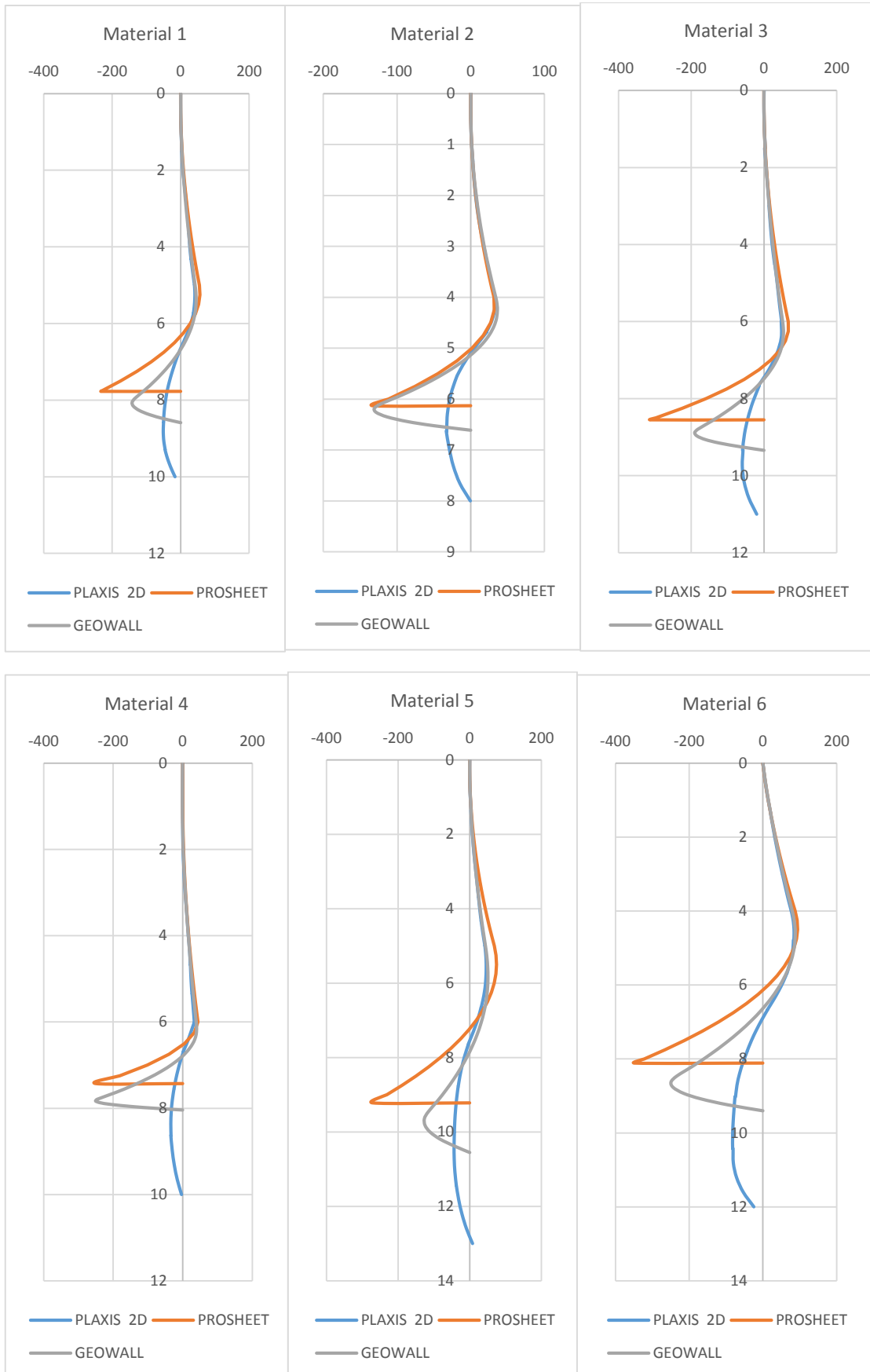
The chart below shows the moment distribution of a cantilever wall for the various materials.

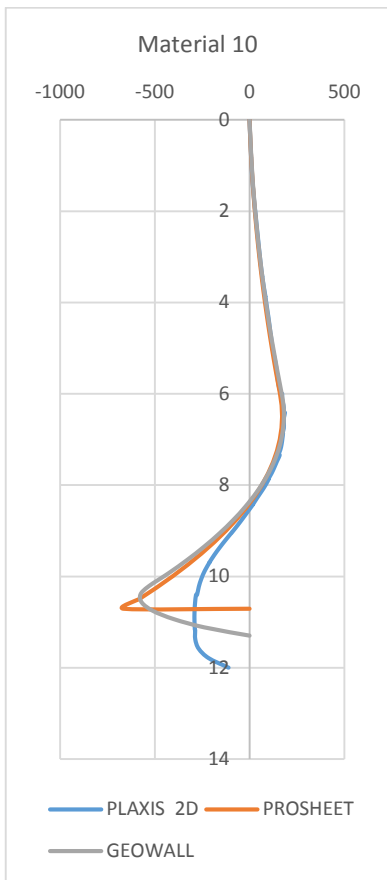
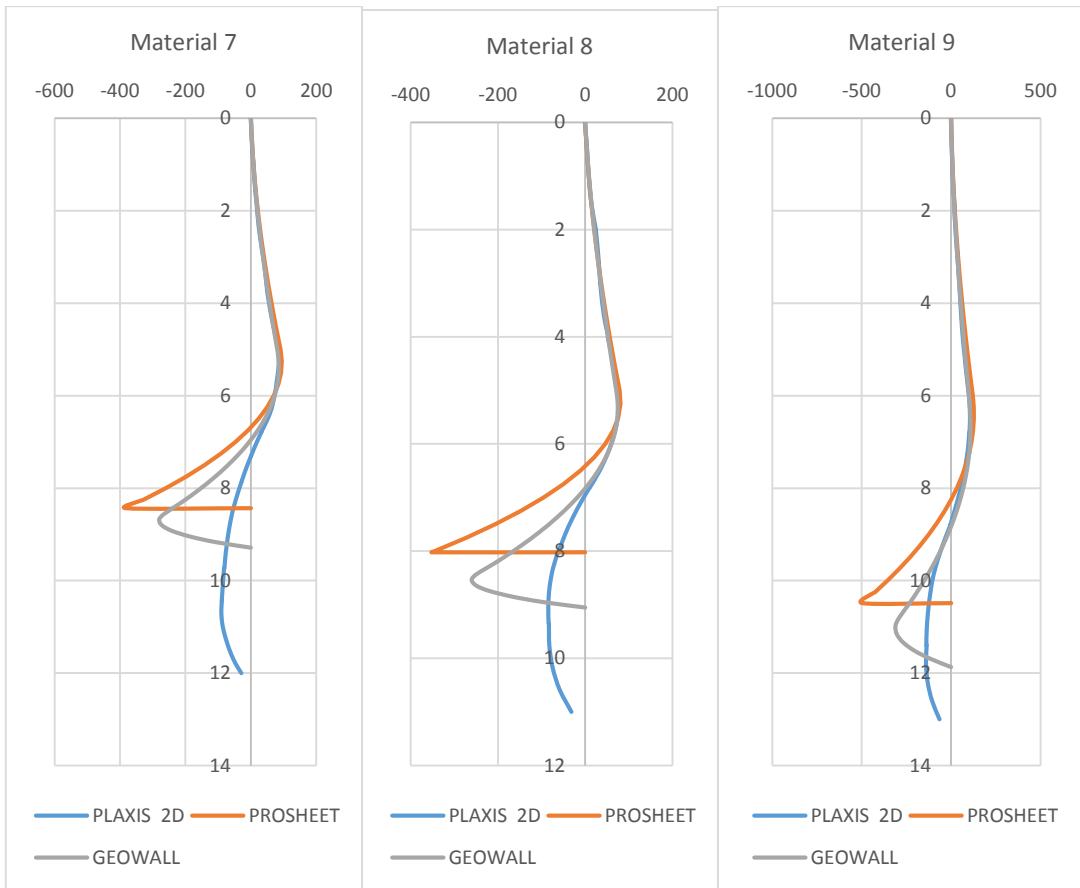




Shear Force Distribution

The chart below shows the shear force distribution of a cantilever wall for the various materials.

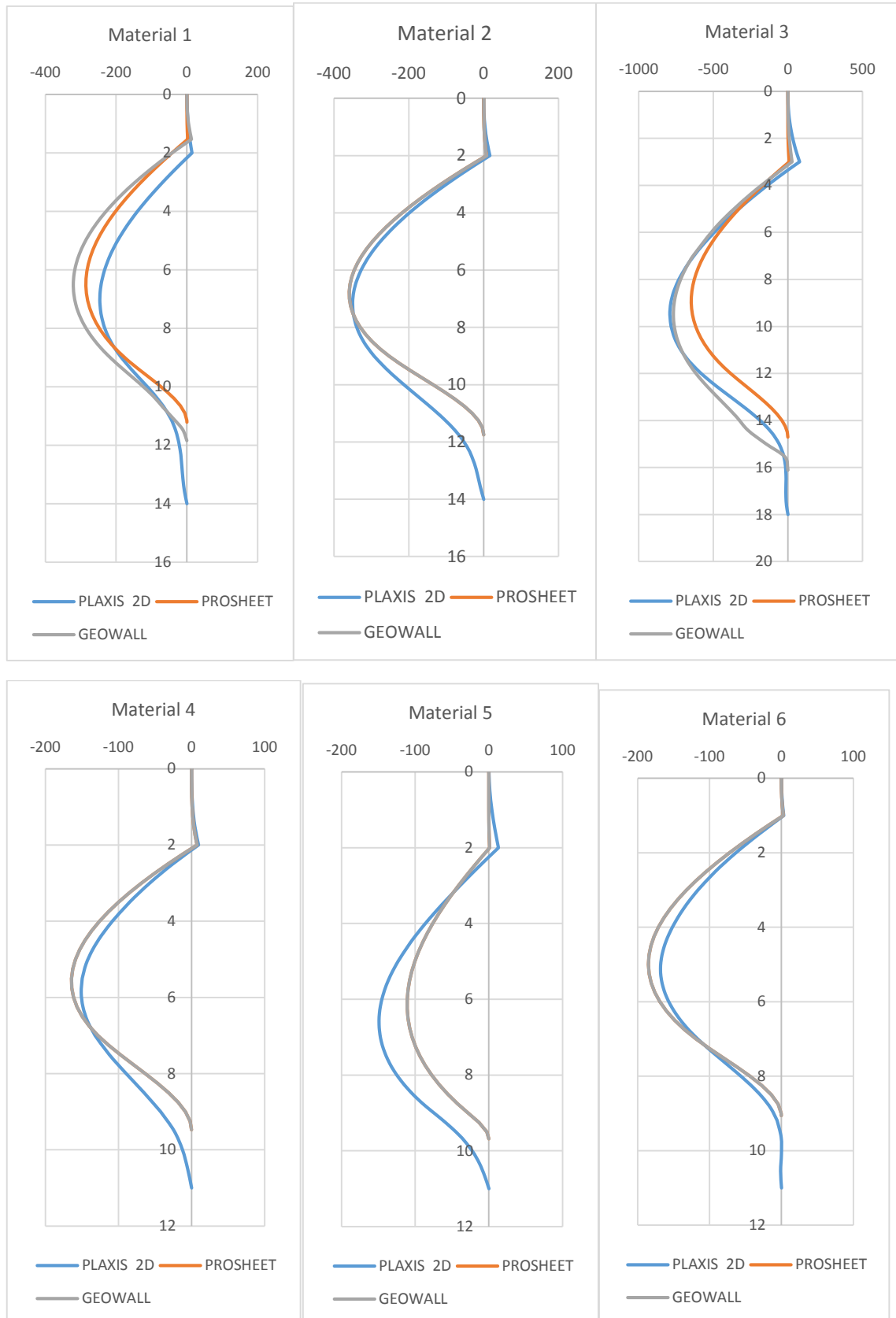


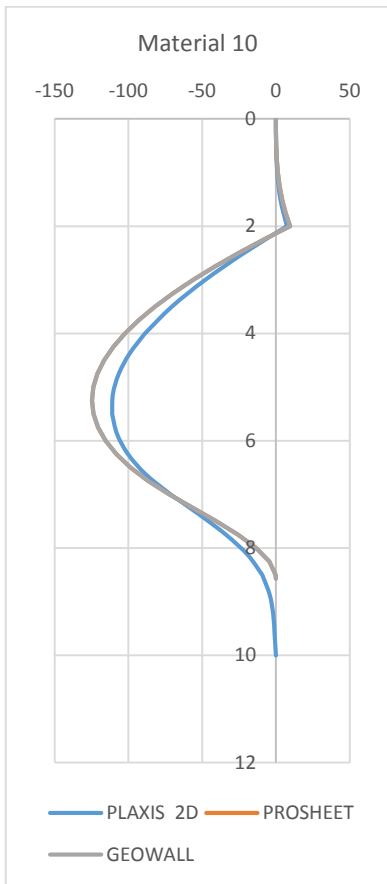
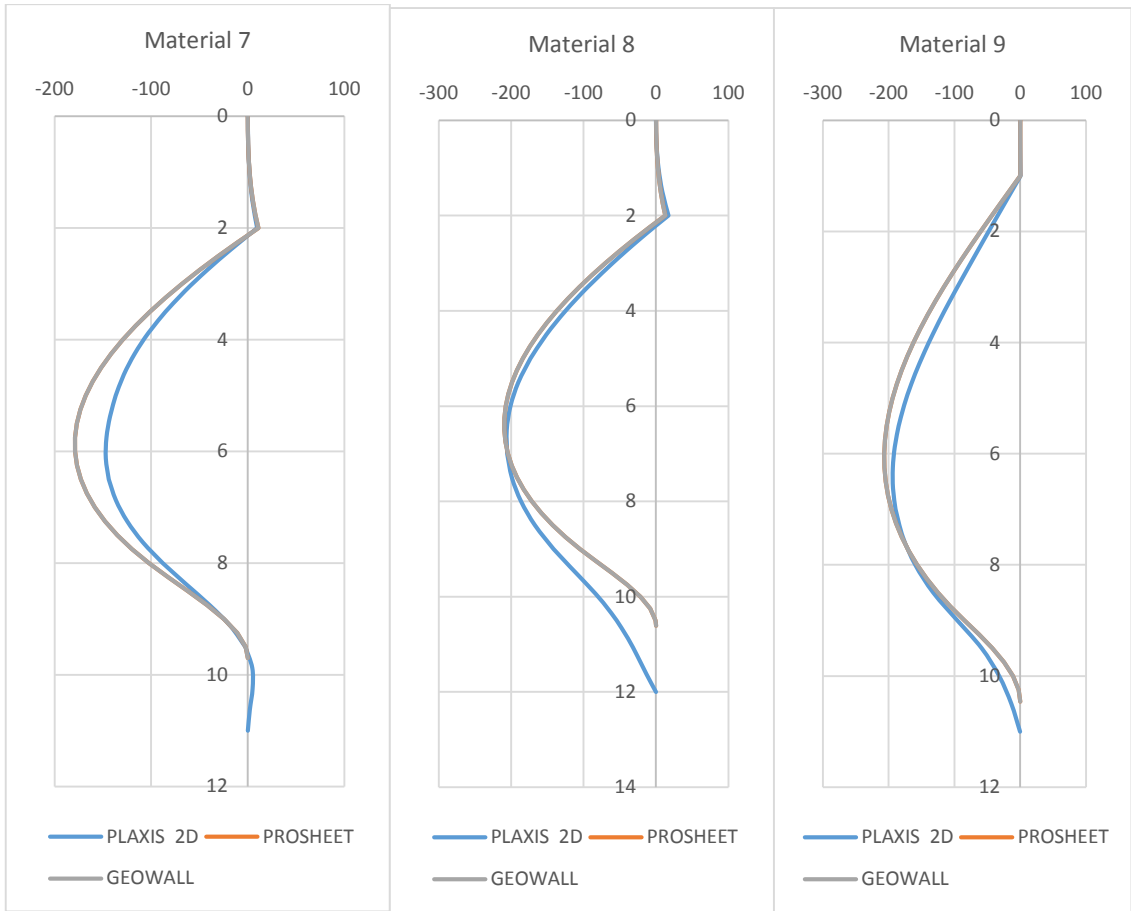


Anchored Sheet Pile Wall

Bending Moment Distribution

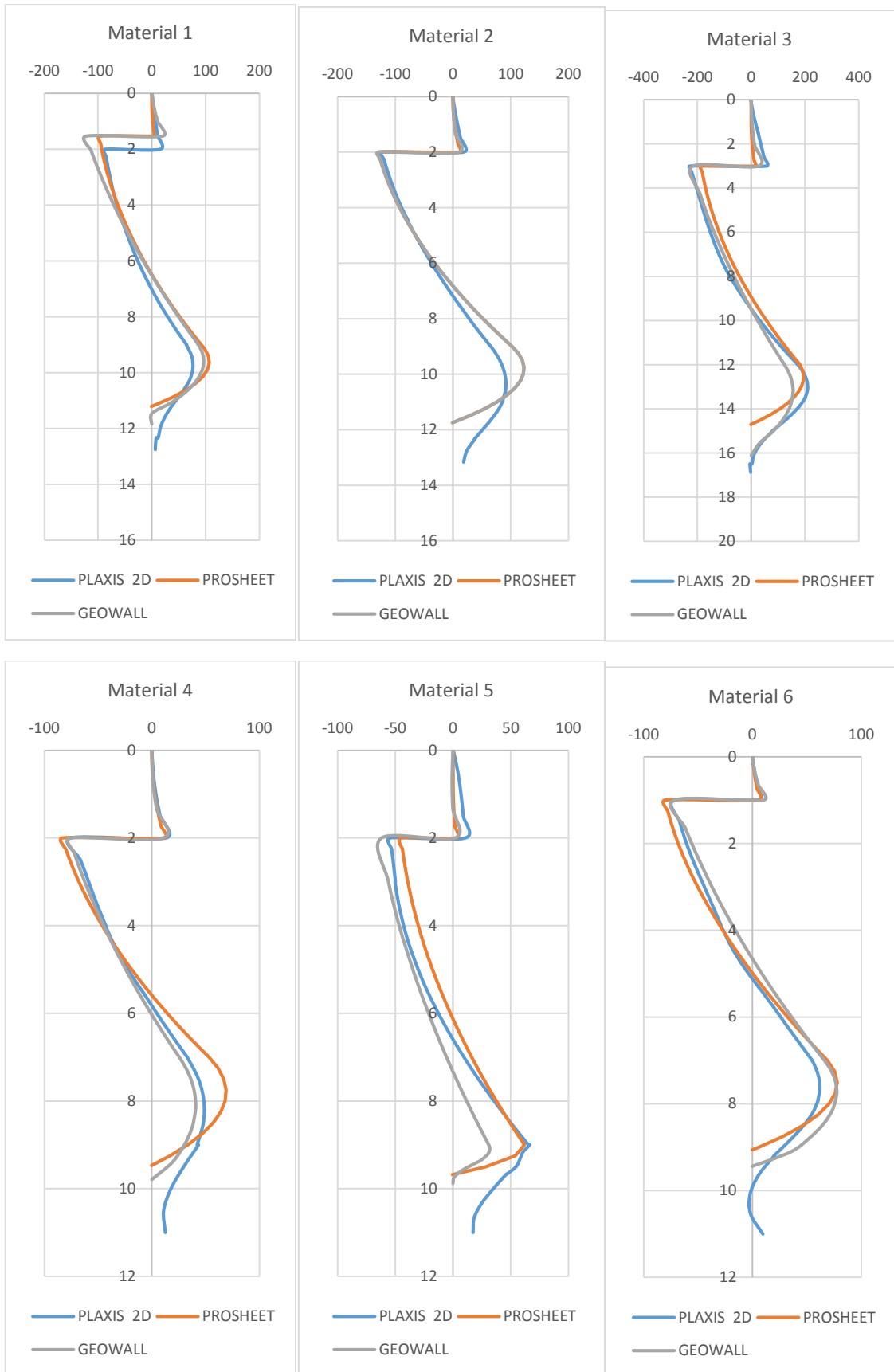
The chart below shows the moment distribution of a cantilever wall for the various materials.

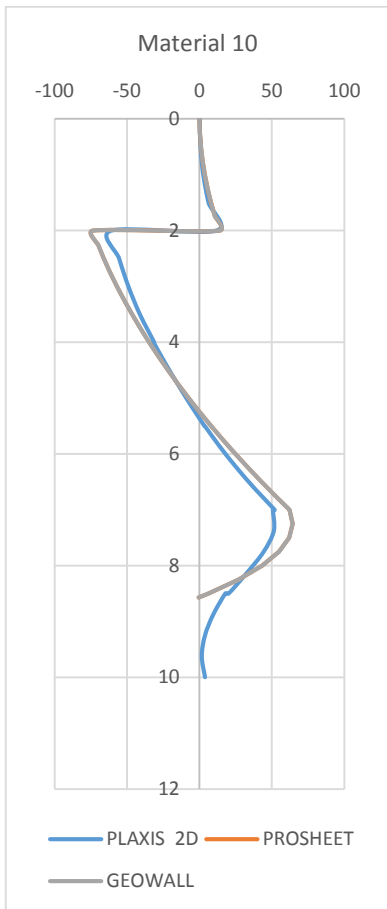
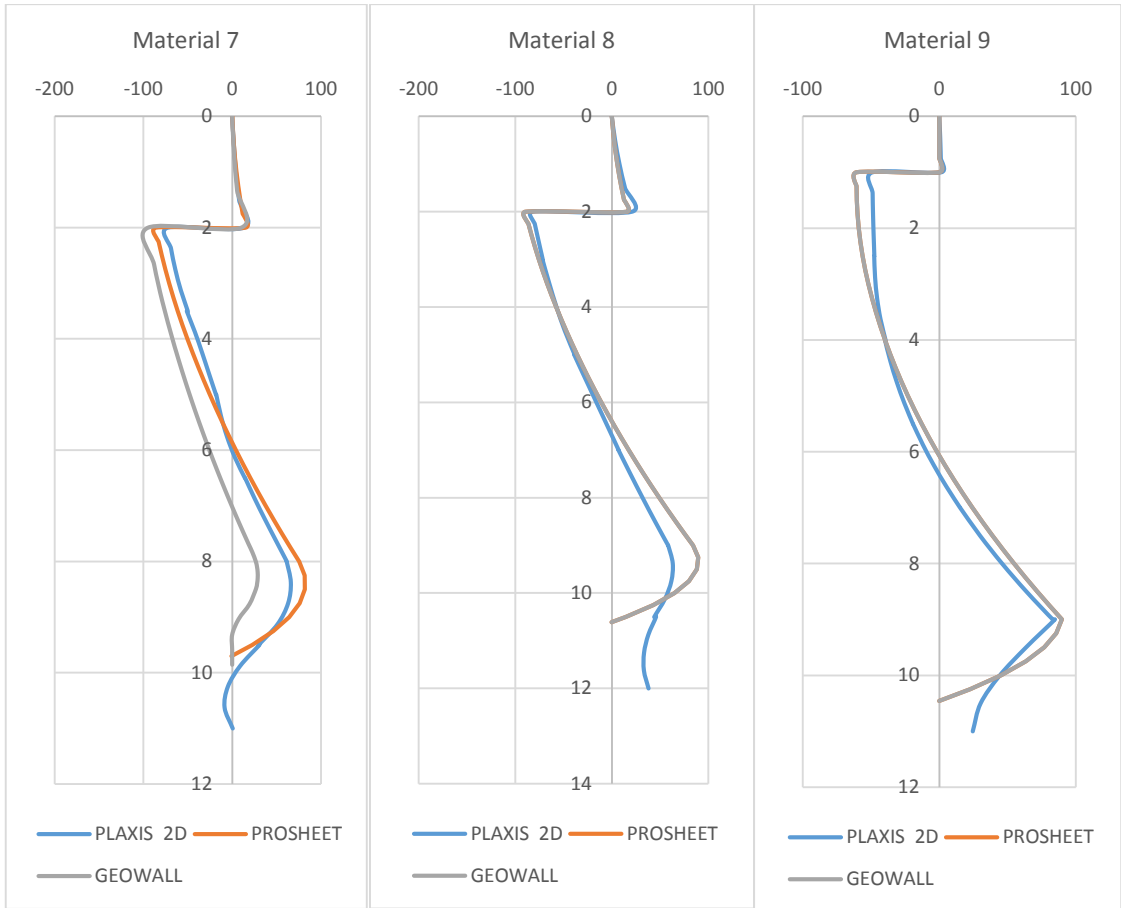




Shear Force Distribution

The chart below shows the shear force distribution of a cantilever wall for the various materials.





ANNEX B GEOWALL ALGORITHM

```
using System;
using System.Collections.Generic;
using System.Linq;
using System.Text;
using System.Windows.Forms;
using System.Threading.Tasks;
using System.Globalization;
using Microsoft.Xna.Framework;
using Thesis.Database;

namespace Thesis.Utilities
{
    public class clsAlgorithm
    {
        #region Public Types

        public double textBoxExcavationHeight;

        public bool IsCantileverNull;
        public bool IsFrictionNull;
        public bool IsGroundWaterAbsent = true;
        public double Surcharge;
        public double _KpFS;
        public double _ExcavationDepth;
        public double _GroundWater_Depth;
        public double _GroundWater_UnitWeight;
        public double _Excavated_UnitWeight;
        public double _Excavated_SatUnitWeight;
        public double _Excavated_Cohesion;
        public double _Excavated_frictionAngle;
        public double _Excavated_InterfaceAngle;
        public double _Dredged_UnitWeight;
        public double _Dredged_SatUnitWeight;
        public double _Dredged_Cohesion;
        public double _Dredged_frictionAngle;
        public double _Dredged_InterfaceAngle;

        public double _anchorL1;
        public double _anchorL2;
        public double _anchorAngle;

        public string _Wall_Name;
        public double _Wall_ElasticModulus;
        public double _Wall_Inertia;
        public double _Wall_AllowableStress;
        public double _Wall_SectionModulus;
        public Color _Wall_Color;

        public int MaximumBM;
        public int MaximumSF;
        public double MaximumDeflection;
        public double MaximumRotation;
        #endregion

        #region Private Types

        double _Z_bar;
        public double _Excavated_EffectiveWeight;
        public double _Dredged_EffectiveWeight;
        double _L3;
        double _L4;
    }
}
```

```

double _Dredge;

#endregion

#region Sheet Pile Wall Algorithm
public double Delta_K()
{
    return Kp() - Ka_Dredged();
}

public double Excavated_EffectiveWeight()
{
    if (IsGroundWaterAbsent == false)
    {
        _Excavated_EffectiveWeight = _Excavated_SatUnitWeight -
        _GroundWater_UnitWeight;
    }
    else
    {
        _Excavated_EffectiveWeight = _Excavated_UnitWeight;
    }
    return _Excavated_EffectiveWeight;
}

public double Dredged_EffectiveWeight()
{
    if (IsGroundWaterAbsent == false)
    {
        _Dredged_EffectiveWeight = _Dredged_SatUnitWeight -
        _GroundWater_UnitWeight;
    }
    else
    {
        _Dredged_EffectiveWeight = _Dredged_UnitWeight;
    }
    return _Dredged_EffectiveWeight;
}

public double Cohesion()
{
    return 2 * _Dredged_Cohesion * Math.Cos(_Dredged_InterfaceAngle *
    Math.PI / 180) * (Math.Sqrt(Kp()) + Math.Sqrt(Ka_Dredged()));
}

#region Excavation Layer
public Double Ka_Excavated()
{
    //return Math.Pow((Math.Tan((45 - (_Excavated_frictionAngle / 2)) /
    (180 / Math.PI))), 2);
    return (Math.Pow(Math.Cos(_Excavated_frictionAngle * Math.PI / 180),
    2)) / (Math.Cos(_Excavated_InterfaceAngle * Math.PI / 180) *
    Math.Pow(1 + Math.Sqrt((Math.Sin((_Excavated_frictionAngle +
    _Excavated_InterfaceAngle) * Math.PI / 180) * Math.Sin(_Excavated_frictionAngle *
    Math.PI / 180)) /
    (Math.Cos(_Excavated_InterfaceAngle * Math.PI / 180))), 2));
}

public Double Sigma0()
{
    return (Surcharge * Ka_Excavated()) - (2 * _Excavated_Cohesion *
    Math.Sqrt(Ka_Excavated()) * Math.Cos(_Excavated_InterfaceAngle * Math.PI / 180));
}

```

```

        public Double Sigma1()
        {
            return Sigma0() + (_Excavated_UnitWeight * _ExcavationDepth *
Ka_Excavated());
        }

        public Double Sigma2()
        {
            return Sigma1() + (Excavated_EffectiveWeight() * _GroundWater_Depth *
Ka_Excavated());
        }

        public Double Area0()
        {
            return Math.Abs(_ExcavationDepth * Sigma0());
        }

        public Double Area1()
        {
            return Math.Abs(0.5 * _ExcavationDepth * Sigma1());
        }

        public Double Area2()
        {
            return Math.Abs(_GroundWater_Depth * Sigma1());
        }

        public Double Area3()
        {
            return Math.Abs(0.5 * _GroundWater_Depth * (Sigma2() - Sigma1()));
        }

#endregion

#region Dredge Layer
public Double Ka_Dredged()
{
    //return Math.Round(Math.Pow((Math.Tan((45 - (_Dredged_frictionAngle
/ 2)) / (180 / Math.PI))), 2), 2);
    return (Math.Pow(Math.Cos(_Dredged_frictionAngle * Math.PI / 180),
2)) / (Math.Cos(_Dredged_InterfaceAngle * Math.PI / 180) *
Math.Pow(1 + Math.Sqrt((Math.Sin((_Dredged_frictionAngle +
_Dredged_InterfaceAngle) * Math.PI / 180) * Math.Sin(_Dredged_frictionAngle *
Math.PI / 180)) /
(Math.Cos(_Dredged_InterfaceAngle * Math.PI / 180))), 2));
}

public Double Kp()
{
    //return Math.Round(((Math.Pow((Math.Tan((45 +
(_Dredged_frictionAngle / 2)) / (180 / Math.PI))), 2)) * _KpFS), 2);
    return (Math.Pow(Math.Cos(_Dredged_frictionAngle * Math.PI / 180),
2)) / (Math.Cos(_Dredged_InterfaceAngle * Math.PI / 180) *
Math.Pow(1 - Math.Sqrt((Math.Sin((_Dredged_frictionAngle +
_Dredged_InterfaceAngle) * Math.PI / 180) * Math.Sin(_Dredged_frictionAngle *
Math.PI / 180)) /
(Math.Cos(_Dredged_InterfaceAngle * Math.PI / 180))), 2) /
_KpFS);
}

public Double L3()

```

```

    {
        if (IsFrictionNull == false)
        {
            _L3 = (Sigma2() + (2 * _Excavated_Cohesion *
Math.Sqrt(Ka_Excavated()) * Math.Cos(_Excavated_InterfaceAngle * Math.PI / 180))
+ (2 * _Dredged_Cohesion * Math.Sqrt(Kp()) * Math.Cos(_Dredged_InterfaceAngle *
Math.PI / 180))) / (Dredged_EffectiveWeight() * Delta_K());
        }
        else
        {
            _L3 = Dredge() - L4();
        }
        return _L3;
    }

public Double Area4()
{
    if (IsFrictionNull == false)
    {
        return Math.Abs(0.5 * L3() * Sigma2());
    }
    else
    {
        return 0;
    }
}

#endregion

#region General Methods
public Double P()
{
    return Area0() + Area1() + Area2() + Area3() + Area4();
}

public Double Z_bar()
{
    if (IsCantileverNull == false)
    {
        if (IsFrictionNull == false)
        {
            if (IsGroundWaterAbsent == false)
            {
                //In the presence of groundwater
                _Z_bar = ((Area0() * ((_ExcavationDepth / 2) +
_GroundWater_Depth + L3())) + (Area1() * ((_ExcavationDepth / 3) +
_GroundWater_Depth + L3())) +
                (Area2() * ((_GroundWater_Depth / 2) + L3())) +
                (Area3() * ((_GroundWater_Depth / 3) + L3())) + (Area4() * (L3() * 2) / 3)) /
                P();
            }
            else
            {
                //If groundwater doesn't exist
                _Z_bar = (((Area0() * ((_ExcavationDepth / 2) + L3())) +
                (Area1() * ((_ExcavationDepth / 3) + L3())))) / (Area0() + Area1());
            }
        }
        else
        {
            if (IsGroundWaterAbsent == false)
            {

```

```

        //In the presence of groundwater
        _Z_bar = ((Area0() * ((_ExcavationDepth / 2) +
_GroundWater_Depth)) + (Area1() * ((_ExcavationDepth / 3) + _GroundWater_Depth))
+
        (Area2() * (_GroundWater_Depth / 2)) + (Area3() *
(_GroundWater_Depth / 3))) / P();
    }
    else
    {
        //If groundwater doesn't exist
        _Z_bar = ((Area0() * (_ExcavationDepth / 2)) + (Area1() *
(_ExcavationDepth / 3))) / (Area0() + Area1());
    }
}
else
{
    if (IsGroundWaterAbsent == false)
    {
        //In the presence of groundwater
        _Z_bar = ((Area0() * ((_ExcavationDepth / 2) +
_GroundWater_Depth + L3())) + (Area1() * ((_ExcavationDepth / 3) +
_GroundWater_Depth + L3())) +
        (Area2() * ((_GroundWater_Depth / 2) + L3())) + (Area3()
* ((_GroundWater_Depth / 3) + L3())) + (Area4() * (L3() * 2) / 3)) / P();
    }
    else
    {
        //If groundwater doesn't exist
        _Z_bar = (((Area0() * ((_ExcavationDepth / 2) + L3())) +
(Area1() * ((_ExcavationDepth / 3) + L3()))) / (Area0() + Area1()));
    }
}
return _Z_bar;
}

public Double Sigma5()
{
    return ((Surcharge + (_Excavated_UnitWeight * _ExcavationDepth) +
(Excavated_EffectiveWeight() * _GroundWater_Depth)) * Kp())
        + (Dredged_EffectiveWeight() * L3() * Delta_K());
}

public double A1()
{
    if (IsCantileverNull == false)
    {
        if (IsFrictionNull == false)
        {
            //return (Sigma5() - (12 * Cohesion())) /
(Dredged_EffectiveWeight() * Delta_K());
            return (Sigma5() + (2 * Cohesion())) /
(Dredged_EffectiveWeight() * Delta_K());
        }
        else
        {
            return (Cohesion()) - (Surcharge + (_Excavated_UnitWeight *
_ExcavationDepth) +
                (Excavated_EffectiveWeight() * _GroundWater_Depth));
        }
    }
    else

```

```

        {
            return (1.5 * (_ExcavationDepth - _anchorL1 + _GroundWater_Depth
+ L3())) + (Cohesion() / (Dredged_EffectiveWeight() * Delta_K()));
        }
    }

    public double A2()
    {
        if (IsCantileverNull == false)
        {
            if (IsFrictionNull == false)
            {
                //return (8 * P()) / (Dredged_EffectiveWeight() * Delta_K())
+
                // ((Cohesion() * ((6 * Sigma5()) + (13 * Cohesion())) /
(Math.Pow((Dredged_EffectiveWeight() * Delta_K()), 2)));
                return ((8 * P()) / (Dredged_EffectiveWeight() * Delta_K()))
-
                ((Cohesion() * (Sigma5() + Cohesion())) /
(Math.Pow((Dredged_EffectiveWeight() * Delta_K()), 2)));
            }
            else
            {
                return 2 * P();
            }
        }
        else
        {
            return 1.5 * ((Cohesion() * (_ExcavationDepth - _anchorL1 +
_GroundWater_Depth + L3())) / (Dredged_EffectiveWeight() * Delta_K()));
        }
    }

    public double A3()
    {
        if (IsCantileverNull == false)
        {
            if (IsFrictionNull == false)
            {
                //return (6 * P() * ((2 * Z_bar() * Dredged_EffectiveWeight()
* Delta_K()) + Sigma5() + (4 * Cohesion() / 3)))
// / Math.Pow((Dredged_EffectiveWeight() * Delta_K()), 2);
                return (6 * P() * ((2 * Z_bar() * Dredged_EffectiveWeight() *
Delta_K()) + Sigma5() + (4 * Cohesion() / 3)))
/ Math.Pow((Dredged_EffectiveWeight() * Delta_K()), 2);
            }
            else
            {
                return (P() * (P() + (3 * Cohesion() * Z_bar()))) / ((2 *
Cohesion()) + ((_Excavated_UnitWeight * _ExcavationDepth) +
(Excavated_EffectiveWeight() * _GroundWater_Depth) +
Surcharge));
            }
        }
        else
        {
            return 3 * P() * (((_GroundWater_Depth + _ExcavationDepth + L3())
- (Z_bar() + _anchorL1)) / (Dredged_EffectiveWeight() * Delta_K()));
        }
    }

    public double A4()

```

```

    {
        if (IsCantileverNull == false)
        {
            if (IsFrictionNull == false)
            {
                //return (P() * ((6 * Z_bar() * Sigma5()) + (4 * P()) - (12 *
Z_bar() * Cohesion())) /
                // Math.Pow((Dredged_EffectiveWeight() * Delta_K()), 2);
                return (P() * ((6 * Z_bar() * Sigma5()) + (4 * P()) + (12 *
Z_bar() * Cohesion())) /
                    Math.Pow((Dredged_EffectiveWeight() * Delta_K()), 2);
            }
            else
            {
                return 0;
            }
        }
        else
        {
            return 0;
        }
    }

    public Double f(double x)
    {
        if (IsCantileverNull == false)
        {
            if (IsFrictionNull == false)
            {
                return (x * x * x * x) + (A1() * x * x * x) - (A2() * x * x)
- (A3() * x) - A4();
            }
            else
            {
                return (A1() * x * x) - (A2() * x) - A3();
            }
        }
        else
        {
            return (x * x * x) + (A1() * x * x) + (A2() * x) - A3();
        }
    }

    public Double g(double x)
    {
        if (IsCantileverNull == false)
        {
            if (IsFrictionNull == false)
            {
                return (4 * x * x * x) + ((A1() * 3) * x * x) - ((A2() * 2) *
x) - A3();
            }
            else
            {
                return (A1() * 2 * x) - A2();
            }
        }
        else
        {
            return (3 * x * x) + ((A1() * 2) * x) + A2();
        }
    }
}

```

```

public String NewtonRaphson(double x_0, double precision)
{
    try
    {
        double x = x_0;
        do
        {
            x++;
        }
        while (f(x) < precision);

        while (f(x) > precision)
        {
            x = x - (f(x) / g(x));
            if (f(x) <= precision)
            {
                return x.ToString();
            }
        }
    }
    catch (Exception ex)
    {
        ex.ToString();
    }
    return "";
}

public Double L4()
{
    if (IsCantileverNull == false)
    {
        if (IsFrictionNull == false)
        {
            try
            {
                double.TryParse(NewtonRaphson(0, 1e-10), out _L4);
            }
            catch (Exception ex)
            {
                MessageBox.Show(ex.ToString());
            }
        }
        else
        {
            _L4 = ((Dredge() * A1()) - P()) / Cohesion();
        }
    }
    else
    {
        try
        {
            double.TryParse(NewtonRaphson(0, 1e-10), out _L4);
        }
        catch (Exception ex)
        {
            MessageBox.Show(ex.ToString());
        }
    }

    return _L4;
}

```

```

public Double Dredge()
{
    if (IsCantileverNull == false)
    {
        if (IsFrictionNull == false)
        {
            _Dredge = L3() + L4();
        }
        else
        {
            try
            {
                double.TryParse(NewtonRaphson(0, 1e-10), out _Dredge);
            }
            catch (Exception ex)
            {
                MessageBox.Show(ex.ToString());
            }
        }
    }
    else
    {
        _Dredge = L3() + L4();
    }
    return _Dredge;
}

public Double Sigma3()
{
    return (Dredged_EffectiveWeight() * Delta_K() * L4()) + Cohesion();
}

public Double Sigma4()
{
    return Sigma5() + (Dredged_EffectiveWeight() * Delta_K() * L4()) +
Cohesion();
}

public Double L5()
{
    return ((Sigma3() * L4()) - (2 * P())) / (Sigma3() + Sigma4());
}

public Double Sigma6()
{
    if (IsFrictionNull == false)
    {
        //return Sigma2() - ((Dredge() - L5()) *
(Dredged_EffectiveWeight() * Delta_K())) + (2 * _Dredged_Cohesion *
Math.Sqrt(Kp()) * Math.Cos(_Dredged_InterfaceAngle * Math.PI / 180));
        return Sigma2() - ((Dredge() - L5()) * (Dredged_EffectiveWeight()
* Delta_K())) + Cohesion();
    }
    else
    {
        return Cohesion() - ((_Excavated_UnitWeight * _ExcavationDepth) +
(Excavated_EffectiveWeight() * _GroundWater_Depth));
    }
}

public Double Z_Prime()

```

```

{
    if (IsCantileverNull == false)
    {
        if (IsFrictionNull == false)
        {
            return Math.Sqrt(2 * P() / ((Dredged_EffectiveWeight() *
Delta_K()) + Cohesion()));
        }
        else
        {
            return P() / Sigma6();
        }
    }
    else
    {
        double x, x1, x2;
        double a = 0.5 * Excavated_EffectiveWeight() * Ka_Excavated();
        double b = (Sigma1() - Sigma0());
        double c = (0.5 * (Sigma1() - Sigma0()) * _ExcavationDepth) -
Anchor_Force();
        double sqrt = b * b - 4 * a * c;
        if (sqrt > 0)
        {
            x1 = (-b + Math.Sqrt(sqrt)) / (2 * a);
            x2 = (-b - Math.Sqrt(sqrt)) / (2 * a);
        }
        else
        {
            return 0;
        }
        if (x1 > x2)
        {
            x = Math.Abs(x1);
        }
        else
        {
            x = Math.Abs(x2);
        }
        return Math.Round(x, 2);
    }
}

public Double Practical_Dredge()
{
    return 1.2 * Dredge();
}

#endregion

#region Anchored Force Algorithm

public Double Anchor_ForceTotal()
{
    return P() - (0.5 * Sigma3() * L4());
}

public Double Anchor_Inclination()
{
    return _anchorAngle * Math.PI / 180;
}

public Double Anchor_Force()

```

```

{
    return Anchor_ForceTotal() / Math.Cos(Anchor_Inclination());
}

#endregion

public double Flexural_Modulus()
{
    return _Wall_ElasticModulus * _Wall_Inertia * Math.Pow(10, -8);
    //return 100000;
}

public double Calculated_Section_Modulus()
{
    double _sectionModulus;
    _sectionModulus = MaximumBM / _Wall_AllowableStress;
    if(_sectionModulus > _Wall_SectionModulus)
    {
        MessageBox.Show("Wall Section Modulus of " + _Wall_SectionModulus
+ " is less than the calculated section modulus ("
        + Math.Round(_sectionModulus, 6) + "). Wall structure CAN'T
resist maximum bending moment! Please select a different wall and resimulate.");
    }
    else
    {
        MessageBox.Show("Simulation Successful!");
    }
    return _sectionModulus;
}

#endregion

#region Interpolation

List<double> _Depth_Interpolation;
List<double> _Pressure_Interpolation;
List<double> _ShearForce_Interpolation;
List<double> _BendingMoment_Interpolation;
List<double> _EI_BendingMoment_Interpolation;
List<double> _Rotation_Interpolation;
List<double> _Deflection_Interpolation;

int countXX;
int countYY;

public List<double> Depth_Interpolation()
{
    double _Practical_Dredge = Practical_Dredge();
    double _Dredge = Dredge();
    double _L3 = L3();
    double _L5 = L5();
    double _Z_Prime = Z_Prime();

    List<double> _depth = new List<double>();
    if (IsCantileverNull == false)
    {
        if (IsGroundWaterAbsent == false)
        {
            double paso1 = _ExcavationDepth / 5;
            for (double i = 0; i < _ExcavationDepth; i = i + paso1)
            {

```

```

        _depth.Add(Math.Round(i, 2));
    }

    double paso2 = _GroundWater_Depth / 10;
    for (double i = _ExcavationDepth; i < (_ExcavationDepth +
_GroundWater_Depth); i = i + paso2)
    {
        _depth.Add(Math.Round(i, 2));
    }
}
else
{
    double paso1 = _ExcavationDepth / 5;
    for (double i = 0; i < _ExcavationDepth; i = i + paso1)
    {
        _depth.Add(Math.Round(i, 2));
    }
}
double paso3 = _L3 / 3;
for (double i = (_ExcavationDepth + _GroundWater_Depth); i <
(_ExcavationDepth + _GroundWater_Depth + _L3); i = i + paso3)
{
    _depth.Add(Math.Round(i, 2));
}

double paso4 = Z_Prime() / 6;
for (double i = (_ExcavationDepth + _GroundWater_Depth + _L3); i <
< (_ExcavationDepth + _GroundWater_Depth + _L3 + _Z_Prime); i = i + paso4)
{
    _depth.Add(Math.Round(i, 2));
}

double paso5 = (_Dredge - _L5 - _Z_Prime - _L3) / 6;
for (double i = (_ExcavationDepth + _GroundWater_Depth + _L3 +
_Z_Prime); i < (_ExcavationDepth + _GroundWater_Depth + _Dredge - _L5); i = i +
paso5)
{
    _depth.Add(Math.Round(i, 2));
}

double paso6 = _L5 / 6;
for (double i = (_ExcavationDepth + _GroundWater_Depth + _Dredge
- _L5); i <= (_ExcavationDepth + _GroundWater_Depth + _Dredge); i = i + paso6)
{
    _depth.Add(Math.Round(i, 2));
}
_depth.Add(Math.Round((_ExcavationDepth + _GroundWater_Depth +
_Dredge), 2));

//_depth = _depth.Distinct().ToList();

for (int i = 1; i < _depth.Count; i++)
{
    if (_depth[i] - _depth[i - 1] <= 0.04)
        _depth.RemoveAt(i);
}
_depth = _depth.Distinct().ToList();

//bool auxiliar = true;

//while (!auxiliar)

```

```

//{
//  auxiliar = true;
//  for (int i = 0; i < _depth.Count - 1; i++)
//  {
//      if (_depth[i + 1] - _depth[i] <= 0.04)
//      {
//          _depth.RemoveAt(i);
//          auxiliar = false;
//          break;
//      }
//  }
//}

//_depth.Add(Math.Round((_ExcavationDepth + _GroundWater_Depth +
_Practical_Dredge), 2));
}
else
{
    if (IsGroundWaterAbsent == false)
    {
        double paso1 = _anchorL1 / 3;
        for (double i = 0; i <= _anchorL1; i = i + paso1)
        {
            _depth.Add(Math.Round(i, 2));
        }
        countYY = _depth.Count;

        double paso2 = (_ExcavationDepth - _anchorL1) / 3;
        for (double i = _anchorL1; i < _ExcavationDepth; i = i +
paso2)
        {
            _depth.Add(Math.Round(i, 2));
        }

        double paso3 = _Z_Prime / 12;
        for (double i = _ExcavationDepth; i < (_ExcavationDepth +
_Z_Prime); i = i + paso3)
        {
            _depth.Add(Math.Round(i, 2));
        }

        double paso4 = (_GroundWater_Depth - _Z_Prime) / 8;
        for (double i = (_ExcavationDepth + _Z_Prime); i <
(_ExcavationDepth + _GroundWater_Depth); i = i + paso4)
        {
            _depth.Add(Math.Round(i, 2));
        }

        //for (int i = 6; i < _depth.Count; i++)
        //{
        //    if (_depth[i] - _depth[i - 1] < 0.03)
        //        _depth.RemoveAt(i);
        //}
        countXX = _depth.Count;
    }
    else
    {
        double paso1 = _anchorL1 / 3;
        for (double i = 0; i <= _anchorL1; i = i + paso1)
        {
            _depth.Add(Math.Round(i, 2));
        }
    }
}

```

```

        countYY = _depth.Count;

        double paso2 = _Z_Prime / 12;
        for (double i = _anchorL1; i < (_anchorL1 + _Z_Prime); i = i
+ paso2)
        {
            _depth.Add(Math.Round(i, 2));
        }

        double paso3 = (_anchorL2 - _Z_Prime) / 8;
        for (double i = (_anchorL1 + _Z_Prime); i < _ExcavationDepth;
i = i + paso3)
        {
            _depth.Add(Math.Round(i, 2));
        }

        //for (int i = 6; i < _depth.Count; i++)
        //{
        //    if (_depth[i] - _depth[i - 1] < 0.03)
        //        _depth.RemoveAt(i);
        //}
        countXX = _depth.Count;
    }

    double paso5 = _L3 / 5;
    for (double i = (_ExcavationDepth + _GroundWater_Depth); i <
(_ExcavationDepth + _GroundWater_Depth + _L3); i = i + paso5)
    {
        _depth.Add(Math.Round(i, 2));
    }

    double paso6 = _L4 / 5;
    for (double i = (_ExcavationDepth + _GroundWater_Depth + _L3); i
<= (_ExcavationDepth + _GroundWater_Depth + _L3 + _L4); i = i + paso6)
    {
        _depth.Add(Math.Round(i, 2));
    }
    // _depth.Add(Math.Round((_ExcavationDepth + _GroundWater_Depth +
_L3 + _L4), 2));
}

//for (int i = 27; i < _depth.Count; i++)
//{
//    if (_depth[i] - _depth[i - 1] < 0.03)
//        _depth.RemoveAt(i);
//}

    return _depth;
}

public double interMedia()
{
    //return Sigma6() * ((_ExcavationDepth + _GroundWater_Depth + _L3 +
Z_Prime()) - (_ExcavationDepth + _GroundWater_Depth + _L3))
    // / ((_ExcavationDepth + _GroundWater_Depth + Dredge() - L5()) -
(_ExcavationDepth + _GroundWater_Depth + _L3));

    return Sigma6() * Z_Prime() / (_Dredge - L5() - _L3);
}

public double anchorCohesion_l1()
{

```

```

        return (_Excavated_UnitWeight * _anchorL1 * Ka_Excavated()) - (2 *
        _Excavated_Cohesion * Math.Sqrt(Ka_Excavated()) *
        Math.Cos(_Excavated_InterfaceAngle * Math.PI / 180));
    }

```

```

public List<double> Pressure_Interpolation()
{

```

```

    double _Sigma0 = Sigma0();
    double _Sigma1 = Sigma1();
    double _Sigma2 = Sigma2();
    double _Dredged_EffectiveWeight = Dredged_EffectiveWeight();
    double _Delta_K = Delta_K();
    double _L3 = L3();
    double _interMedia = interMedia();
    double _Sigma6 = Sigma6();
    double _Sigma4 = Sigma4();

```

```

    List<double> _pressure = new List<double>();
    if (IsCantileverNull == false)
    {

```

```

        if (IsGroundWaterAbsent == false)
        {
            double paso1 = (_Sigma1 - _Sigma0) / 5;
            for (double i = _Sigma0; i < _Sigma1; i = i + paso1)
            {
                _pressure.Add(Math.Round(i, 2));
            }

```

```

            double paso2 = (_Sigma2 - _Sigma1) / 10;
            for (double i = _Sigma1; i < _Sigma2; i = i + paso2)
            {
                _pressure.Add(Math.Round(i, 2));
            }

```

```

        }
        else
        {
            double paso1 = (_Sigma1 - _Sigma0) / 5;
            for (double i = _Sigma0; i < _Sigma1; i = i + paso1)
            {
                _pressure.Add(Math.Round(i, 2));
            }
        }

```

```

        double paso3 = -_Sigma2 / 3;
        for (double i = _Sigma2; i > 0; i = i + paso3)
        {
            _pressure.Add(Math.Round(i, 2));
        }

```

```

        double paso4 = _interMedia / 6;
        for (double i = 0; i > _interMedia; i = i + paso4)
        {
            _pressure.Add(Math.Round(i, 2));
        }

```

```

        double paso5 = (_Sigma6 - _interMedia) / 6;
        for (double i = _interMedia; i > _Sigma6; i = i + paso5)
        {
            _pressure.Add(Math.Round(i, 2));
        }

```

```

        double paso6 = (_Sigma4 - _Sigma6) / 6;

```

```

        for (double i = _Sigma6; i <= _Sigma4; i = i + paso6)
        {
            _pressure.Add(Math.Round(i, 2));
        }
        _pressure.Add(Math.Round(_Sigma4, 2));
        //_pressure.Add(0);

        for (int i = 0; i < _pressure.Count - 1; i++)
        {
            if (Math.Abs(Math.Abs(_pressure[i + 1]) -
Math.Abs(_pressure[i])) <= 0.05)
                _pressure.RemoveAt(i);
        }
    }
    else
    {
        double _anchorCohesion_l1 = anchorCohesion_l1();
        double _Excavated_EffectiveWeight = Excavated_EffectiveWeight();
        double _Dredged_EffectiveWeight = Dredged_EffectiveWeight();
        double _Ka_Excavated = Ka_Excavated();
        _Depth_Interpolation = Depth_Interpolation();
        double _pressureActive;

        double paso1 = (_anchorCohesion_l1 - _Sigma0) / 3;
        for (double i = _Sigma0; i <= _anchorCohesion_l1; i = i + paso1)
        {
            _pressure.Add(Math.Round(i, 2));
        }
        //_pressure.Add(Math.Round((_Excavated_UnitWeight * _anchorL1 *
_Ka_Excavated), 2));

        double paso2 = (_Sigma1 - _anchorCohesion_l1) / 3;
        for (double i = _anchorCohesion_l1; i <= _Sigma1; i = i + paso2)
        {
            _pressure.Add(Math.Round(i, 2));
        }
        //_Depth_Interpolation.Count - 10
        for (int i = _pressure.Count; i < countXX ; i++)
        {
            _pressureActive = _pressure[i - 1] +
(( _Excavated_EffectiveWeight * _Ka_Excavated) * (_Depth_Interpolation[i] -
_Depth_Interpolation[i - 1]));
            _pressure.Add(Math.Round(_pressureActive, 2));
        }

        for (int i = countXX; i < _Depth_Interpolation.Count; i++)
        {
            _pressureActive = _pressure[i - 1] -
(( _Dredged_EffectiveWeight * _Delta_K) * (_Depth_Interpolation[i] -
_Depth_Interpolation[i - 1]));
            _pressure.Add(Math.Round(_pressureActive, 2));
        }
    }
    }
    return _pressure;
}

public List<double> ShearForce_Interpolation()
{
    _Depth_Interpolation = Depth_Interpolation();
    _Pressure_Interpolation = Pressure_Interpolation();
    double _AnchorForce = Anchor_Force();
}

```

```

double _shearForce;
List<double> SFInterpolation = new List<double>();
SFInterpolation.Add(0);

if (IsCantileverNull == false)
{
    for (int i = 1; i < _Depth_Interpolation.Count; i++)
    {
        _shearForce = SFInterpolation[i - 1] +
(((_Depth_Interpolation[i] - _Depth_Interpolation[i - 1]) *
        (_Pressure_Interpolation[i] + _Pressure_Interpolation[i -
1]) / 2);
        SFInterpolation.Add(Math.Round(_shearForce, 2));
    }
}
else
{
    //_Depth_Interpolation.Count - 34
    for (int i = 1; i < countYY; i++)
    {
        _shearForce = SFInterpolation[i - 1] +
(((_Depth_Interpolation[i] - _Depth_Interpolation[i - 1]) *
        (_Pressure_Interpolation[i] + _Pressure_Interpolation[i -
1]) / 2);
        SFInterpolation.Add(Math.Round(_shearForce, 2));
    }

    //_Depth_Interpolation.Count - 33
    for (int i = countYY; i < countYY + 1; i++)
    {
        _shearForce = SFInterpolation[i - 1] +
(((_Depth_Interpolation[i] - _Depth_Interpolation[i - 1]) *
        (_Pressure_Interpolation[i] + _Pressure_Interpolation[i -
1]) / 2) - _AnchorForce;
        SFInterpolation.Add(Math.Round(_shearForce, 2));
    }

    for (int i = SFInterpolation.Count; i <
_Pressure_Interpolation.Count; i++)
    {
        _shearForce = SFInterpolation[i - 1] +
(((_Depth_Interpolation[i] - _Depth_Interpolation[i - 1]) *
        (_Pressure_Interpolation[i] + _Pressure_Interpolation[i -
1]) / 2);
        SFInterpolation.Add(Math.Round(_shearForce, 2));
    }
}
return SFInterpolation;
}

public List<double> BendingMoment_Interpolation()
{
    _Depth_Interpolation = Depth_Interpolation();
    _ShearForce_Interpolation = ShearForce_Interpolation();

    List<double> BMInterpolation = new List<double>();
    BMInterpolation.Add(0);
    double _bendingMoment;
    for (int i = 1; i < _Depth_Interpolation.Count; i++)
    {

```

```

        _bendingMoment = BMInterpolation[i - 1] +
        ((_Depth_Interpolation[i] - _Depth_Interpolation[i - 1]) *
        (_ShearForce_Interpolation[i] + _ShearForce_Interpolation[i -
1]) / 2);
        BMInterpolation.Add(Math.Round(_bendingMoment, 2));
    }
    return BMInterpolation;
}

public List<double> EI_BendingMoment_Interpolation()
{
    _BendingMoment_Interpolation = BendingMoment_Interpolation();

    _EI_BendingMoment_Interpolation = new List<double>();
    double _EI_BM_Interpolation;
    for (int i = 0; i < _BendingMoment_Interpolation.Count; i++)
    {
        _EI_BM_Interpolation = _BendingMoment_Interpolation[i] /
Flexural_Modulus();
    }
    _EI_BendingMoment_Interpolation.Add(Math.Round(_EI_BM_Interpolation, 5));
    return _EI_BendingMoment_Interpolation;
}

public List<double> Rotation_Interpolation()
{
    _Depth_Interpolation = Depth_Interpolation();
    _EI_BendingMoment_Interpolation = EI_BendingMoment_Interpolation();

    List<double> RotationInterpolation = new List<double>();
    RotationInterpolation.Add(0);
    double _rotation;
    for (int i = 1; i < _Depth_Interpolation.Count; i++)
    {
        _rotation = RotationInterpolation[i - 1] +
        ((_Depth_Interpolation[i] - _Depth_Interpolation[i - 1]) *
        (_EI_BendingMoment_Interpolation[i] +
        _EI_BendingMoment_Interpolation[i - 1]) / 2);
        RotationInterpolation.Add(Math.Round(_rotation, 5));
    }
    return RotationInterpolation;
}

public List<double> Deflection_Interpolation()
{
    _Depth_Interpolation = Depth_Interpolation();
    _Rotation_Interpolation = Rotation_Interpolation();

    List<double> DeflectionInterpolation = new List<double>();
    DeflectionInterpolation.Add(0);
    double _bendingMoment;
    for (int i = 1; i < _Depth_Interpolation.Count; i++)
    {
        _bendingMoment = DeflectionInterpolation[i - 1] +
        ((_Depth_Interpolation[i] - _Depth_Interpolation[i - 1]) *
        (_Rotation_Interpolation[i] + _Rotation_Interpolation[i - 1])
/ 2);
        DeflectionInterpolation.Add(Math.Round(_bendingMoment, 5));
    }
    return DeflectionInterpolation;
}

```

```

public List<double> Rotation_Interpolation_Degrees()
{
    _Rotation_Interpolation = Rotation_Interpolation();

    List<double> RotationInterpolation_deg = new List<double>();
    double _rotation_deg;
    for (int i = 0; i < _Rotation_Interpolation.Count; i++)
    {
        _rotation_deg = _Rotation_Interpolation[i] * 180 / Math.PI;
        RotationInterpolation_deg.Add(Math.Round(_rotation_deg, 3));
    }
    return RotationInterpolation_deg;
}

public List<double> Deflection_Interpolation_mm()
{
    _Deflection_Interpolation = Deflection_Interpolation();

    List<double> DeflectionInterpolation_mm = new List<double>();
    double _deflection_mm;
    for (int i = 0; i < _Deflection_Interpolation.Count; i++)
    {
        _deflection_mm = _Deflection_Interpolation[i] * 1000;
        DeflectionInterpolation_mm.Add(Math.Round(_deflection_mm, 3));
    }
    return DeflectionInterpolation_mm;
}

#endregion
}
}
}

```